ANL/RAS 80-17

# FAST-NEUTRON HODOSCOPE AT TREAT: METHODS FOR QUANTITATIVE DETERMINATION OF FUEL DISPERSAL

by

A. De Volpi, C. L. Fink, G. E. Marsh, E. A. Rhodes, and G. S. Stanford



Reactor Analysis and Safety Division
Argonne National Laboratory
Argonne, Ill. 60439

ANL/RAS 80-17

# FAST-NEUTRON HODOSCOPE AT TREAT: METHODS FOR QUANTITATIVE DETERMINATION OF FUEL DISPERSAL

by

A. De Volpi, C. L. Fink, G. E. Marsh, E. A. Rhodes, and G. S. Stanford



Reactor Analysis and Safety Division
Argonne National Laboratory
Argonne, Ill. 60439

CONTENTS



ABSTRACT

Fuel-motion surveillance using the fast-neutron hodoscope in TREAT experiments has advanced from an initial role of providing time/location/velocity data to that of offering quantitative mass results. The material and radiation surroundings of the test section contribute to intrinsic and instrumental effects upon hodoscope detectors that require detailed corrections. Depending upon the experiment, count rate compensation is usually required for deadtime, power level, nonlinear response, efficiency, background, and detector calibration. Depending on their magnitude and amenability to analytical and empirical treatment, systematic corrections may be needed for self-shielding, self-multiplication, self-attenuation, flux depression, and other effects. Current verified hodoscope response (for 1- to 7-pin fuel bundles) may be parametrically characterized under optimum conditions by 1-ms time resolution; 0.25-mm lateral and 5-mm axial-motion displacement resolution; and 50-mg single-pin mass resolution. The experimental and theoretical foundation for this performance is given, with particular emphasis on the geometrical response function and the statistical limits of fuel-motion resolution. Comparisons are made with alternative diagnostic systems.

## I. INTRODUCTION

In the ongoing transient test program at TREAT, fuel-motion surveillance using the fast-neutron hodoscope has advanced from an initial role of providing time/location/velocity data to that of offering quantitative mass results. Previous reports (1), (2), (3), (4) have surveyed the status of hodoscope development and given typical results; however, the analysis methods employed to obtain mass data were not described. Recent improvements (5) in hardware and software provide more precise mass-movement resolution. In view of the significance to the licensing and safety program of detailed fuel-motion information having suitable precision and accuracy, this paper traces the steps necessary to achieve quantitative fuel-mass surveillance, as well as methods of validation and correlation of results.

Fuel-motion surveillance differs from other applications of transient-radiation diagnostics because of the material and radiation surroundings of a fuel-pin test section. Substantial thicknesses of sodium, steel, nuclear-heated walls, or thermal-neutron filters usually surround the test section; the reactor-driver causes neutron and gamma background; and the test section itself tends to scatter and absorb the emitted radiation that is a characteristic signature of the fuel. The fission rate in the fuel is neither spatially uniform nor related in a simple way to the neutron-driver flux. In addition to these inherent problems, the instruments utilized to observe the motion of fuel can have a nonlinear response, particularly in view of the wide power range and the large mixed background arising during the transient.

Selection of diagnostic technique and optimization of design for a given technique are critical in leading to results that meet experiment objectives over a wide range of test conditions. Among the important diagnostic parameters are time resolution, signal rate, sensitivity to fuel displacement, signal/background ratio, spatial dependence of background, and spatial resolution of fuel motion. In addition, the diagnostic instrumentation should not sacrifice meaningful performance on account of detector drift, nonlinear response to power or fuel changes, background impact, or difficulties in calibration, processing, and data reconstruction.

In order to respond to experiment needs, the hodoscope at TREAT has been configured to have a high specific sensitivity to fission neutrons from fuel, low sensitivity to gamma ray and neutron background, and good statistical precision over a wide range of reactor power. A conscious tradeoff has been made, with given collimator designs, to sacrifice static spatial resolution in order to satisfy more critical experiment requirements, such as time and mass resolution.

In particular, the hodoscope is designed for high sensitivity to the motion of fuel; it is thus legitimate, when tradeoffs are involved, to forego static resolution -- to do without well-resolved "pictures" of stationary fuel disposition. There is some confusion in the technical community on this point. A diagnostic device that offers good resolution of static images may be of very limited value unless it yields adequate mass, time, and spatial resolution of moving fuel. Conversely, a system that provides adequate imaging of moving fuel need not produce good resolution of stationary objects. During transients the hodoscope has high-quality resolution of fuel movement (with appropriate tradeoffs in time and spatial resolution) but relatively coarse resolution of stationary fuel. However, before or after a transient, when the hodoscope collimator can be moved in small increments to cause the relative motion of detector channels with respect to the fuel, static-fuel distributions may be reproduced with higher resolution imaging.

## I-A. Data Processing and Analysis

Recent improvements in the manner of recording hodoscope data permit direct and prompt processing of the results of an experiment. The data are recorded on a magnetic disk system (5), with the digital photographic system (1) operational as a backup.

Digital data are transferred after the experiment to interactive computer facilities at Argonne, Illinois. Count-rate data are generated for each detector channel, and a time-base consistent with other instruments is established. With a variety of available power monitors, the channel data are power-normalized to compensate for the effect of transient power changes upon the count rate.

Corrections are developed for deadtime and nonlinear detector response at high peak power levels by doing a minimum-variance fit to a model for each channel. The next major stage in data processing is the normalization of channels for efficiency in order to provide uniform image reconstruction. Efficiency-normalization data can be obtained either from a steady-state scan performed before the transient or from a low-power portion of the transient prior to fuel relocation. In the latter case, a computer code goes through an iterative process, based on a minimum-variance fit to a response model, taking into consideration the axial-flux profile.

Background subtraction is based on supplementary data and on calculations that lead to the appropriate magnitude of the background distribution. Depending on the desired time and space resolution, data-recording intervals may be summed and spatial regions may be averaged in various stages of analysis.

## I-B. Fuel Masses

Quantitative mass determination depends on establishing the proper proportionality between the observed signal rate and the amount of fuel present at any instant. The observed fission rate depends not only on the fuel mass but also -- largely to second order -- upon self-shielding, self-multiplication, self-attenuation, and flux depression. The applied calibration factor is derived from the experimentally determined signal rate per unit power, from the known amount of fuel initially in the test section, and from the posttest examination when available.

Before reaching specific conclusions regarding reportable data, systematic and statistical tests for internal consistency are made. Satisfactory data are then interpreted to establish time and location of fuel motion. A variety of presentation modes have been programmed to aid in visualization of the data.

After analysis and initial reporting, an effort is made to cross-check the data against the posttransient hodoscope scan, as well as any radiographic or other posttest data that may be available. Appropriate correlations are noted with other instrumentation, including power level, flow, temperature, pressure, and acoustic monitors. Eventually reconciliation is attempted against the full range of pretest predictions, posttest calculations, physical examinations, and other test-train data.

The results of this process will be illustrated graphically later in this report in various formats, with the precision and accuracy of time/location velocity/mass data noted.

## II. HODOSCOPE PERFORMANCE REVIEW

Because of changes that have taken place since publication (1) of a complete description of the hodoscope system at TREAT, the system and its experimental role are reviewed below. The hodoscope has been active in fuel-motion monitoring for about 15 years.

### II-A. Hodoscope System Description

The apparatus installed at TREAT makes use of either the north or south beam access-facilities of the reactor. Most experiments are imaged by the hodoscope collimator at the north side because its view has a vertical extent of 1.2 m. The collimator that can be installed at the south slot views only a height of 0.5 m, but it has intrinsically better spatial and mass resolution. Much of the electronic-support system is shared by the two collimator and detector arrays.

Each collimator is situated at or inside the biological shield, as shown in Fig. 1. Ordinarily, the core is loaded with slotted elements between the test sample and the collimator to permit unimpeded viewing. For some experiments, slotted elements may be loaded on both sides of the test capsule, thereby allowing diagnostic devices to be installed at each end of the slot. Some experiments, reactivity allowing, have been performed with both the hodoscope at the north side and pinhole-camera devices at the south side. With the slot running fully through the core, the hodoscope signal/background ratio is typically twice as good as with a half-slot.

The test capsule is located at the center of the TREAT core. Capsules at TREAT have contained 1, 3, and 7 pins, in addition to those with dummy fuel for calibration. Some capsules have stagnant coolant and others have flowing coolant.

The radiation and containment test environment for a fuel sample dominates diagnostic-design considerations. The opaque surroundings of the fuel include one or two centimeters of steel wall, sodium coolant, a solid heat sink, thermal-neutron filters, and occasionally nuclear-heated walls. The radiation field incident on the test section is time-varying and contains a large component that can be scattered from the test section and interfere with the signal emanating from the fuel.

The new 1.2 m collimator (Fig. 2) has been amply described elsewhere (6). Its primary feature is the extended viewing height.

Hornyak-button detectors with improved linear response (7) are the main fast-neutron detection elements of the hodoscope at present. Gamma detectors are mounted in tandem for development of steel-blockage detection (8). A power monitor independent of TREAT core instrumentation is used for purposes of intercomparison of reactor-power profiles.

The signal-processing electronics is basically unchanged (1). Detector signals are amplified and shaped, and pulses of adequate amplitude trigger digital scalers assigned to each channel. These scalers periodically transfer their count total to the magnetic-disk recording system. Control equipment initiates the storage of data and carries out other operations during a transient.

The hodoscope is operated by TREAT personnel, who check out, calibrate, and set up the remote-triggering link prior to a transient, in accordance with specifications established at Argonne, Illinois. After an experiment, they are responsible for handling data, which is transferred to magnetic tape for

permanent storage. Tape data may be transmitted by either electronic link or physically by mail to Illinois, where processing, analysis, and reporting will take place.

## II-B. Summary of Performance Characteristics

Table I contains a summary of the key performance features of the fast-neutron hodoscope at TREAT. Not all of the limiting characteristics can be achieved simultaneously. Nor are the mass-displacement resolution capabilities obtainable with every experiment configuration. Although the reference values in Table I are based on experimental results, resolution will be degraded for a capsule surrounded by very thick walls. Normal settings need not be at the minimum level; for instance, rather than 0.1 ms, typical data-collection intervals are set in the several-millisecond range.

TABLE I

Hodoscope Capabilities

| | |
|---|---|
| Maximum Viewing HEIGHT | 1.2 m (48 in.) (North face of TREAT)<br>0.5 m (21 in.) (South face of TREAT) |
| Maximum Viewing WIDTH | 7 cm (2.6 in.) (North face of TREAT)<br>5 cm (2.0 in.) (South face of TREAT) |
| Maximum CHANNEL CAPACITY | 360 |
| Interchannel HORIZONTAL spacing | 7 mm (0.26 in.) (1.2 m collimator) |
| Interchannel VERTICAL spacing | 34 mm (1.35 in.) (1.2 m collimator) |
| Detectable HORIZONTAL MOTION | 0.2 mm (10 mils) |
| Detectable VERTICAL MOTION | 6 mm (0.25 in.) |
| 1-pin MASS-DISPLACEMENT RESOLUTION | 0.05 g/channel (minimum) |
| 7-pin MASS-DISPLACEMENT RESOLUTION | 0.35 g/channel (minimum) |
| Data-collection INTERVALS | 0.1 ms (minimum) |
| Data-interval CAPACITY | 8000 intervals (maximum) |
| Minimum TREAT power | 10 kW |
| Maximum TREAT power | 20,000 MW |
| Dynamic-power RANGE | 10,000 |

## II-C. Experimental Information Resulting from Hodoscope

Certain types of fuel motion have been observed in experiments monitored by the hodoscope. The effects may be categorized as below:

1. Pin bowing
2. Axial and radial expansion
3. Prefailure motion (within cladding)
4. Internal fuel motion (within annular fuel)
5. Fuel breach into coolant channels
6. Sweepout by coolant
7. Eructation
8. Slumping
9. Blockages
10. Breach of test container
11. Compaction

The direct characteristics of these effects that are measured are:

1. Timing
2. Location
3. Velocities
4. Normalized mass

In addition, certain information has been derived from this data, for example, the equivalent reactivity-worth of a large core (9) as a function of time.

Additional material-motion capabilities under development include clad-blockage (8) and sodium-voiding (10) detection.

The effect of fuel motion can be simulated under controlled stationary conditions by scanning the collimator (11, 12). This technique has been fundamental in development of the hodoscope and evaluation of its basic properties. In addition, scanning has proven to be of unique value in leading to radiographic reconstructions before or after a transient with the following properties:

1. Highly penetrating fast-neutron radiography, resulting in images that are:
    a. characteristic of fissile (in distinction to fertile or structural) material distribution
    b. insensitive to thermal-neutron filters and containment
    c. undisturbed by removal of test section from reactor
    d. indicative of pre- and posttest distributions
2. Complementary radiographic results depicting steel-blockage accumulations.
3. Digital-reconstructions subject to quantitative calibration and utilization.

Future applications of this technique include tomographic reconstruction, achieved by rotating the test assembly -- and higher resolution, achieved by deconvolution and by having a special collimator with smaller slots (13).

## III. METHODOLOGY FOR FUEL MOTION ANALYSIS

Achievement of quantitative results in fuel-motion analysis is dependent upon many factors. Success is affected by the experimental situation, choice and design of diagnostic hardware, as well as the methodology of processing, analysis, and reporting.

Keeping in mind that the usual objectives are to achieve quantitative values for masses, locations, velocities, and timing of material motions, a number of parameters can be identified as important to good results. Some factors contribute in a direct, positive sense--others indirectly, by their absence as an impediment. In general, the data should be as unambiguous as possible; in particular, the diagnostic system should discriminate fuel from other moving materials (structural and coolant), exclude background of the surroundings to the maxiumum extent possible, and be free of artifact generation. Also, the data should be available soon after an experiment and should be subject to as direct an analysis as possible.

The best results arise from situations where:

1. Fuel motion is highly correlated.
2. Good counting statistics are available (a high count rate without saturation).
3. There is a high signal-to-background ratio.
4. The background level is low and well understood.
5. The background is uniform rather than highly structured.
6. Detector efficiencies are constant in time (and power level).
7. Detector efficiencies are uniform over the array of pixels.
8. Intrinsic effects on emission (or transmission) rate are understood and properly applied.
9. Supplementary data -- from calibrations, alignment, and scanning -- are available.
10. The diagnostic system is insensitive to extraneous factors, such as thermal-neutron filters.
11. Flux gradients, self-shielding, and attenuation consequences are minimal.

The extent that these conditions can be met is a measure of the likelihood of a given diagnostic system achieving the objectives of a certain experiment. Because conditions for adequate fuel-motion diagnostics are frequently marginal, the weighing of these values in the selection and design of a diagnostic system, as well as in the experimental application, is a judgement factor that strongly influences ultimate success.

Subsequent sections of this paper will describe the different stages necessary to assimilate the data obtained. While some stages may appear to be trivial, the marginal nature of diagnostics in some situations necessitates careful attention to each stage to avoid loss of information. There are six separable stages: preparation of experiment and diagnostic equipment, collection of data, posttransient handling of data records, processing of data, analysis, and reporting. The following paragraphs briefly describe the salient aspects of the first three stages. A user-oriented document (Operating Manual for the Hodoscope) has been prepared to give explicit guidance in these three stages.

### III-A. Preparation

The hodoscope system is prepared for an experiment in accordance with written specifications. These specifications are derived from information supplied by the experimenter and from standard operating parameters of the hodoscope system. In order to reduce error in instrument settings, the specifications are combined

with a check list that requires independent verification. Appropriate documentation-control procedures are utilized.

Quality controls in documentaton, preparation, checkout, verification, and periodic evaluation are essential to minimizing malfunction and operator errors. Failure rate of the hodoscope system from all causes has been about two percent.

In addition to pretransient startup and checkout, the system is calibrated and aligned prior to each experiment. Also a pretransient scan for radiographic comparison and fuel-location validation is usually performed before most experiments. This has turned out to be an important attribute in checking for proper test-section assembly and orientation.

III-A. Collection

Once a remote-triggering signal is obtained, the collection of data is carried out automatically by the recording equipment. This signal is linked to the TREAT transient-initiation system. Interlocks are provided to prevent false starts.

Transient data are stored simultaneously on three media: disk, magnetic tape, and photographic film. The disk is the primary recording system; the magnetic tape stores digital data with a minimum time resolution of 32 ms, but for an interval much longer than the disk. The photographic system (1) acts as a backup; after chemical development, the film is placed in storage.

Data from pretransient and posttransient scans are also recorded on magnetic tape.

III-C. Handling

Since June 1977 (Experiment R-12), the magnetic-recording system has been operational. Several steps are involved in conveying the data to Argonne, IL (ANL/E).

First, the data on the fixed disk must be copied onto a transportable medium, namely magnetic tape. In order to minimize possible losses due to procedural or power-supply failures, this transfer is accomplished automatically at a preset time after a transient. The disk data is stored as a separate file ("Trancopy") in the latter half of the magnetic tape which runs during the transient. When it is possible to return to the reactor building after an experiment, a fresh tape is loaded and another copy of the disk contents is transferred to this tape ("Diskcopy").

Before the disk may be erased for any reason, the contents of the Trancopy tape are verified by preliminary processing and plotting of key data.

There are two ways of transmitting data to ANL/E. The most rapid is over an existing digital-data transmission link ("HASP"). A special tape is copied for this purpose and arrangements are made to transmit and receive at the ANL/E computer facilities. The magnetic-tape image produced at ANL/E may then be brought to RAS PDP-11 computer facilities for processing. It may take several hours to transmit the hodoscope data of the most significant portion of a transient.

The magnetic-tape reels may be shipped to ANL/E, as required, or stored at ANL/W. The tapes include data taken from the pre- and posttransient scans, the

transient, and the delayed-neutron phase of the transient. The tapes are usually sent in special containers by means of registered air mail pouch.

The photographic film is also mailed to ANL/E, where it undergoes chemical processing and printing. After editing, as mentioned, the film is stored, unless it utilized due to malfunction of the magnetic system. Facilities exist for the scanning and decoding of the digital photographic data (2).

## IV. DATA PROCESSING

In order to minimize memory capacity and achieve desired time resolution and recording duration, data are recorded during a transient in compressed formats. These formats are not immediately compatible with subsequent data-processing programs, nor are the formats appropriate for direct count-rate information. Consequently, during processing the data undergo conversion in several stages. Although this section describes data processing, while Section V is reserved for data analysis, there is no sharp line of distinction. In general, we use the term "processing" to signify a fairly straightforward treatment of the data without the human intervention and judgement that enters increasingly during "analysis."

### IV-A. Computer Programs

Stage I: The first stage of processing converts the digital data stored on film to digital data stored on 9-track magnetic tape. Stage I processing of film data takes place entirely on the ANL/AMD PDP-10 Alice scanning facility (2). Since film recording of data has been relegated to a backup role, this stage is rarely activated any more.

Stage II: Conversion of digital data to count-rate information was originally accomplished at the PDP-10, through a program called DIGLITES, which resulted in a 7-track tape compatible with input to the ANL/RAS PDP-11 computer facilities (2). Film data would enter through Stage I; magnetic data would go directly to Stage II. The new program DIGLITES-11 permits the magnetic data to be read directly by 9-track magnetic-tape facilities at ANL/RAS, and subsequent conversions to count-rate data take place under the control of that program.

Stage III: A third stage of programming takes place at the PDP-11 RAS interactive-computer facilities. Corrections for efficiency and supralinearity, and other normalizations, are applied, resulting in various displays or plots of data. Now, except for special-purpose programs, much of the Stage II and Stage III activities are combined into the single program DIGLITES-11.

In the subsequent discussion, it is assumed that the data have been processed through these programs in routine fashion, in accordance with the type of input. Only the salient steps are described below, with the program details omitted. Fig. 3 is a block diagram of the key program steps.

### IV-B. Total-Count Conversion

Although it is necessary that the output image have a one-to-one correspondence with the viewed object, that relationship need not be preserved within the data-recording system. The 1.2-m collimator has positions for up to 360 fast-neutron Hornyak-button detectors, but so far it has not been fully instrumented. There are also gamma detectors for steel-blockage detection. The recording system is capable of storing data from 704 channels of detectors; it may also be switched over to accepting data from the 0.5-m collimator in place of the 1.2-m unit. In that case, in addition to Hornyak-button and gamma detectors, the 336-channel collimator can be instrumented with a 31-channel fission-counter array (14).

Some experiments will not require the use of the same detectors as other experiments. In some cases only the Hornyak buttons are utilized; in others, as many gamma detectors as possible are desired. In addition, the number of operational detectors will vary from one experiment to the next due to failure of one component or another. Also, the allocation of detectors to the magnetic

and/or digital-photographic storage-systems may be made according to current needs.

As a result of these mismatches and changing conditions, detectors may be arbitrarily assigned to different storage locations. The key to unravelling this arrangement is contained in a table of channel organization. One table is maintained to relate detector type and location to sequential storage location. There also exist other tables that allow tracing for maintenance of detector assemblies, cables, electronic-processing boards, high-voltage supply, scalers, and storage channels.

In general, it is possible to have detectors allocated on output according to three arrays: Hornyak button, gamma, and fission. One of the first roles of the data processing is to reconstruct these arrays in accordance with the detector-organization tables. This then provides a potential matrix of total counts for each detector array for each count interval.

## IV-C. Time Base and Intervals

Accurate and precise time information is necessary in order to correlate data with the sample energy input and other instruments, and to provide a basis for converting from counts to counting rates. (Counting rates are needed for supralinearity and deadtime corrections, as well as to adjust for the effect of non-constant counting intervals.)

Several methods are used to record time data. The primary method is based on timing oscillators, one associated with the magnetic system and one with the camera system. When an experiment is initiated, the TREAT program-timer triggers, through the TREAT program-computer, a signal that activates both hodoscope recording systems simultaneously. When they are activated, the constant-frequency timing oscillators introduce counts into their respective systems. Each recording system has at least 24 bits of non-resettable scaler capacity set aside to record the timing counts. The time resolution for both systems is 0.01 ms. In the magnetic system the timing scaler has 40 bits, which can store a total time of $10^5$ sec (in BCD format). During each readout cycle, the contents of the timing scalers are transferred, along with the data from the other channels, to the recording medium.

To activate the camera-recording system, there is a mechanical relay that must close, introducing a known delay of 3.0 ms. There is also a correction for oscillator frequency of 0.4 ms/s to force agreement with the TREAT timing oscillator. In the magnetic-data system there is no appreciable startup delay, and the clock frequency has been found to be in satisfactory agreement with the TREAT clock (DAS Modcomp oscillator) frequency. However, a time shift has been observed -- see below.

In parallel with these oscillators, time is recorded in the magnetic system from an IRIG standard real-time clock. The IRIG time for each cycle is stored in a 13-decimal-digit field, the information being day of the year (0 - 366: 3 digits), hour (0 - 23: 2 digits), minute (0 - 59: 2 digits), second (0 - 59: 2 digits) and tenths of milliseconds (0 - 9999: 4 digits). The IRIG time is also fed to the TREAT analog-data readout system.

The IRIG data are not used for routine hodoscope data processing, except as a check and backup on the hodoscope-clock oscillator. There has been good agreement between the hodoscope and IRIG clock frequencies.

In order to determine counting intervals, it is necessary to correct for the time that the system is dead while data are being transferred from the scalers

to the recording medium. This is a fixed time for each cycle: 67 μs for the film system, but only 1 μs for the magnetic sytem. The true count interval is simply the difference between adjacent time readings, less the fixed recording-system correction.

To set the time base for data reporting, the hodoscope zero time must be brought into agreement with the zero time of the TREAT program (DAS) timer by application of an empirical time shift that is determined by matching the TREAT and hodoscope power profiles for the test. Typically, a time shift of the order of 5 ms has been needed to match the hodoscope data with the TREAT "Safety 1" instrument-power readout from DAS (TREAT digital data-acquisition system). While the IRIG time is not used by the DAS, it is the basis for the TREAT analog tapes, which are later digitized and used for analyzing the test.

The next problem is to define a mean time for the purpose of characterizing the data of a given interval. This mean is computed by summing the end-times for all the counting cycles in the interval and dividing by the number of cycles.

Time-base marks are emitted at preset times by each of the recording systems. They may be used for a variety of purposes, including that of establishing an independent accurate time difference. In one experiment, these time marks were transferred to the loop-instrumentation analog-recording system to gain further accuracy in intersystem timing. In the magnetic system, there are three such marks available, labeled A, B, and C, settable by thumbwheel switches. As each of those preset times is reached, a signal is produced on each of four lines: two 100-μs, 5-V pulses, one positive and one negative, and two 5-V level changes, again one positive and one negative. As of 1980, these signals are not exploited.

In the camera system there are two time marks, labeled A and B. At each of these two times, most of the neon lamps of the camera-system readout array are turned on for 10 ms, to serve as a timing marker on the film. The resulting film frames also provide an indication of any malfunctioning lamps, and are useful in setting parameters for the optical film scanner. The settings for the film points A and B are called out in the Hodoscope Test Specifications -- point A to come at a time that allows the camera to have accelerated the film to full speed, and point B to occur while the film is still running, but near the end. TREAT Operations sets up each test so that the transient will take place entirely between the two marks.

## IV-D. Count Rates

In order to determine count rates, corrections must be introduced for deadtime effects. Counting circuits are classified as "paralyzable" or "non-paralyzable" depending on whether the dead time following a pulse that is counted is extended by a subsequent, unresolved pulse. (If the dead interval is extended, the counter can be paralyzed by a sufficiently high counting rate.) If $R_z$ is the observed counting rate and $\theta$ the pulse-pair resolving time (deadtime) of the system, then the corrected counting rates R are given by:

$$\text{Non-paralyzable:} \quad R = R_z / (1 - R_z\theta); \tag{1}$$

$$\text{Paralyzable:} \quad R = R_z * \exp(R\theta). \tag{2}$$

In practice, both of these models are approximations (equivalent at low counting rates). It has been found that the non-paralyzable model is adequate most of the time, but that in some cases where very high counting rates are reached (as in the EOS experiment series), some of the channels are definitely

in the paralyzable category. The data-processing code DIGLITES permits the desired type of deadtime treatment to be specified for each channel -- requiring, of course, the analyst to inspect the data from each channel in order to make the decision. The nominal default value for $\theta$ is 0.5 μs.

Each scaler stores up to 4095 counts. It is possible for overflow to take place, in which case the scaler clears to zero and starts to accumulate again. Generally, care is taken to select counting intervals such that at peak power scaler overflow is unlikely to occur. For example, at 4 ms the rate would be kept below $10^6$ c/s. However, supralinear effects have occasionally caused the scaler limit to be exceeded. If only one or two overflows take place, that event is usually unambiguously marked by a step-function drop of about 4000 counts per cycle as the power rises, with a corresponding sudden rise while the power is falling. Overflow corrections are automatically invoked within the data-processing program, without difficulty.

### IV-E. Data Inspection

It is standard practice to make a preliminary inspection of the data before proceeding with detailed processing. The inspection may involve examining printed tables of count rates, plotting of selected channel count-rate histories, or reconstruction of full-image arrays (hodographs). Within a time range of particular interest, the data may be examined for general patterns, malfunctioning channels, and spurious interference. Some preliminary filtering of outlying data may take place at this time, particularly for malfunctioning channels or intervals of time where there appears to be electronic interference. To avoid scale distortion, a clearly malfunctioning data channel (e.g., all zeros) will be replaced with an average of four neighbors. Occasionally entire counting cycles of data are deleted because of a burst of noise; such deletion is rarely necessary except during the low-power phases of some experiments.

### IV-F. Count-rate Composition

The count rate achieved in each channel may be partitioned into two basic components: (1) signal, resulting from fuel within the effective channel field of view, and (2) background, resulting from all other sources. Further decomposition of the rate will be described in the following simplified expressions. It should be kept in mind that each term actually represents an average over space (at the test fuel and at the detector) and time (the duration of measurement). This practice may be justified because in the TREAT hodoscope system, the collimator-acceptance angle is quite small (several microsteradians) and detectors are biased for fast neutrons (over 1 MeV). For the detected neutrons, relevant cross sections and detector-response functions vary weakly in energy, and scattering is nearly isotropic. Also, relatively small test bundles of 1 to 7 pins are currently used.

The total deadtime-corrected count rate R is composed of a signal component S (primarily uncollided neutrons from the test fuel), background component B (uncollided and scattered neutrons from behind the test capsule and neutrons scattered from the test capsule), and ambient background A (other background sources, such as detection-system noise and Cosmic-ray background). Thus we may write for a single channel or pixel i:

$$R_i = S_i + B_i + A_i \quad , \tag{3}$$

where

$$S_i = \nu \, \alpha_i \, k_i \, \epsilon_i \, M_i \, \omega_i \, P \quad , \tag{4}$$

with $\nu$ = average number of neutrons/fission

$\alpha$ = attenuation factor characteristic of the test fuel and capsule structure, in neutrons-transmitted per incident neutron

$k$ = calibration factor (power coupling to reactor) for test fuel, in fissions/s-g-MW(TREAT)

$\omega$ = collimator-slot solid angle, in steradians

$\epsilon$ = detector efficiency for signal, in counts/neutron-transmitted

$P$ = power level, in MW(TREAT)

$M$ = fuel mass viewed by the given detector channel, in g

and

$$B_i = h_i \, \epsilon_{bi} \, \omega_i \, P \quad , \tag{5}$$

with $h$ = coupling factor for background (including attenuation and scattering effects), in neutrons/s-MW(TREAT)

$\epsilon_b$ = detector efficiency for background, in counts/neutron.

The neutron yield $\nu$ is a constant common to all channels. Because of possible slight variations in slot dimensions, the solid angle $\omega$ is a constant that depends upon the channel. The power level P depends explicitly on time according to the reactor transient. The efficiencies $\epsilon$ and $\epsilon_b$ may depend upon the power level to the extent that the detectors are not linear in response; otherwise they would be constants characteristic of each detector channel. The fuel mass M varies with time, though not in any prescribed manner; we are ultimately interested in tracking M by means of the signal rate S. The power-coupling factor k may have some dependence upon the mass of fuel and its geometry. The background-coupling factor h is generally found to be invariant during TREAT transients.

The ambient background A is basically independent of power level. For the hodoscope, the ambient background is negligible except for power levels below 100 kW. If shielding is not adequate, it is possible to have a component of background B that is proportional to the power level and reaches the detector by indirect pathways.

Note in particular that the signal (Eq. 4) is directly proportional to the fuel mass M viewed by a particular channel, except insofar as there might be second-order effects contained in $\alpha$ and k. For example, the penetrating nature of fission neutrons is sufficient to allow neglect of the attenuation-factor dependence on source mass for 1-pin tests but not necessarily in 7-pin tests. On the other hand, self-shielding factors can be important even for single-pin tests.

For any given detector in which data are collected during an interval at t:

$$S(t)/S(r) = [\alpha(t)/\alpha(r)] \, [k(t)/k(r)] \, [P(t)/P(r)] \, [M(t)/M(r)] \quad , \tag{6}$$

where the parameter r refers to an initial, reference interval chosen because it is unlikely that fuel has moved up to that point in time. In practice, a large number of data intervals are averaged together to form the reference interval. In the hodoscope system, the power-level ratio may be directly measured by a

variety of means. If the coupling factor were not dependent (as a result of shielding perturbations from both the fuel and the shaping collars) upon mass changes, then the power-normalized count-rate differences would be directly proportional to the mass changes. Sometimes this is not a good approximation; so it is necessary to devise both an analytical and experimental foundation for the coupling-factor k ratio. For Eq. 6 it has been assumed that efficiency factors have been corrected for any possible dependence upon power level.

In current hodoscope-analysis practice, the power-normalized count rate forms the primary basis for data analysis. We have for any given channel from Eq. 3:

$$R(t)/P(t) = S(t)/P(t) + B(t)/P(t) + A(t)/P(t) \quad , \tag{7}$$

and for any single channel, with B/P constant and A/P constant or negligible,

$$R(t)/P(t) - R(r)/P(r) = S(t)/P(t) - S(r)/P(r)$$

$$= [\nu \alpha \epsilon \omega k(r)] \{[k(t)/k(r)] M(t) - M(r)\} \quad , \tag{8}$$

which is proportional to the mass difference, subject to correction for self-shielding type effects. Equation 9 below indicates the form of the channel equation fitted by least-squares methods in the program EFFI to determine the overall efficiency factor that is within the first bracket of Eq. 8.

$$R(r)/P(r) = [\nu \alpha \epsilon \omega k(r)] M(r) + B(r)/P(r) \quad . \tag{9}$$

The reference interval for determination of the overall efficiency factor may be a low- or constant-power phase of a transient or it may be a pretransient scan phase or both. In any case, the initial fuel-mass and background distributions are the primary non-statistical parameters introduced. The statistical parameters are the channel counts, the adjacent background counts, and the power level for normalization. Once the coefficient in the brackets has been determined by fitting the experimental data to a model that makes use of Eq. 9, the coefficient may be applied to determination of mass differences through Eq. 8, subject to correction for self-shielding variations.

Another relationship of some use is derived from the assumption that detection efficiencies for signal and background, while not necessarily the same due to spectral differences, are at least related to each other by a constant that is characteristic of each channel:

$$\epsilon_i(P) = \gamma_i \epsilon_{bi}(P) \quad . \tag{10}$$

In that case, we may write:

$$S_i/B_i = \nu \gamma_i \alpha_i (k_i/h_i) M_i \quad , \tag{11}$$

which defines the signal-to-background ratio for the channel. Typically the mass (and structure) dependence of $\alpha$ and the k/h ratio decreases the S/B ratio faster than M increases it.

The detector efficiencies vary with power because of some intrinsic nonlinear response at high powers. Under the assumption of Eq. 10, the program SUPRA (see Appendix A) provides correction factors for each channel to diminish this power dependence.

## IV-G. Power-Level Normalization

Count-rate normalization to remove power-level dependence is an important process, as it avoids the necessity for absolute reactor-power measurements. To provide the proper normalization for use in Eqs. 7-9, one must allow for effects that lead to a nonlinear dependence of counting rate on reactor power. These effects may be conveniently partitioned into intrinsic and instrumental.

### IV-G.1. Intrinsic Factors

Power normalization validity depends upon the position of the power monitors, upon the influence of perturbations, and upon the manner of normalization. Perturbations may be traced to flux and spectral changes due to temperature gradients and control-rod motion.

If feedback from the test assembly to the reactor is small, as is the case with experiments now conducted at TREAT, and if there are no time-dependent flux tilts, then the time profile for power normalization may be measured almost anywhere in the reactor or shield. One of the primary methods of monitoring power with the hodoscope is to use detectors aimed at portions of the viewing area where fuel motion does not occur. The flux through such a slot is composed of fast neutrons scattered from the test section. Possible locations for other flux-monitoring instruments would be within the core, in the reflector, at a beam hole perpendicular or tangential to the core or reflector, or in or outside the biological shield.

In the past, the primary monitors of transient reactor power have been the uncompensated ionization chambers designated S-1 and S-2; these are located in corners of the core. Their power traces are primarily reported along with data from experiment-loop instrumentation. Because these monitors are safety-related instruments, it has not been possible to make a direct recording of a signal taken from them during transients. Accordingly, a dedicated hodoscope monitor has been assembled. Finding a suitable location for it has been difficult, because it is desirable to have a single monitor to use both for transients and steady-state operation, so that data adjustment may be more direct. It is now located at the north side of the reactor, just above the hodoscope collimator.

There are a number of perturbations of power-monitor reading that require attention. Power monitors located near control rods are subject to changes in both rod position and neutron spectrum during transients. Furthermore, in interpreting differences from one experiment to another, differences in control-rod configuration can affect monitor calibration, as can changes in core loading. Finally, care must be taken to ensure that massive test-fuel movement is not likely to affect the monitor signal.

As a result of the preceding considerations, the primary monitor normally used is a hodoscope detector subarray that does not view the fuel-motion zone and thus is relatively insensitive to fuel movement. However, because this array focusses on scattered neutrons, it might be sensitive to spectral shifts. An alternative monitoring scheme is to average all the detectors in the array, which works as long as the net effective amount of fuel in the viewing region remains constant. By comparison with the TREAT power profile, the array average may sometimes be used as an indicator of fuel displacement out of the region. For experiments that do not result in fuel losses out of the viewing region, the array average is an indicator of self-unshielding trends. The signal from TREAT monitor S-1 (not part of the hodoscope data) is always used for comparative normalization at some point.

IV-G.2. Instrumental Factors

Aside from the inherent factors that must be considered in power normalization, there are certain instrumental effects that may arise:

1. Noise at low powers
2. Saturation at very high powers
3. Nonlinearity
4. Sensitivity to gamma rays
5. Statistical fluctuations
6. Drifts and instabilities

Each type of monitor is subject to these effects in different ways. To avoid vulnerability to a single systematic effect, several monitor profiles are obtained and compared. For example, the S-1 signal is sensitive to gamma rays and has a relatively high noise level at low powers. However, it is less subject to saturation at very high powers and is more linear than the Hornyak buttons. If agreement can be achieved between different types of power monitors, the most convenient monitor may be considered validated for normalization purposes.

## IV-H. Correction for Supralinearity and Deadtime

The response of a detector as a function of reactor power level can be distorted by deadtime, saturation, and other nonlinear effects. Deadtime is an effect imposed by the finite response time of the electronic circuitry. It is usually defined to be the pulse-pair resolving time. As mentioned in Section IV-D, a counting channel can be "paralyzable" or "non-paralyzable" (or somewhere in between).

Saturation effects occur when the count rate reaches such a high level that the deadtime models begin to fail and the output rate can no longer be corrected for counting-rate losses. There is little that can be done within a fixed electronic design, other than to attempt to keep the rate well below saturation. This can be accomplished by adjusting the efficiency of the detectors, thus sacrificing statistical significance at low powers. This is done by interposing a count-rate attenuating medium such as a lead filter. Besides attenuating the neutrons, the lead preferentially attenuates gamma rays, which, although not directly counted, may contribute to nonlinearity.

The supralinearity experienced with the Hornyak-button detectors shows up as a count rate that increases more rapidly than the reactor power rises. This supralinear effect may be due to any of several candidate causes. The model presently used is discussed in Appendix A. The corrected count rate may be found from a least-squares fit of an expression that depends either on the power level or on the measured rate, subject to determination of two (sometimes three) constants.

The constants must be determined channel-by-channel. Their values are derived from the transient data by fitting a curve to the rising portion of the power profile before fuel motion occurs.

As shown in Appendix A, agreement may be obtained in a typical channel between the calculated and measured supralinearity correction. Without the correction for supralinearity, the count rate in that channel would be high by a factor of ~1.5 at the top of the power range indicated.

## IV-I. Efficiency Normalization

Although individual channel efficiencies are normalized prior to a transient by calibrating against a standard neutron source, the efficiencies for use in a transient are not assumed to be accurately known. There are several reasons: The Hornyak-button detector systems are not electronically stabilized, the neutron source is subject to positioning error, the calibration has statistical variance, the slots are not necessarily lined up with detectors in a manner consistent with the method of source calibration, the detectors are subject to occasional spurious fluctuations, and the energy differences between the neutron source and the fission spectrum could have an influence. In addition, the "efficiency" normalization includes necessary compensation for the axial (and radial) flux profile.

There are two important facets to the efficiency normalization: absolute and relative calibration. A non-quantitative reconstruction of general fuel motion may be presented by knowledge of relative efficiencies. Our practice, however, is to calibrate each experiment based on the known quantity of initial fuel loaded in the test section. Thus, effects that vary from one experiment to another, such as self-shielding and fuel enrichment, are less likely to influence the quantitative outcome.

Equation 9 represents the form through which efficiency factors are determined for each channel; the overall efficiency factor (the term in brackets) subsumes all the relevant effects of channel-dependent attenuation, effective solid angle, detector and electronic efficiency, and initial self-shielding factor. To minimize the possibility for drift, the efficiency is best determined just prior to the period of use, namely during an early phase of a transient. This process is statistically as good or better than prior determination during a low-power steady-state run. Care must be taken to ensure that data are accumulated with minimal systematic perturbation from nonlinear effects.

Appendix B contains a detailed description of the data-fitting process, which matches the array response to a geometrical and neutronic model of the test section. No corrections for self-shielding are made at this point, so that in effect the efficiency factor has buried within it a self-shielding term. If the geometry changes suffiently to affect self-shielding, a correction would have to be made to explicitly correct for that effect. As mentioned previously, self-shielding could have as much as a 10- or 20-percent effect, though it is usually less.

In addition to the radial variation in the coupling factor (which causes the self-shielding effects), there is an axial variation due to the chopped-cosine distribution of the reactor flux, fuel end-effects, and axial-shaping collars. These must be taken into account in the neutronic model of the test section. The best information for this purpose is derived from the experimenter's data on axial fission rates obtained from fuel-core samples or flux monitors.

During steady-state pretransient or posttransient scanning a different situation presents itself. Each detector may be scanned horizontally to focus on a sample that was originally covered by an adjacent detector. In this manner it is possible to build up a cross-normalization matrix. By comparing pretransient with posttransient results, an absolute fuel-mass calibration may be derived and rather small differences may be detected. On occasions when the detector efficiencies have been set to abnormally high values in order to reduce the power level and duration of the scanning, a time-dependent drift-compensation may be required.

## IV-J. Mass Calibration

It is important to determine mass displacement on a quantitative basis. This could be done in two ways. One, which we make use of, is to calibrate on the basis of the known initial mass of fuel in the viewing area. The other is to make use of the calibration factor by which the reactor-power input is coupled to the sample fission rate; however, this method would require the intervention of additional possible systematic and statistical effects that depend upon the measurement quality of the calibration factor. Making use of initial fuel conditions avoids this unnecessary step. However, it should be noted that the reactor-coupling factor is a useful parameter in predicting diagnostic performance for a given experiment.

As indicated in Eq. 9, after removal of background, the power-normalized count rate is proportional to the fuel mass. The constant of proportionality contains, besides the detector efficiency and the channel solid angle, several intrinsic factors -- neutron yield, capsule attenuation, and self-shielding. Having a known mass of fuel during the reference interval and a measured normalized count rate provides the unknown properties lumped together in a single constant. That constant is, of course, strictly applicable only as long as the geometry of the fuel is unchanged. The mass-proportionality constant is determined using the EFFI program, as described in Appendix B.

When the fuel geometry undergoes a transition, changes in self-attenuation, self-shielding, and flux depression must be considered. In addition, there are possible higher-order effects of flux perturbation, test-section induced multiplication, etc. that are ignored at present. Effects due to geometric changes appear as a fuel-measurement error of up to 20% when not taken into account.

### IV-J.1. Collar Corrections

The nonuniform flux distribution in TREAT causes the fission rate in test fuel to vary axially. A partial compensation for this variation is effected in hodoscope data processing by EFFI. In making its fit, EFFI assumes a constant signal-to-background ratio over the length of the fuel. The use of thermal-neutron absorbers to shape the flux profile can affect the quantitative interpretation of hodoscope data. This is so because the efficiency multipliers of counters viewing regions under the flux-shaping collars are increased to compensate for the reduced test fuel signal (which is basically proportional to fission rate in the pins), while the background (which is determined by fast flux in the test capsule) may not be proportionally reduced by the collars as much as the signal. Thus the count rate from regions under the flux-shaping collars may consist disproportionately of background.

A semi-empirical correction for the effect of flux-shaping collars has been derived. It is given in Appendix C along with some comparisons with experimental data. The correction is currently in a development phase.

The advisability of making collar corrections without also correcting for fuel self-shielding variations is in doubt. Self-shielding in the test region has an opposite effect from that of the flux-shaping collars. On the one hand, a small amount of fuel moved away from the original fuel zone will be seen by the hodoscope to have a larger mass as a result of reduced self-shielding. On the other hand, fuel that moves to an axial position under a collar will appear to lose mass because of the collar effect of flux depression.

### IV-J.2 Self-Shielding

Corrections for self-shielding are difficult to perform. If there is adequate filtering of the entire zone where fuel is originally located or where it is displaced to, then the correction may be only a few percent. In experiments lacking extensive filtering in certain zones, the correction could amount to 20%.

Gailar and Klickman (15) have made an estimate of the correction magnitude by performing three-dimensional computations with a Monte Carlo program. The seven-pin E8 experiment was studied. Major simplifications were made in order to expedite computation. The results -- for this specific case and for the assumptions made -- showed a radial dependence of as much as 11% self-shielding due to changes in fuel density and distribution, and a axial effect of up to 35% due to redistribution for extreme cases of fuel motion not usually realized experimentally. Some of the effects were also thought to be attributable to self-induced fission in the fuel.

Albrecht (16) has recommended that the problem be tackled systematically by a global approach. This approach may be characterized as having the following major elements: (1) identification of regions in space and time that have restructured and unrestructured fuel; (2) correction with calibration factors that depend upon a first-order estimate of fuel quantity based on observed fission rate; (3) re-analysis in order to recalculate fuel distributions; and (4) testing iteratively to see if a converging and adequate fuel distribution is obtained. Lacking a global program, it is likely that an incremental approach will be utilized for ad-hoc corrections on an interim basis.

### IV-J.3 Other Effects

Gailar and Klickman (15) indicate that interactions between the test fuel and the TREAT driver are likely to be negligible. On the other hand, flux tilting due to control-rod motion may induce time-dependent changes resulting from flux magnitude and spectrum changes. Temperature effects causing spectral shifts could be a factor too. These and other potential effects are currently ignored because of the lack of theoretical or experimental indication that they require attention in comparison with known limitations.

## V. DATA ANALYSIS

The data treatment that we classify as analysis (which could be called evaluation) involves a higher degree of judgement than the previously described processing. At this stage, data is available from several hodoscope and non-hodoscope sources, and -- in some cases -- choices must be made between conflicting information.

There are three relevant experiment phases: pretransient, transient, and posttransient. During the pretransient phase, several operations take place that generate useful data. Aside from calibration experiments, which could have preceded the transient by several months, certain heat-balance and trial transients may be run in conjunction with the experiment series. Hodoscope data may also be taken during some of these runs, partly as backup in case of unexpected fuel movement and partly to establish hodoscope response for special test conditions or detector settings. Except for rare situations, the hodoscope does not require any transient calibration experiments.

Prior to an experiment, a pretransient scan is arranged, primarily for the purpose of aligning the hodoscope with respect to the test section. However, the information derived is of use in setting preliminary values of efficiency factors and in providing the necessary geometric correlation for initial position of the fuel in the hodoscope object grid.

During a transient, the data taken may be categorized by three phases: flattop, spike, and delayed neutron. Some experiments have a simple natural-transient shape without any flattop; some have a flattop (steady-state) profile only; and others have a flattop followed by a spike. The early phase of a spike, prior to fuel movement, is generally used to generate supralinearity correction factors. The delayed neutron phase occurs after scram and is due to core multiplication of delayed neutrons circulating primarily within the core. There is usually enough fission intensity in the fuel sample to permit hodoscope viewing during the delayed neutron phase with adequate statistics if time integration takes place over increasing intervals. Up to ten seconds of data may be taken after scram, with time resolutions starting from 0.1 s and approaching 1 s. The backup (TRANDATA) tape accumulates data for six minutes or more after a transient.

One reason for collecting data during the delayed-neutron phase is to determine if there continues to be fuel movement even though the reactor-driven fission rate in the test has been shutoff. Delayed fuel movement has occurred in a few experiments. It is also important to have this knowledge for the purposes of comparing and interpreting the post-transient radiography. Moreover, in some experiments it has not been possible to obtain posttransient in-situ or ex-situ radiography; so the delayed-neutron data is all that is available.

During the posttransient phase, a hodoscope scan is frequently performed. This is accomplished in the same manner as the pretransient scan, namely horizontal translation of the hodoscope collimator with the reactor at a relatively low steady-state power, typically 80 kW. The scanning operation provides the relative motion necessary to improve the effective static resolution of the hodoscope and thus provides data for a digital radiograph.

### V-A. Background Determination

Determination of the correct background component is always important in these experiments because, in the first case, the initial signal is rarely more than a few times the background level and, in the second case, the mass

displacements of interest induce count rates that are often much less than background level.

The determination of correct background is complicated by a mismatch between information needs and available methods of measurement. Background varies both vertically and horizontally; also, it is unlikely to have as hard a spectrum as the fission-source component. It is not always possible to directly measure a background profile with the sample removed and no other perturbations.

For the purposes of calculating a mass-calibration factor and determining efficiencies, our practice is to deduce the background by a least-squares fit to a known fuel distribution. Detectors in the non-fuel region of the viewing area act to provide a bridge between computation and experiment. The program EFFI (See Appendix B) estimates the background on the basis of a model of the known initial fuel distribution fitted to the experimental data.

In determining fuel motion, normalized count rates of subsequent intervals are subtracted from those of a reference interval. It is assumed that the power-normalized background remains constant and is thus eliminated by substraction. This is found experimentally to be the case to first order.

There are two sources of experimental data on background -- scan and/or transient data. In the scanning mode, the hodoscope may be operated in such a manner that efficiency differences from one channel to another may be cancelled out. The data taken during early phases of a transient, prior to likely fuel motion, may also be used for normalization; this data has the advantage of being least susceptible to detector instabilities.

At the moment there remains an unresolved disparity between the two methods of efficiency normalization. The disparity may be connected either with detector responses or with spectral shifts or some combination of the two. For data analysis, we rely upon the background derived from transient data.

V-B. Averaging

In general, hodoscope data is collected in intervals shorter than needed for time resolution of most events. Consequently, it is possible to average together adjacent intervals in order to smooth out fluctuations in data. It is sometimes convenient to do this in initial analysis and then to subsequently back off from this averaging for time domains of particular interest to the experimenter. In addition, it is not necessary to average an entire transient by a constant interval.

By the same token, spatial averaging may be implemented, both as a tentative and as a final result. All members of a row of detectors may be averaged together, thereby suppressing lateral fuel movements in favor of the axial component of fuel motion. Alternately, adjacent columns may be averaged together.

For purposes of presentation of data in graphical form it is frequently useful to average adjacent channels. Otherwise, the graphical presentation will be speckled due to fluctuations. In cases where there is outlying data, it is also valuable to replace the outlyer with an average of adjacent channels.

Care must be taken to avoid masking of events that take place in short intervals or within limited spatial domains. An iterative process is often utilized to isolate particular events.

V-C. Graphic Presentations

In order to visualize progress made in analysis, it is necessary to undertake a variety of graphical displays of the data. The displays depend upon the nature of the data, the purpose in visualization, and the complexity of the data.

Much of the standard plotting capability is built into a computer program FPLOT. It is sufficiently flexible to make use of a variety of inputs and to adapt output to either cathode ray screen or electrostatic plotter. Because of the importance of data presentaton, considerable development, both hardware and software, has been devoted to generation of suitable printing and plotting capability. These developments have also been necessary to foreshorten the process of reporting data by avoiding unncessary intermediate steps.

One of the first pieces of information to be plotted is the time history of the power profile, which is rendered is standard form, either linear or logarithmic. Comparisons may be made between various sources of power level data (See Fig. 4).

A fundamental approach to representation of data is a simple time history of any given channel or combination of channels. This feature permits the most straightforward comparison of data results on a common time scale (See Fig. 5). Various time interval and spatial averages may be applied.

A "picture" of the fuel motion may be reconstructed in an analog fashion by means of an intensity-modulated "hodograph." This gives, by means of a dot matrix, a linear representation of the fuel location in the array at any time (See Fig. 6).

A more quantitative mode of pictorial presentation is the use of a "symbolic" hodograph, in which structured symbols are utilized to represent linear intensities. Each symbol may be equated with a fixed amount of fuel (See Fig. 7).

In order to enhance the visual effect of small changes in fuel motion, differential symbolic hodographs may be generated. In this case, differences may be created between adjacent time intervals or between one interval and some reference time used for normalization (See Fig. 8).

The data contained in either type of hodograph -- intensity-modulated or symbolic -- may be averaged across rows or columns to indicate the axial or transverse fuel profile at any time. Axial profiles may also be drawn up graphically, with count rate or fuel mass as a function of axial elevation. This process may be extended to the point that the axial component of fuel may be represented in multi-parameter form, as shown in Fig. 9.

The above array of presentation modes has evolved from the necessity of depicting events taking place amidst a large amount of data. To a certain extent, the personal taste of an analyst may influence the choice of presentation. The intended audience is another factor. The intensity-modulated profiles are useful for qualitative presentations and for the production of movies. The symbolic hodographs and the time plots are important quantitative analysis tools. The multi-parameter representations are useful renditions for the purpose of transmitting key information to the experimenter and the accident-analysis code modeler. Derived information about reactivity worth of fuel motion as a function of time is beginning to play an important role (9).

V-D. Interpretation of Time, Location, and Quantity

With the data adjusted to take into account known influences that would cause a departure from a linear relationship between measured rate and fuel mass, the task of determining key events may be undertaken. Making use of the array of graphical displays of the corrected data, statistically significant changes in normalized counting rate are noted. These changes may take the form of shifts in normalized rate, of deviations from zero in Eq. 8, or in patterns that appear in the various types of hodographs.

The general time and location of an event are determined by the channel in which the event takes place and the time frame to which its initiation can be assigned. By comparison with adjacent channels, interpolation methods -- utilizing a model of point-response function -- can readily localize an event to an elevation or transverse location between channels. Likewise, events may be traced to the smallest data-recording interval or interpolated between intervals. The limits of application of these interpolation processes are naturally bounded by the available statistical precision. Moreover, because of the possibility of fluctuations due to artificial noise sources, it is necessary to have internal consistency between adjacent channels. Fig. 5, for instance, shows how adjacent channels reflect the propagation of a common effect. There is an ultimate uncertainty limit for which the statistical imprecision and the lack of coherence will not allow simultaneous, precise determination of time, location, and quantity of fuel.

V-E. Velocities

In principle, having obtained a sequence of time and location of fuel displacement, adequate information is on hand for determining the velocity of the displacement. However, there is neither adequate information nor suitable means of representation of the three-dimensional mass flow that takes place. It is necessary to simplify the flow and categorize the movement into discrete events. One simplification is breaking the data into either axial or radial movement, one to the exclusion of the other. This is accomplished by averaging over either rows or columns.

Another essential simplification is to quantize movement into center-of-mass or frontal velocities. Either of these two representations may be chosen on the basis of the nature of the data.

As a result, the velocities that are reported are abstracted to represent the most noticeable events, usually those of net axial displacement. Such discrete velocities may mask fuel movement that takes place in multiple phases or that could be of a more continuous nature. Fortunately, users of our data have found the level of information available to be more than adequate for the range of application.

V-F. Verification Against Posttransient Scans

As a matter of routine, all transient data is compared against the post-transient scan, if one is carried out. Although scans are recommended for every experiment in which significant fuel motion is expected, the experimenters do not always permit them because of limits upon reactor heating of the test section that might cause further fuel relocation. Usually the post-transient data verifies the final location of the transient image that is reconstructed from data taken a few seconds after scram. On a few occasions there have been disparities between the thermal-neutron radiograph and the hodoscope transient data; in one case, the disparity could be traced to a fragile post-transient

fuel arrangement that was likely to have collapsed during handling. Consequently, the post-transient scan serves the role of providing an in-situ radiograph (with coarse resolution) that may differentiate between two possible causes of relocation: (1) thermal contraction or sodium reentry immediately after the transient and (2) mechanical disturbance due to subsequent handling prior to thermal-neutron radiography.

Because the in-situ fast-neutron radiograph obtained by the hodoscope reflects the fission distribution, its reconstruction represents an image of fissile material. On the other hand, the higher-resolution thermal-neutron radiograph later obtained is sensitive to absorption of low energy neutrons, which may be caused by either fertile fuel or steel. As a result, the two types of radiography complement each other -- one giving an image of all materials, the other providing an image of the fissile component.

The capability also exists for the hodoscope to provide a distinctive image of the steel distribution after a transient. Although this option has not been fully developed yet, it offers the possibility of being able to distinguish between steel and fuel blockages.

### V-G. Correlation with Test-train Instruments

During a transient a number of instruments may be associated directly with the test train. Typically there are flow meters, thermocouples, pressure transducers, and occasionally there may be some special instrumentaion, such as acoustic monitors. In general, it is the responsibility of the experimenter to reconcile diverse sources of information. After an analysis has been made of the hodoscope data based entirely on fuel motion information, it is appropriate that some preliminary comparison be made by the analyst against test-train instrumentation data to ensure that no key events will have been overlooked in the hodoscope analysis. Sometimes the experimenter asks for additional detailed information about fuel motion during a given time zone.

In a few experiments the quality of fuel motion data is not self-explanatory without an external crutch, such as guidance from test-train transient information; in that case, the dependence will be noted in the report.

### V-H. Examination of Post-scram Data

After scram, count rates decrease greatly, substantially reducing the statistical significance of the hodoscope data. However fuel motion can be observed if large enough, by judicious averaging of channels and time intervals. Post-scram fuel motion has been observed in a number of transients. Beyond the point at which no further fuel motion is observed, it' is customary to average all remaining time intervals to obtain an estimate of final fuel disposition.

Approximately an hour after the transient, a horizontal scan of the hodoscope collimator is conducted at low (~80 KW) reactor power, provided the resultant thermal energy input to the test capsule is permissible (as is normally the case). This scan serves several useful functions. An independent picture of final fuel disposition is generated for comparison with the final transient picture mentioned above and with radiographs. For diagnostic purposes, an independent normalization of the hodoscope channels may be performed which can be compared to those generated from transient data (EFFI) and pretest scan data, for determining drifts and malfunctions of channels. Also, the scan data may be deconvoluted from the hodoscope spatial response, to obtain increased horizontal spatial resolution of final fuel disposition.

A file of efficiency multipliers for each hodoscope channel can be generated by the SPLOT program for scan data (either pre- or posttest). The count rate for each channel is adjusted to be equal for the background regions scanned to the left or right of the test fuel. Unlike the EFFI efficiency normalization, no model of the test fuel and background is involved, and normalization is independent of test fuel configuration (at least to first order). Differences among the three normalizations (EFFI using transient data, SPLOT using pretest scan data, and SPLOT using posttest scan data) have been noted and may be due to channel drifts or malfunctions and other causes. SPLOT also provides plotting capabilities similar to FPLOT for analysis of scan fuel profiles. A composite of graphs for a typical posttest scan derived from SPLOT is shown in Fig. 10. A dotted line outlines the initial position of a bundle of three fuel pins.

The observed pretest scan signal-to-background ratios (S/B) vary slightly among hodoscope channels, leading to irregularities in test-fuel profiles when using SPLOT efficiency multipliers. A normalization of the scan data which enforces both constant background and constant S/B can be performed using EFAX, a modified version of EFFI. An efficiency multiplier and an additive number are computed for each channel. EFAX can determine S/B only from the pretest scan (for which test fuel geometry is known) and only for channels viewing fuel in that scan (an arbitrary S/B may be assumed for other channels). Pre- and posttest scans for a particular test of a 7-pin bundle obtained using EFAX are shown in Fig. 11. Fuel mass is roughly proportional to dot density in the figure and the rectilinear grid serves to indicate hodoscope channel positions.

Because the horizontal scan increments are small compared to the width of the hodoscope channel spatial response function at the test fuel plane, it is possible to obtain increased lateral spatial resolution by deconvoluting the scan data from the response function, provided noise in the data is sufficiently small. The amount of resolution increase that can be obtained is limited by count statistics and spurious noise in the scan data, because deconvolution amplifies noise and/or produces distortions in the resulting image. Shown in Fig. 12 is the deconvolution of the scan of a single channel in the 1.2-m collimator viewing a fuel pin containing a fabricated hole. The pin is contained in a relatively thick capsule. No correction for self-shielding, which depresses the signal in the pin interior, has been made. The overall fuel profile is rather accurately portrayed and a signature associated with the hole is obtained. However the hole profile is not accurately portrayed and several spurious peaks can be seen in regions outside the pin. Nevertheless, this deconvolution represents a substantial gain in resolution for a scan which is relatively noisy.

Noise can be reduced without sacrificing spatial resolution by summing over scans from all channels in a given row. Also, the scan data will be improved in the near future by installation of a proportional-counter detector array, which will provide immunity to spurious noise, better count statistics, and greater stability. A vertical-scanning capability is planned for the hodoscope collimator, which may allow improvement of axial resolution using deconvolution. And several promising deconvolution techniques are presently under investigation.

### V-I. Comparison With Other Radiography

Conventional thermal-neutron radiographs are routinely obtained both before and after an experiment. These radiographs depict the location of material which absorbs thermal neutrons. If it has not been possible to remove the test train from the loop, a thermal-neutron radiograph may not be of value if the loop is surrounded by a thermal neutron filter. In most experiments it is possible to have the test train isolated from the filter, thus permitting a

comparison of the hodoscope final results with the radiograph. Two possible sources of disparity must be kept in mind: possible posttransient fuel relocation and the inability of the thermal-neutron radiograph to distinguish between steel and fuel.

One attribute of a thermal-neutron radiograph is that it may be obtained at more than one angle with respect to the vertical axis of the test train. Consequently, it can provide complementary dimensional information 90° to the hodoscope view.

Other forms of radiography -- autoradiography or gamma radiography -- may be utilized, but they rarely introduce information not already provided by the thermal-neutron radiographs. Research is underway on the use of higher energy, more penetrating neutrons.

V-J. Comparison with Post-test Examinations

Usually a test assembly is sectioned, and macroscopic examinations of the vertical and horizontal cross sections are performed, with particular attention to a cut transverse to the hodoscope line of sight. Inspection and photography of the surface normally reveal significant information on the final state of the test, particularly information on the disposition of fuel, steel, and sodium. The amount of fuel removed from the hodoscope viewing area may be estimated. Ultimately a metallurgical examination is performed in order to determine the physical condition of the residue.

Upon completion of the hodoscope analysis, a comparison of final-state data may be achieved if the post-test examination is available at the time. If not, the experimenter will perform the comparison during assembly and analysis of all of experiment data. If the post-test examination has been used to aid interpretation of any hodoscope event, a special note will be made in the report.

## VI. ERROR ESTIMATION

Data error-band determination depends upon thorough recognition of sources of error, proper estimation of precision and accuracy, and valid propagation of the uncertainties. In evaluating the sensitivity of proposed alternative diagnostic-measurement devices, difficulties in interpretation have led to disputed claims of performance. Consequently, the following discussion goes into some required detail.

### VI-A. Sources of Error

It is convenient to divide error sources into two categories: inherent and instrumental. Inherent errors are defined here as those that arise from the test sample and environment, largely external to the devices involved in the measurement process, though sensitive to the method of observation (i.e., emissive vs. transmissive). Instrumental errors originate with the devices used in diagnostic measurement (e.g., type of neutron or gamma detector).

Instrumental corrections and errors are characteristic of a particular instrument system. All systems are subject to instrumental errors, but each list of corrections and errors will differ.

Given below in Table II is a general tabulation of primary sources of error. Caution should be exercised in avoiding a misinterpretation of the length of the list. Having a large number of entries is sometimes misunderstood to mean that it is intrinsically difficult to arrive at precise and accurate results. In fact, the relative size of a list of adjustment factors is sensitive to the degree of maturity of the diagnostic system and reflects understanding of the corrections that are needed. A short list may only provide an illusion of simplicity.

TABLE II

Primary Sources of Fuel-Motion Diagnostic Error

Inherent (any emissive system)
Reactor power normalization
Background
Initial fuel inventory
    Fuel enrichment
    Fuel geometry
    Axial profile
    Radial profile
    Azimuthal symmetry
Fuel redistribution
    Radiation attenuation/transmission
    Self-shielding
    Self-multiplication
    Shaping collars (axial flux)
    Neutron filters (radial flux)
    Reactor flux coupling
Nuclear-heated walls
Calibration factor
Control-rod perturbations
Spectrum shifts
Statistical limits

Instrumental
Deadtime
Efficiency of detectors
    Normalization
    Collimator precision
    Absolute
Non-linearity
Time base
Noise
Statistics (power-level dependence)
Saturation
Gamma effects
Drift
Anomalous detector channels
Spectrum sensitivity
Fluctuating instabilities

The meaning of the terms in Table II is described, for the most part, in preceding sections. Their significance varies from test to test, depending upon the experiment geometry and environment, and varies during any given experiment, depending upon power level and fuel movement.

In general, each instrument system has capability of simulating its instrumental corrections under conditions which do not require the movement of fuel. With a dummy capsule, it is possible for the hodoscope to derive correction factors that are appropriate for almost any experiment. In addition, during various phases of any given meltdown transient, the instrumental correction factors may also be determined. The errors in these correction factors depend upon the nature of the transient. For the high-power phase (over several thousand MW-TREAT) of a transient, usually the nonlinear aspect of Hornyak-button response will dominate the error. At lower power levels the efficiency normalization becomes relatively more important. Any test with fuel motion is a useful exercise of all of the factors. High-power tests on dummy samples can provide adequate information on power-dependent corrections (deadtime, nonlinearity, and saturation). The higher the power level that can be reached for a dummy capsule, the more that these factors can be evaluated in conjunction with fuel motion.

On the other hand, the determination of accurate fuel-mass displacement is not readily tested under existing programs. Proper compensation for background can be a serious problem in experiments involving thick or nuclear-heated walls. Reactor-power normalization must, of course, be accurately and precisely performed over the entire viewing region for the full span of the transient. Hodoscope fuel-mass normalization is based on knowledge of the initial fuel inventory. The extent that the initial fuel and flux characteristics can be understood is the limit to which normalization is valid. Normalization of this type has a fairly good foundation because of the existence of pre- and posttest validation.

The most significant contributors to error in quantitative analysis arise after fuel redistribution. The effective signal strength may then vary over conditions which are no longer well established, with particular concern for changes in self-shielding and the impact of axial fuel movement within shaping collars. The loss of known geometry makes compensation under such conditions difficult. In simulating such conditions it should be noted that transient effects or power levels are not, to first order, important.

A test that is most effective in determining critical fuel parameters is one in which the parameters may be separately evaluated without the complicating role of other simultaneous effects. For this purpose a special diagnostic capsule had been under development by General Electric Co. with support by the U.S. Dept. of Energy.

## VI-B. Error Magnitudes

Inasmuch as calibration is effected for the hodoscope on the basis of the known initial emplacement of fuel, errors in the initial fuel inventory are relatively small, per se. However, compensation for the actual radial and azimuthal profile introduces some uncertainty due to fluctuations in detector response.

The range of self-shielding correction depends very much on the hardness of the spectrum of neutrons that induce fission, and the hardness is tied to the degree of neutron filtering. A typical range for self-shielding correction factors has been below 25%. In the future, errors in some experiment situations due to self-shielding variations may eventually amount to 20% to 50% of a

correction that may run up to 50% or 100%. Errors from axial-shaping collars may contribute as much as 10% or 20% of a 50% correction in the involved axial region.

Self-multiplication is probably of little importance for tests involving seven pins or less, with present fuel enrichments. Assuming that a change in fuel mass equivalent to two pins would be the most seen by a channel, error due to attenuation could amount to 10% at most. Enrichment-gradation error would occur as fuel of a different enrichment came into view of a given channel and would have a maximum magnitude given by the ratio of relative enrichment (in case the fuel viewed were completely replaced, with no self-shielding differences). For transient data, errors of magnitude up to ~ 20% have been observed, which may be due to control-rod motion and/or spectral shift, but it has never been ascertained that either of these effects was a primary cause.

Although only a few tests conducted to date suffer in part from such extremes, we expect future tests to require systematic corrections. The utilization of fuel-motion data has not required greater precision and accuracy than obtained so far, though we expect that more refined analysis will be needed in the course of time.

### VI-C. Error Propagation

Random errors due to normalization of hodoscope data are usually synthesized and propagated in quadrature; they need not contribute more than 10% uncertainty (68% confidence level). Errors due to counting statistics can also be as low as a few percent.

On the other hand, systematic errors, which may have to be appended linearly, are larger and more difficult to ascertain. Wherever possible, a return to boundary conditions is utilized to estimate the uncertainty. For example, the final fuel disposition determined by weighing and by radiograph may be compared against the measured locations from hodoscope data.

Errors for measurements as reported usually follow the convention of directly indicating the random-error range, and in a final compilation of the results estimates are made of the likely systematic errors.

### VI-D. Relative vs. Absolute Error

Not all reportable data requires an estimation of absolute errors, that is, uncertainties associated with the the quantity of fuel. We may consider some of the measurements to be relative in nature, so that absolute calibrations cancel out. Examples are measurements of time and location of initial or subsequent fuel movements. Velocities determined without respect to mass of fuel are also relative measurements. As a result, a series of important data on time, location, and velocity may be determined without recourse to absolute calibrations and without suffering from the uncertainties in those calibrations.

### VI-E. Statistical Error

One type of error that cannot be avoided is stochastic in nature. The statistical uncertainty associated with the finite number of collected counts underlies the error estimate of both relative and absolute determinations. If one disregards the contribution of systematic error, then the following analysis will provide a guide to estimation of either the error to expect under various experimental conditions or the total count required to achieve a specified

confidence level.

In view of the fact that the primary information sought in fuel-motion experiments is the change in fuel disposition with respect to known initial conditions, we may concentrate our interest upon the standard deviation of the difference between two measurements. Given an initial count rate (signal plus background) of $R_o$ at corresponding power level $P_o$ during interval $t_o$, and a count rate of R at power level P during interval t, then the difference D may be formed simply as:

$$D = R/P - R_o/P_o = (s + b)/P - (s_o + b_o)/P_o \quad , \tag{12}$$

where $s_o$ and $b_o$ are the reference-interval signal and background count rates, and s and b are the signal and background count rates during interval t. Inherent in use of the terms "signal" and "background" are the assumptions that signal is independent of background, they both vary linearly with reactor power (constant background cancelling), and the power-normalized background rate is a constant ($b/P = b_o/P_o$).

In practice, the measurement of the normalized reference rate $R_o/P_o$ is taken over an interval $t_o$ that is preferably much larger than t; in fact, we shall set

$$t_o = mt \quad . \tag{13}$$

$P_o$, then, is in reality a mean value, averaged over all the m, usually equal, intervals. The reference interval is often rather long during transient experiments so that m may have a value two or three orders of magnitude greater than one. Also, $P/P_o$ may be substantially greater than unity, a characteristic of an experiment initiated with a constant power interval and terminated with a short transient excursion of higher power.

Under almost all conditions of practical interest, the experimenter succeeds in making the statistical uncertainty connected to the measurement of the normalizing factor (reactor power) much smaller than the uncertainty in the detector count rates. Accordingly, we can neglect $\sigma_p$, the standard deviation in the power level, realizing that at worst the variance of the difference could be twice as large if the power monitor had the same variance as the detector count rate.

The standard deviation of the difference D may then be written as:

$$\sigma_D = [(R/P)/(Pt) + (R_o/P_o)/(P_o t_o)]^{1/2} \quad . \tag{14}$$

The relative standard deviation in the difference depends upon the change in signal. The equation above has been derived on the assumption that no significant contribution to statistical uncertainty is introduced by the power normalization process; i.e., $\sigma_p$ is relatively small. This can be attained in hodoscope-type measurements by employment of either a number of detectors simultaneously measuring background, which is proportional to power level, or by use of other power monitors that have improved precision.

It is useful to compare the variance in D with the initial normalized signal rate, $s_o/P_o$. From straightforward considerations in the estimates of variance (17), the following expression for the relative variance may be derived from Eqs. 12-14:

$$(\sigma_D)^2/(s_o/P_o)^2 =$$

$$(1/ms_o t)\{1 + [(s/P)/(s_o/P_o)/E] + (b_o/s_o)(1 + E)/E\} \quad , \qquad (15)$$

where $E = Pt/P_o t_o = (P/P_o)/m$ is equivalent to the relative energy or time-at-power with the interval of interest referenced to the initial normalization interval.

VI-F. Detection Sensitivity

Although there are a number of factors that affect detection sensitivity, the statistical components may be boiled down to a few -- in particular, the initial signal/background ratio, the number of collected counts, the amount of signal change anticipated, and the proportion of time assigned to a precision determination of the minuend in Eq. 12.

It is convenient to recast Eq. 15, in order to determine the number of counts required as a function of several convenient parameters. We introduce the parameter $\delta$, such that a value of 1 corresponds to 100% loss of signal compared to initial conditions and a value of 0 represents no change in signal rate in going from interval $t_o$ to t. Then the fractional signal loss is:

$$\delta = 1 - (s/P)/(s_o/P_o) \quad , \qquad (16)$$

with standard deviation $\sigma_\delta$.

In order to predict the total-count requirement, given known power ratios, relative time at power, and the fractional fuel loss, we write:

$$ms_o t\sigma_\delta^2 = (1 + b_o/s_o - \delta)/E + (1 + b_o/s_o)(1 - \delta)^2 + \delta^2(b_o/s_o)/k \quad , \qquad (17)$$

where the errors in power normalization ($\sigma_P$, $\sigma_{P_o}$) have been dropped and the background can be reduced by increasing the number of background-measurement channels (k).

A plot of the results for selected parameters (with E and k = 1) is contained in Fig. 13. The total signal count $s_o t$ needed to achieve a given statistical confidence may be determined from knowledge of the signal/background ratio. The detector sensitivity is defined here as the standard deviation in $\delta$ -- essentially $\sigma_\delta$. Thus, if one desires to have a measure of the system sensitivity at a given confidence level, application of the total number of signal counts collected and the s/b ratio will give the appropriate value of $\delta$ from Eq. 17 or Fig. 13.

An alternative application is, given all the parameters on the right-hand-side of Eq. 17, to determine the time resolution possible for an anticipated signal source rate, or vice-versa, the signal rate needed to satisfy a desired measurement time.

In evaluation of detection sensitivity, one normally wants to answer questions such as the following: (1) Find if fuel has been entirely depleted from a channel; i.e., if $\delta$ is 0 or 1 with $\sigma_\delta$=1. (2) Find if $\delta$ is in the range of 0, 0.5, or 1; i.e., calculate $\delta$ with $\sigma_\delta$=0.5. (3) Find $\delta$ between 0 and 1 with a precision of 0.2 in $\delta$; i.e., $\sigma_\delta$=0.2.

The first case is of nominal interest, in which data has been collected with a statistical confidence of one standard deviation (confidence level = 68%, $\sigma_\delta = 1$). For the case where the counting times for signal and background are equal (m = 1), the required initial signal count $s_o t$ may be found from the upper-most curves of the graph for $\delta$ ranging from 0 to 1. The total count collected during t would be $(s + b)t$.

As a rule of thumb, for large $s_o/b_o$, about 2 counts are sufficient to distinguish (at 68% confidence level) a 100% loss of the source. With background equal to signal strength, about 4 counts are needed. For a relatively large background fraction, one or two hundred counts are required. However, this latter situation can be improved by monitoring background for a larger fraction of time (m>1) or suppressing the statistical variance due to background by allocating additional channels to simultaneous background (k>1). Thus, for most practical cases, a few counts per channel will suffice to detect a radical change in signal rate.

For the second and third cases, we must amplify the count totals plotted in Fig. 13 by $1/(\sigma_\delta)^2$. Note that care is taken here not to introduce an anomalous, diverging, and unrealistic criterion of infinetisimal precision. We must take into account the fact that the entire signal source may be eliminated (s=0) due to fuel loss.

For convenience $\sigma_\delta$ may be set equal to $\delta$, in which case the measure of sensitivity at the 68% confidence level is equivalent to the limit of signal change sensitivity. This is a more common definition. For a flattop experiment, which means that $P = P_o$, and assuming large m, which is usually easy to attain, the expression for sensitivity approaches:

$$s_o t\delta^2 = 1 - \delta + b_o/s_o. \qquad (18)$$

Table III is constructed on this basis, assuming fractional mass change is equal to fractional signal change. It applies to the case where the measure of fuel displacement (or signal change) is understood to be the disposition of source term at t compared to the reference interval $t_o$. Another important case which would yield different results arrives when we are interested in the interval-by-interval progression of fuel displacement (essentially m=1).

TABLE III

Sensitivity of the 1.2 m Hodoscope for Various Conditions
(single pin; flattop)
(Random Errors Only; CL = 68%; $\sigma_\delta = \delta$; m = 100)

| COUPL. FACTOR W/g-MW | $s_o/b_o$ | INITIAL MASS g | FINAL MASS g | FUEL LOSS $\delta$ | $s_o t$ | SPECIFIC ENERGY J/g | ENERGY FRACTION* % | SPECIFIC POWER W/g@6ms | TREAT POWER MW@6ms |
|---|---|---|---|---|---|---|---|---|---|
| 1 | 0.5 | 4.0 | 0.0 | 1.0 | 2 | 0.048 | 0.004 | 8 | 8 |
| | | | 2.0 | 0.5 | 10 | 0.43 | 0.04 | 72 | 72 |
| | | | 3.6 | 0.1 | 290 | 7.0 | 0.6 | 1200 | 1200 |
| | 0.05 | 0.4 | 0.0 | 1.0 | 20 | 0.48 | 0.04 | 80 | 80 |
| | 0.01 | 0.1 | 0.0 | 1.0 | 100 | 2.4 | 0.2 | 400 | 400 |
| 2 | 1.0 | 4.0 | 0.0 | 1.0 | 1 | 0.024 | 0.002 | 4 | 2 |
| | | | 2.0 | 0.5 | 6 | 0.14 | 0.01 | 23 | 11 |
| | | | 3.6 | 0.1 | 190 | 4.6 | 0.4 | 770 | 340 |
| | 0.1 | 0.4 | 0.0 | 1.0 | 10 | 0.24 | 0.02 | 40 | 20 |
| | 0.02 | 0.1 | 0.0 | 1.0 | 50 | 1.2 | 0.1 | 200 | 100 |
| 4 | 2.0 | 4.0 | 0.0 | 1.0 | 0.5 | 0.012 | 0.001 | 2 | 0.5 |
| | | | 2.0 | 0.5 | 4 | 0.096 | 0.008 | 16 | 4 |
| | | | 3.6 | 0.1 | 140 | 3.4 | 0.3 | 570 | 140 |
| | 0.2 | 0.4 | 0.0 | 1.0 | 5 | 0.12 | 0.01 | 20 | 5 |
| | 0.05 | 0.1 | 0.0 | 1.0 | 20 | 0.48 | 0.04 | 80 | 20 |

HODOSCOPE REF.: $s_o$=10 cps @ 80 kW for 3 W/g-MW [no Pb; half-slot; $s_o/b_o$=1.5]
*out of assumed 1200 J/g limit at TREAT

Note that in Table III the degree of assignable statistical confidence depends somewhat on whether a small amount or all of the signal is displaced, as well as the initial signal/background ratio.

The statistical quality may be improved substantially by improving the minuend $R_o/P_o$ in Eq. 12. In other words, the statistical quality of a measurement of the difference between two large, statistically uncertain quantities, can be improved by causing one of the two quantities to be measured with improved precision. That effect is visible in Fig. 13 as m increases; note also that this improvement factor already reaches a limiting value close to m=10.

For small $s_o/b_o$, the initial signal count requirements are nearly identical because of the dominance of background in forming the difference. The background is measured with relatively high precision both in the minuend and the subtrahend of Eq. 12.

Given a certain signal/background ratio and an expectation of count rates, then the confidence level that might be attributed to the measurement in a single interval can be determined. This allows an estimate of the number of intervals that might have to be averaged together in order to achieve a statistical goal.

Some examples of recent application will be given. Experiments to optimize detector choice and manner of operation recently revealed that for a certain experiment capsule configuration (F3/4), $s_o/b_o$ of 0.65 was achievable at an efficiency one-eighth of that achievable at $s_o/b_o$ = 0.3. At what $s_o/b_o$ should the detector be operated? From Fig. 13, clearly the lower $s_o/b_o$ is better because of the beneficial influence of the much higher signal rate. However, $s_o/b_o \ll 1$ should be avoided, as then systematic errors not considered here become critical.

Table III contains estimates based on Poisson statistics for a variaty of conditions (assuming a flattop). For relative measurements, Table III may be used to estimate the power level or sample energy required to attain statistical confidence in a given displacement of fuel. For example, with a reactor coupling factor of 2 W/g-MW, if all of 4 g of fuel moved out of a single channel, then a TREAT power level of 2 MW would be sufficient to give the required count of 1 for a 68% confidence level in 6 ms data-collection time. The error associated with the collection of 1 count gives only the relative error connected with measurement of the displacement of all the fuel; if the precision of the measurement is to be based on the question of whether 0.0 or 0.4 g of fuel remained, then an entirely different statistical question is being asked, the count requirement being about 190 times larger.

We can calculate with 68% confidence the time and location of an event while having lower confidence in the quantitative mass estimate. We can also designate a higher threshold of confidence, for example 95%, which would require four times as many counts.

From the data in Table III, remaining rate and time parameters of interest may be found from the statistic $s_o t$. For example, on the first line, with $s_o t=2$, we would have $st=0$, $(s+b)t=4$, $(s_o+b_o)t=6$, and $(s_o+b_o)t_o=600$. These parameters then allow us to estimate that an initial signal rate of 2000 cps would meet the two-count criterion with 1 ms time resolution; or, given a desired time resolution of 5 ms, we would need a count rate of 400 cps.

Some estimates have been made of comparative performance between the hodoscope and the pinhole-camera apparatus developed by LASL (18). We are

obligated to take note of the data because of the unique opportunities of having two different diagnostic systems viewing the same test object under simultaneous and identical experiment conditions. Based on their data (19) for PINEX-3A experiment, which had a coupling factor of 6.6 W/g-MW, they report a threshold of 130 W/g. At 16-ms time resolution this corresponds to 2.1 J/g. We interpret this to be sufficient to measure an initial mass of 0.6 g. Under these conditions the hodoscope would have an S/B value of 1.0 and would require, for a flattop, about 100 times less reactor energy to achieve the pinhole-camera detection threshold.

We would extrapolate these estimates to suggest for PINEX-3, with a coupling factor of 4.2, assuming two-fold improvement in sensitivity, that the pinhole-camera should be able to image the pin at about 15 MW, which is 25 times below peak power level. However, the mass-sensitivity requirement (of fuel moving within the annulus of the pin) is about 0.2 g, which implies a signal change ($\delta$) of only 0.03. Thus, the sensitivity of the pinhole camera should not be adequate to see fuel motion within the annulus without further improvement. A useful level of about 1 g may be ascertainable, though.

For the same experiment, PINEX-3, hodoscope sensitivity (for comparable 16 ms interval) would be, from Eq. 18, about 0.6 g at 50 MW or 0.25 g at 300 MW. This appears to be roughly consistent with observations from the actual experiment.

In evaluating diagnostics systems for the F3 experiment, which has two-thirds the power level and one-third the coupling factor of PINEX-3, we would conclude that the pinhole-camera would be unlikely to image the motion of fuel at the required sensitivity level (about 0.2 g). The hodoscope, on the other hand, has a sensitivity threshold of about 70 MW.

It should be noted that statistical analysis is useful in anticipating relative performance under comparable conditions. But systematic effects could be sufficiently large to alter conclusions. In addition, fluctuating instabilities (such as interference from external noise sources) can mask the statistical quality of the data.

## VI-G. Figure of Merit

From the above formulae, a comparative figure of merit may be devised. We are interested in two systems, designated 1 and 2. We may write the figure of merit to be:

$$F = [\sigma_\delta(s_o, P_o)]_1 / [\sigma_\delta(s_o, P_o)]_2 \quad , \tag{19}$$

such that a value of F greater than than 1.0 would favor system 2 because of its lower relative standard deviation. The equation then becomes:

$$F = [(s_o)_2/(s_o)_1]^{1/2} \times \{[1 - \delta + (b_o/s_o)_1]/[1 - \delta + (b_o/s_o)_2]\}^{1/2} \quad . \tag{20}$$

The assumption has been made that E approaches zero (corresponding to very good statistics during the reference interval). This helps simplify the expression without affecting the relative universality of the conclusions.

The above figure of merit exhibits within the range of assumptions an established (17) pattern of dominance on the square root of the inverse-signal ratio. There is little dependence for most applications upon $\delta$ in the limits of 0 or 100% signal change. As an example, a factor of two loss in s/b -- in going

from 0.6 to 0.3 -- sacrificed for a factor of eight gain in count rate yields a figure of merit of about 2 for the system with higher count rate, despite the lower signal/background ratio.

## VII. DATA REPORTING AND RESULTS

Although the procedure for reporting results may not initially appear to be of sufficient intellectual stature to warrant attention in a journal, a description of the methods utilized in reporting data serves two purposes: (1) it is an important formality in satisfying inquiries about methodology, and (2) it leads to some graphic illustrations of typical results. Unless experimental data can be presented in useful form, they can be of little specific or general use, particularly in the case of complex multiparameter data. The extraction of the most useful information and the development of the best visual format is an essential exercise.

### VII-A. Reports

A technical report on hodoscope data is ordinarily addressed to the experimenter. Depending on whether it is in preliminary or final form, the report contains as much contextual information as needed to be understood without unnecessary reference to other reports.

Introductory material describing the experiment, the test parameters, and hodoscope operation are included. In particular, note is made of special test conditions that may affect diagnostic performance and of changes that may have taken place in either the hodoscope instrumentation or its operation. Because there is a constant milieu of modification and improvement, it is important for at least archival purposes to make note of such changes.

Results are presented in a variety of ways. Usually by reference to certain types of graphical illustrations, the significant data is abstracted, discussed, and interpreted by the hodoscope analyst. Details are provided in both graphical and tabular form, and appropriate summaries of key fuel-motion events are prepared.

At this stage, data is always compared with other available information. Instrumentation results from the test train are usually available, and normally there is a radiograph. In a time frame comparable to completion of the hodoscope report, the posttest destructive examination has usually been completed and reported. Pretest and posttest calculations may also be on hand. The hodoscope analyst will make an intercomparison with this other data and note agreements and disparities. Occasionally, on the basis of clues derived from the other instrumentation, certain fuel-motion events may be identified that might otherwise have been overlooked. More likely there will be hodoscope detected events that have no correspondence in other instrumenation data or calculations. If reinterpretation of an event takes place as a result of the data intercomparison, specific note in the report is made of this. In one or two experiments it has been necessary to lean heavily on outside information because of a low signal/background ratio or other difficulty in hodoscope data.

All known uncertainties and limitations are routinely noted. Estimates are made of statistical and systematic effects. Where judgement is involved in the interpretation -- which will almost always occur at the limits of sensitivity -- note is made of the role of human interpretation.

In order to structure reports in a readable fashion, much detail material is relegated to appendices. This will include archival data that allow the tracing of data back to original sources, copies of important experiment records, and details of corrections or operational features.

The procedures involved in report preparation have been simplied to allow an expedited schedule. The text portions of all reports are originated at the TXT

terminals (20); graphics are derived from programs stored on the same support-computer system. All editing and revisions of composite reports are facilitated by this interactive environment. Long lead times and some sources of inaccuracy have been eliminated.

All reports are internally reviewed within the Diagnostics Section, then reviewed in draft form by the experimenter, before being issued in final form. Copies of hodoscope reports are given limited distribution until further disseminated as part of the full report by the experimenter.

### VII-B. Report Illustrations

Several techniques are available to make use of hodoscope data. All processed data is indefinitely retained on disk or tape. Tabulations or condensed numerical summaries can be made and incorporated in reports. More generally, various image forms are devised to communicate salient features of the fuel motion. Examples of simple time-plots, profiles, and intensity-modulated graphics were given in Section V. Additional graphic forms are given in Figs. 14 through 18. Other than some occasional flaw-correction, image-enhancement techniques are not systematically applied or necessary because of the sufficient signal/background ratio of the hodoscope.

Figs. 14 and 15 are results from 7-pin bundle tests. For experiment R7 the fuel extended beyond the vertical range of the 0.5 m hodoscope collimator then in use. Figure 16 depicts the primary motion stages of a 3-pin bundle of short fuel. In all cases, intervals of selected interest are shown. Internal reports will frequently carry additional intervals, but rarely will all the data be presented in graphic form because of the overwhelming amount of it.

Quantitative data is not well represented by intensity-modulated images. The human eye, though rather discriminating on a relative basis, is a rather crude quantitative measuring instrument for pictures with grey tones. Consequently, we have devised a method of rendering the data using symbols that quantize various levels. Fig. 17 is such an example (as is Fig. 7). Shown in Fig. 17 is only the axial component of the fuel motion, which is usually of dominating importance.

Multiparameter presentations are often made in order to condense the graphics, as Fig. 9 illustrated. We may also on rare occasions make use of artists' reconstructions (Fig. 18) in cases where the straightforward presentation of computer data lacks sufficient contrast. In such a case, a subjective form of image enhancement is applied in order to achieve the end objective.

A final example is that of data taken before and after the transient. When the hodoscope is operated in a scanning mode with the reactor at low steady-state power (nominal 80 kW), a radiographic reconstruction of the fuel disposition can be achieved in about a half-hour. A pair of pre- and post-test scan data reconstructions are shown in Fig. 11. Figure 12 provides an example of a typical pair of unconvoluted and deconvoluted horizontal profiles for an annular fuel pin (PINEX-3).

### VII-C. Movies

Most of the illustrations provided above may be displayed on a cathode-ray tube screen; accordingly, by displaying successive intervals of data, the effect of motion can be simulated in slow motion. By speeding up the display of intervals, a real-time display can also be presented. Algorithms for refreshing

and blanking the screen must be utilized to take into account human perception. These types of display are useful in creating a qualitative impression of the fuel motion events.

If warranted by the quality of the data and the significance of the fuel-motion events, the information stored on the screen may be photographed with a pin-register type of framing camera and a motion-picture film assembled from suitable frame repetitions. Both slow-motion and real-time presentations have been incorporated into motion-picture films. One film presented at the Fast Reactor Safety meeting in Seattle (4) contained a succession of animated sequences representing fuel motion during the PINEX-2 experiment, of which some selected intervals are shown in Fig. 18.

Future activities for motion representation are directed towards interactive-computer control and use of color videotape and/or color film as storage media. Animation and titles will be devised on a graphics terminal, and these scenes will be integrated with the data display onto a single medium by computer-controlled editing.

## VIII. APPLICATIONS OF DATA

In the previous section, some of the results obtained from the hodoscope were illustrated. In order to show the range of applicability, examples will be given in this section of some known applications. In general terms, the information has been applicable to LMFBR design and licensing.

### VIII-A. Experimenter Applications

Initial application of hodoscope data is usually carried out through the experimenter who is interested in evaluating the performance and outcome of the test. There are many examples of test reports (21) which indicate the role of hodoscope data in conjunction with other available information. In addition, there are summary reports (22) in which significant dispersal trends are abstracted.

Many phenomena of interest have been observed. In single-pin experiments, we have noted the initial bowing of the pin, in some cases followed by extensive helical distortion upon failure of the cladding. In multi-pin experiments, both individual-pin warpage and coherent-bundle distortion have been detected. Where the expansion exceeds the axial resolution threshold of the particular collimator design, axial expansion has been measured in early phases. Some experiments have been characterized by internal fuel motion, with or without subsequent cladding failure. Internal fuel motion has taken place through a preformed cavity in annular pellets or through the transport of voids in pre-irradiated fuel pins. In cases where molten fuel has been ejected into coolant channels, sweepout by sodium has been noted.

The preceding phenomena in a few cases challenge the sensitivity limits of the diagnostic system. When much larger restructuring takes place, the events are easier to detect -- though not necessarily easier to quantify. Extensive relocation has been observed in loss-of-flow and transient-overpower simulations as dispersive forces acted upon melted or disintegrated fuel. Some of the dispersal mechanisms include sodium sweepout, fission-gas pressure, steel-vapor pressure, and fuel-vapor pressure -- in addition to gravitational slumping. Eructations resulting from steel vaporization in contact with molten fuel were first discovered from hodoscope data as a prominent dispersal mechanism in loss-of-flow tests.

Many experiments undergo an assortment of phenomena. Events are usually separated sufficiently in time to allow characterization from the hodoscope data. In other cases, certain phenomena tend to dominate the course of the experiment at a given time. It has been rare that simultaneity has resulted in ambiguous results.

### VIII-B. LMFBR Applications

The application of hodoscope data to various whole-core scenarios has been accomplished in several ways: incorporation of data in codes, comparison with code calculations, or computation of reactivity worth.

Two codes that have been devised with hodoscope fuel-motion data factored in are SLUMPY and PLUTO (23). Figure 19 contains a comparison of PLUTO2 post-test computations against L-8 experimental data from the hodoscope. At the selected intervals it can be seen that there is significant qualitative agreement. Also it can be noted that there are some disparities that warrant both instrumental and analytical evaluation.

Hodoscope data has been frequently utilized in code comparison. A recent example is in LEVITATE (24), where the code gave fair agreement with the hodoscope-measured early fuel dispersal. Figure 20 compares fuel density for the measured and calculated data. A comparison between the relative fuel-reactivity worth calculated by PLUTO2 and the experimental data from the hodoscope is shown in Fig. 21. Simms (9) has made a broad range of reactivity worth calculations and Fig. 22 is such a plot against reactor energy release, compared with LEVITATE and SLUMPY.

## VIII-C. Experiment Decisions

An interesting class of applications arises in connection with operational decisions regarding a future test. One example is the R-6 test, which preceded R-7 by about six weeks. At the request of the experimenter, data handling for R-6 was accelerated and results were available as a series of qualitative images on a cathode ray tube within 60 hours of the experiment. (This was at a time when it was necessary to go through a film-processing stage). The information presented in R-6 was used to decide upon the transient termination time for R-7.

In a more recent experiment (J1), the first attempt in performing the planned transient was aborted under computer control before reaching anticipated power. In order to determine if the initial portion of the transient resulted in damage to the fuel, the hodoscope data was evaluated promptly, and no sign of displacement was found. In addition, detailed scans were performed and compared against the pretransient scan. This data, in conjunction with other instruments and calculations, indicated that the fuel bundle was undisturbed and the transient could be rerun without compromising test objectives.

## VIII-D. Rapid Data Turnaround

Interest in expediting data processing accrues from two directions: (1) to aid in operational decisions and (2) to minimize the information delay between shots. In some cases, operational decisions would not directly arise from the results, but planning for succeeding experiments may depend on the outcome of those already accomplished. As a result, a continuing program has been underway to shorten the time between experiment and reporting.

A number of measures can be invoked to expedite the turnaround. First of all, the data may be transferred to the processing facilities more rapidly. This has been accomplished by making use of a dedicated 9600-baud (HASP) data transmisson line from ANL-W to ANL-E. The data can now be available within a few hours of an experiment.

The data-processing facilities can be optimized to turn data around promptly by having interactive, timesharing hardware and software. The analysis of data is facilitated by providing appropriate analysis tools and graphic aids and having a base of experience. Finally, the rendering of reports takes place more rapidly now due to an advanced text-processing system.

Each of these factors was exploited in an exercise of rapid data turnaround after the AX-1 experiment. The essential processing programs were exported to TREAT, and the data-accumulation control computer was operated as a data processor. Within 45 minutes after the experiment, initial qualitative results were displayed on the videoscreen. In addition, the same information was transmitted over the HASP link and promptly processed in more quantitative fashion at ANL-E. The lessons learned in this experience have been helpful in making a smoother and better process of initial data evaluation.

Consideration is being given to the role of on-line transient termination as a result of a signal derived from the fuel motion detected by the hodoscope. There are experiments in which it is desired to scram the reactor at onset of fuel motion. However, to accomplish such a step with a high probability of success is a major task; it is important to avoid premature termination as a result of invalid interpretation of signals. To derive a reliable terminating signal requires the assimilation of diverse hodoscope information and an extensive program of testing by use of the existing data base and trial transients.

## IX. DISCUSSION AND SUMMARY

The hodoscope has been configured to meet or exceed programmatic goals. Although there has been a general evolution in goals and experiment conditions, efforts have been made to be responsive and keep abreast. In general, it is fair to say that available hodoscope resolution in space, time, mass, and velocity has exceeded the capability of core-destructive models to make use of the data. However, there is a class of experiments involving phenomenology of fuel and clad motion where diagnostic needs are unmet, at least in part. As a result, there has been some impetus to examine alternative diagnostic techniques.

There have been two historic major limitations in hodoscope data. One is that there has been a lag in providing the experimenter with the processed data; this has been a consequence of resource limitations. The other major limitation has been due to the nonlinear response of the detectors at high power. It has been possible to compensate for this deficiency, and work is underway to bypass the problem. In addition, there has been an inadequate base of information for evaluating systematic corrections; efforts have been underway to alleviate this difficulty too.

Before reviewing and comparing the prospects of alternatives, we should clarify possible misconceptions regarding limitations of the hodoscope. Also, cost-effective actions that can be taken to improve hodoscope response should be examined.

### IX-A. Hodoscope Interchannel-Motion Resolution

Fuel-motion resolution better than the interchannel spacing between hodoscope collimator slots can be achieved. This is sometimes not appreciated. To visualize that capability, the following generalized example is provided. Application to a specific situation is complicated by the geometrically complex response function of the hodoscope and by the variety of possible fuel-source scenarios. As a result, a simplified model will be introduced for the sole purpose of illustrating the underlying principle.

It should be kept in mind that there are two extremes encountered in fuel motion: highly correlated motion corresponding to nearly intact geometry or less correlated motion corresponding to significant fuel redistribution. Certain experiments, such as the recent L-series conducted at TREAT, are designed to be of an integral nature for predicting net reactivity effects. In such experiments, the hodoscope has clearly demonstrated better capability in practice than the mesh resolution of existing accident-analysis models. The fundamental limit to resolution, when there is substantial loss of integrity, is established by the interchannel spacing between detectors. That spacing is a design compromise based on experiment requirements, accident-analysis codes and technical feasibility -- factoring in available funds and other practical considerations.

On the other hand, in phenomenological experiments when more subtle fuel motions take place, such as axial or radial expansion, the existing hodoscope collimators yield somewhat marginal performance. Construction of a new collimator is not a large expense, because it is possible to reuse the detectors, electronic system, and methods of analysis. However, before doing so it is useful to have a thorough understanding of the capabilities of existing hodoscope collimators in demanding situations. Within the context of correlated fuel motion, the effective spatial and mass resolutio can be much better than the interchannel spacing between d etectors. Because this is not readily self-evident, the resolution potential of the hodoscope has sometimes been

misunderstood.

The hodoscope senses relative motion; when this relative motion is highly correlated, advantage may be taken of an inherent design resolution-enhancement factor. Relative motion occurs in either of two ways: (1) the fuel moves, and the collimator is stationary, or (2) the fuel is stationary, but the collimator is moved. These situations are physically equivalent and thus allow the testing of hodoscope response functions under controlled conditions, namely systematic scanning of the collimator across a stable source. It is important that the two situations of relative motion are also statistically equivalent, for the statistical limits are a controlling factor. First, one must have a suitable and known response function; second, one must be able to translate this into statistically significant data.

Although all fuel redistribution modes cannot be inferred from scan data, simple highly correlated fuel displacements, in which the initial geometry has not been extensively altered, can usually be identified. Such displacements usually are of prime interest in phenomenological tests. Thus correlation-enhanced resolution is most useful for phenomenological experiments. To visualize a capability for fuel-motion resolution better than interchannel spacing, the following simple model of correlation-enhanced lateral resolution is provided.

Figure 23 shows an idealized trapezoidal response function of two laterally adjacent collimator channels. We shall take the interchannel distance to be D and set the response overlap G = D/2. With top width W = D/2 and bottom width L = 3D/2 for the trapezoid, uniform response is achieved. Let us set the diameter of a uniform line source P to be 3/8 D and locate its centroid between channels at distance D/4 from the center of channel 1. The initial signal/background ratio $s_o/b_o$ is assumed to be 1 for channel 1 (and thus 0.087 for channel 2).

If the source centroid is shifted further toward channel 1, there would be an increase in count rate in channel 1 and a corresponding decrease in channel 2. This propagation and correlation is fundamental to hodoscope resolution of interchannel motion. It is an attribute often not appreciated. Suppose the shift amounts to 25% of the interchannel distance, i.e. D/4, placing the centroid in the middle of channel 1. Then the relative decrease in total rate for channel 2 would be 100% and the corresponding increase for channel 1 would amount to about 9%.

Statistical conditions (Eq. 18) would then suggest that a significant measurement (to 68% confidence level) of the decrement in channel 2 would require about 1.4 ms at an initial signal rate of $10^5$ cps, and that the increment in channel 1 could be measured in about 2.8 ms. Thus, despite the fact that the full-width-at-half-maximum of the hodoscope response function is in the order of the interchannel spacing (not intrinsically, but by design tradeoff), the effective resolution can be and generally is substantially better.

Of course, if the source centroid now shifts from the center of channel 1 by ± D/16 or less, channel 1 and 2 count rates would remain unchanged. However, test fuel pins have diameters significantly greater than W for both collimators. In fact, many fuel pins have diameters greater than interchannel spacing. The original 0.5 m collimator provides a lateral interchannel spacing near the diameter of small EBR-II pins, but the 1.2 m collimator has a spacing that is larger than most pins presently tested.

The reader should take note of two sources of confirmation of the above reasoning: First, the experimental data cited in preceding sections clearly

yields hodoscope resolution consistent with that derived from the preceding analysis of its response function. For example, horizontal motion down to 0.25 mm has been observed under some conditions. Second, similar results, with corresponding experimental verification, have been derived by the hodoscope group at CABRI (25). Their horizontal design precision is given as at least 1-2 mm. As a rule of thumb, spatial resolution an order of magnitude better than the hodoscope interchannel spacing is usually achievable for fuel motion, when initial geometry is not significantly disturbed.

In addition, not yet fully utilized to date in hodoscope analysis are some powerful computational tools, namely, systematic application of correlations in space and time. We do make subjective use of such correlations, particularly in visual examinations of data; for example, adjacent channels should exhibit consistent behaviour. This treatment could be programmed for systematic application: At the moment it is unnecessary because of the more-than-adequate consistency of data processed without this feature.

As a result of the above considerations, one may conclude that hodoscope design parameters meet or exceed the requirements of both phenomenological and integral tests for all but a few existing situations.

## IX-B. Comparison with Other Diagnostic Systems

Several evaluations (1, 26) of alternative diagnostic techniques have taken place. Initial proposals were made in the late 1950's for fuel motion diagnostic measurements at TREAT. Another survey was made at ANL in 1963 in estimating the prospects of the hodoscope. Starting in 1974 a third round of evaluations based on newer technology was made. Laboratories undertook development of several alternatives, and the French-German project chose to build a hodoscope at Cadarache.

Our attention will be confined to systems that are external to the test container or reactor core, because those that are within the core are subject to destruction or irradiation effects during the course of the experiment. In addition, they tend to have inherently limited spatial resolution and complicated response to fuel, coolant, and clad motion.

Three types of alternative ex-core diagnostics systems have reached some degree of experimental verification: flash x-ray, pinhole, and coded-aperture. The flash x-ray system (27) depends on passing a beam of high energy x-rays (up to 20 MeV) through the test section; it requires, accordingly, a full-slot through the core. Because there are many experiments in which the reactivity loss of an additional half-slot cannot be tolerated, we will pass on to those that can operated with only half a slot. Flash x-ray systems have produced excellent tramsmission images of test fuel with thick surroundings, but such machines operating with a repetition rate of at least 1000 pulses/s have not been demonstrated with the beam current and reliability required. Also, x-rays cannot directly distinguish between fuel and steel.

The coded-aperture system (28) has been under development for about five years at Sandia Laboratories. Initial proof tests under combined transient conditions indicated a poor signal-to-background ratio. Redesign of the system has resulted in a delay in achieving fuel motion data.

A pinhole system has been under development by LASL for application to TREAT, based on classified results in the nuclear-weapons underground-testing program. This system has reached the most advanced stage of development, resulting in three comparative tests with the hodoscope at TREAT. Test PINEX-2 (5) ultimately resulted in some quantitative data derived from the pinhole

apparatus; a comparison of papers containing data presented at the International Meeting on Fast Reactor Safety (4, 19) indicates that at the stage of development the pinhole was unable to match the quantity and resolution of the hodoscope. In AX1 a non-redundant pinhole array was tested, but they obtained no fuel motion results. This was due partly to the disadvantageous orientation of the pinhole array with respect to the test section, although the hodoscope would have been able to achieve fuel resolution under such conditions.

In a third comparative test, the pinhole system has made significant progress in increasing sensitivity at lower power levels. Nevertheless, there remain specific differences. For PINEX-3, a data exchange was arranged between the experimenter (HEDL) and the two laboratories that had developed diagnostic systems (LASL and ANL). The exchange took place at a common date about two months after the experiment. The following interpretations may be made of the data as reported:

1. Many detailed features, measured in terms of specific time, location, and mass were reported for hodoscope observations without comparable results reported for the pinhole.

2. There are some features reported in common by both diagnostic systems. These are equivalent to fuel movements interpreted by LASL as "radial expansion" and "central voiding." One specific item is the LASL estimated time of "clad failure," which coincides well with the time of our reported value of "clad breech." Both of these ANL and LASL measurements of loss of clad restraint are consistent with HEDL thermocouple data.

3. Some features were noted by the pinhole but contra-indicated by hodoscope data; these include eight axial fuel expulsion "cases" reported by LASL. The x-radiograph does not support LASL in this, but the post-mortem examination has not yet been performed.

It should be recognized that the data exchange for PINEX-3 was based on preliminary data from both diagnostic systems, and each is likely to improve their analysis for final reports. In addition, the experiment was affected by three factors that that are not characteristic of most TREAT tests:

1. A high power-coupling calibration factor, 50 to 100% greater than usual. Because of its low signal/background ratio, the pinhole apparatus would be severely impacted by lower coupling factors.

2. A full slot through the core. Although this improves the diagnostic performance of both systems, the pinhole system would be hurt the most in experiments performed with a standard slot.

3. Application of the hodoscope under spatial-resolution conditions that are at the limits of its design. The collimator used is primarily intended for integral-type experiments with large fuel motion; a smaller collimator is available with better inherent resolution.

Both the coded-aperture and pinhole devices accumulate results in the form of analog images stored on film and/or video recorders. From a general viewpoint, our experience indicates that the collection of such analog data is inferior to the direct recording of digital data. The process of analog-to-digital conversion often runs the risk of losing significant information or introducing artifacts. There is a comparable problem in converting from digital to analog data; however, of most value are the quantitative results derived from the digital data. The loss in visual appearance that results from conversion of digital to analog data can be tolerated because such reconstructions serve no quantitative purpose -- they are qualitative pictures for communicating

impressions.

Inevitably judgment must play a role in any set of data. One method can be more susceptible to artifacts and judgment than another. We believe that to be the case with the analog systems, such as the pinholes and coded-apertures, because of the large background that must be subtracted.

In terms of specific quality indicators, comparative performance at the time of the PINEX-3 data exchange may be summarized as follows: hodoscope signal-to-background and mass resolution appear to be an order of magnitude better than the pinhole. Hodoscope time and spatial resolution are as good or better than the pinhole. In addition, hodoscope data appears easier to process, analyze, and utilize and is evidently less subject to spurious effects.

It should also be kept in mind that the hodoscope is continuously being upgraded in accordance with a systematic program of develpment (see below).

No system is immune from technical corrections to the data. There are inherent errors common to all diagnostic systems that use the same source. For example, both hodoscope and pinhole systems rely upon emission of radiation from the fuel. Flash x-ray systems would not be subject to these same inherent corrections because they are dependent primarily on transmitted radiation; however, they would have their own list of inherent correction factors and errors. Table IV lists the major corrections needed for each generic type of diagnostic system. An estimate of the relative importance of the correction is also given.

TABLE IV

Comparison of Corrections for Diagnostic Systems

| | EMISSIVE | | | TRANSMISSIVE |
|---|---|---|---|---|
| | HODOSCOPE | FZP | PINHOLE | X-RAY |
| Reactor power | ** | ** | ** | * |
| Dynamic range | | ** | ** | * |
| Self-shielding, etc. | * | * | * | |
| Attenuation | | | | * |
| Linearity | ** | * | * | * |
| Saturation | * | * | * | * |
| Background | * | ** | ** | * |
| Uniformity | * | * | * | ** |
| Drift | * | * | * | ** |
| Absolute fuel-mass normalization | ** | ** | ** | ** |

Code: * A correction must be applied.
** The applied correction is important.

In the continuing process of reassessment, one asks if it is likely that other systems can do better in some situations. Flash x-ray for certain specialized applications with large bundles may be best if a full slot through the core could be tolerated and if the high-current pulsed machine could be built at a reasonable cost with adequate reliability. Those are big "ifs." There is a better possibility for application of accelerators in the safety program: radiography of stationary objects, such as test sections in thick enclosures. Accelerators, though, may not compete well on the basis of cost effectiveness with existing reactors and other radiation sources.

Another approach to radiography that utilizes existing facilities is hodoscope in-situ scanning. In this mode (3) the hodoscope scans both vertically and horizontally to increase its effective spatial resolution for stationary objects. The test section may be rotated to provide three-dimensional tomography. In addition to fuel distribution, it may be possible to sort out the steel relocation using the gamma-ray hodoscope system.

A related development that is being planned is that of plenum radiography. This consists of detection of decay gamma rays emitted by a test section after an experiment. This can be done conveniently when the test section is withdrawn from the core of the TREAT reactor. Tomographic images may be obtained by providing relative rotation. Either hodoscope- or pinhole-type apertures are likely to be employed.

The CABRI hodoscope (24), though developed along the same principles as the TREAT hodoscope, has several significantly different features. It achieves more precise static location of fuel by careful design, machining, and detector selection. Results to date have established its role for high accuracy in measurement of axial fuel motion.

## IX-C. Hodoscope Improvements

As a result of several years of evaluation and testing, certain improvements have reached the stage of design, fabrication, and impending installation. The most significant improvement will be the addition of an array of methane-filled high-pressure proportional counters. The detectors have undergone extensive steady-state and transient proof tests. Compared to the Hornyak buttons, the proportional counters should provide more linear response at high power, higher efficiency, more stability, and be less susceptible to noise -- at a small sacrifice in signal/background ratio. Another modification to be carried out simultaneously is a capability of remote control of the scanning apparatus, with the added dimension of vertical motion.

Improvements that are projected further in the future include equipment and software for better analysis, and detectors with improved efficiency and signal/background ratio for use in future tests where thick test vessels surround the fuel sample.

There is a continual program of improvements for the sake of reliability. In fact, a major portion of the apparent complexity and expense of the hodoscope system results from efforts to assure dependable performance. A strong degree of operational assurance is warranted because of the high cost and long lead-times associated with destructive experiments at TREAT. Consequently, quality control is routinely exercised in procedures and hardware, and considerable redundancy has been designed into the entire hodoscope system. For example, the proportional-counter system will be completely isolated from the Hornyak-button detector system.

## IX-D. Summary

By a combination of instrument design, normalization of data, calibration, and data validation, it has been possible to reliably achieve hodoscope quantitative data with fuel-motion sensitivity limits as small as 1 ms in time resolution; 0.25 mm (lateral) and 5 mm (axial) in displacement resolution; a few m/s velocity resolution; and 50 mg (single pin experiments) in mass resolution. The foundations in hardware and software now exist for advancements in application and for coping with future experiments that contain more fuel pins and have thicker test-vehicle walls. To do so requires an understanding of underlying principles, a convenient means of recovering data, programmed methods of data processing, experience in data analysis, and sufficient recognition of sources of error.

## APPENDIX A

## SUPRALINEARITY AND DRIFT CORRECTIONS

### A1. Introduction

The count rate response from the primary hodoscope-detector system (Hornyak button coupled to a photomultiplier tube) is not directly proportional to changes in the TREAT reactor power. At present, two distinct types of nonlinear behavior have been identified; the most likely cause is a variation in detector efficiency due to changes in the gain of the photomultiplier-amplifier-discriminator electronic system.

The supralinear response consists of the measured count rate increasing at a faster rate than the reactor power. It is observed experimentally that the supralinearity becomes larger as the reactor power increases and that it varies from transient to transient and from detector to detector. Typically, this nonlinear effect produces a factor of two increase in the detector count rate at peak power.

The second nonlinear term, which has only recently been identified, is a drift in the detector count rate at reactor powers greater than a few megawatts. Since the drift term is smaller than the supralinear term, it is most noticeable in the flattop portion of transients where the power level is constant and the supralinear term does not change. As in the case of the supralinear response, the drift response varies from detector to detector, from transient to transient, and in slope -- being predominantly positive. The maximum magnitude of the drift correction is ±50% at the end of a 20-s transient.

Note that, in the analysis of the data, the fact that the correction to the detector response is large does not mean that systematic errors in the detector response need be large. Whether these errors are significant depends to a large extent on how well the mathematical models used to describe the nonlinear effects agree with the experimental data. Experimental analysis of many transients has provided evidence that the current models are capable of giving a good description of the various nonlinear effects and thus the systematic errors are small.

The current explanation for the detector supralinearity is a variation in the detector efficiency resulting from a change in the gain of the detector system. Figure A-1 shows a plot of the detector count rate response as a function of the gain of the detector system. A typical detector threshold is shown for reference. The absence of a plateau in the count rate versus gain curve of Figure A-1, causes the count rate to be a sensitive function of the system gain. In particular, the count-rate change is approximately twice as large as the fractional gain change at typical detector efficiencies.

There are several reasons why the gain of the detector system could vary with reactor power. Recent measurements of the average DC photomultiplier-tube current during transient tests suggests that the supralinearity is due to the tube current being of the same order of magnitude as the bias-string current (29). Other effects, which could contribute to the supralinearity, are: pulse pile-up of small gamma-ray and neutron pulses, changes in the light output of the scintillator due to high ionization densities within the scintillator, and gradual build-up of a direct-current light level due to the long decay components of the ZnS(Ag) scintillator.

A significant portion of the drift may also be due to the large average DC currents in the photomultiplier tube (30). A second effect, which may also be

important, is a nonlinear response of photomultiplier-tube gain to sudden changes in the detector count rate (31). Although this nonlinear response varies exponentially with time, the time constants involved are usually long compared to the duration of a transient. Thus this effect could appear as a slow, linear drift in the detector efficiency.

A2. Theory

The basic assumption in the development of a model for supralinearity and drift is that, in the absence of fuel movement, the power-normalized count rate change, which is observed as the power increases, is due to changes in the gain of the detector system. With this assumption it is reasonable to expand the detector count rate in a Taylor's series about the initial system gain. Figure A-3 shows a typical count rate versus discriminator curve. The true gain of the system is $G_o$ and the true count rate $C_o$ is taken to be the count rate at this gain. If the gain of the system changes to $G_1$, then the measured count rate will change from the true rate $C_o$ to the new count rate $C_1$.

The rate $C_1$ can be determined by a Taylor's expansion about $G_o$. Keeping only the first two terms gives

$$C_1 = C_o + \frac{\partial C}{\partial G}\Big|_{G_o} (G_1 - G_o) \quad . \tag{A1}$$

Figure A1 suggests that the relationship between the counting rate C and the gain G for a small region about $G_o$ is

$$C = G^b \quad , \tag{A2}$$

which leads to

$$\frac{\partial C}{\partial G} = \frac{bC}{G} \quad . \tag{A3}$$

Substituting Eq. A3 into Eq. A1 gives

$$C_1 = C_o(1 + b\Delta G/G_o) \quad . \tag{A4}$$

In order to obtain $C_1$ it is necessary to determine the variation $\Delta G/G_o$. While this could in principal be done theoretically, the present procedure is to use the experimental observation that $b\Delta G/G_o$ can be written as

$$b\Delta G/G_o = AC_o + \Phi t \quad , \tag{A5}$$

where t is the time from the start of the transient, and A and $\Phi$ are constants. The term $AC_o$ corresponds to the supralinear correction and the term $\Phi t$ corresponds to the drift correction. Substituting Eq. A5 into Eq. A4 gives the required analytical relationship between the measured and the true count rates.

$$C_1 = C_o(1 + AC_o + \Phi t) \quad . \tag{A6}$$

It should be noted at this point that there is another model for the supralinear term that would also be in agreement with current experimental data. In this model, $C_o$ in Eq. A5 is replaced by the reactor power P. Since the

change in $C_o$ is proportional to the reactor power unless there is fuel motion, this change produces only a small correction to the detector response. Experimental studies of this approximation are being made, however.

## A3. Determination of A and Φ

While Eq. A6 provides an analytical relationship between $C_1$ and $C_o$ it is not especially useful unless the constants A and Φ are known. These constants can be determined directly from the transient data by noting that prior to fuel motion the true counting rate $C_o$ is proportional to the reactor power P, which is well determined. Thus

$$C_o = \gamma P \quad . \tag{A7}$$

Equation A6 can then be rewritten as

$$C_1 = \gamma P(1 + A\gamma P + \Phi t) \quad . \tag{A8}$$

A least-squares fit between the measured counting rate $C_1$ and the reactor power P gives the constants γ, A, and Φ. Usually the A values vary from 10 to 50 μs and the Φ values from -50 to +50 $(ms)^{-1}$.

A typical fit between the measured count rate and the reactor power is shown for transient H6 in Fig. A-3. The measured count rate has been divided by the reactor power in order to show more clearly the nonlinear portion of the detector response. The dashed line shows the response for a linear detector. The solid line is the least-squares fit using Eq. A8 and the constants given in the caption. The drift correction term is most noticeable between 4 and 6 s when the reactor power was constant and as a consequence the supralinear term did not change. After 6 s the reactor power rapidly increases and the supralinearity becomes the dominant term in the nonlinear detector response.

Once the constants A and Φ are known, the true count rate can be obtained from Eq. A6 by solving for $C_o$. In doing this it is important to note that the measured count rate $C_1$ should be corrected for any deadtime that occurs in the discriminator or scaler portion of the electronics. Typically a non-paralyzable deadtime is used. The final equation for $C_o$ is

$$C_o = \frac{-\Gamma + \{\Gamma^2 + 4AC_r\}^{1/2}}{2A} \quad , \tag{A9}$$

where the deadtime corrected count rate $C_r$ is given by

$$C_r = C_1/(1 - \tau C_1) \quad , \tag{A10}$$

and the quantity Γ is

$$\Gamma = 1 + \Phi t \quad . \tag{A11}$$

## APPENDIX B

## HODOSCOPE DATA NORMALIZATION BY PROGRAM EFFI AND ASSOCIATED ERRORS

### B1. Introduction

Even though hodoscope channels are calibrated prior to each transient experiment, variations in relative efficiency of 50% or more over the array are found subsequently in transient data. Although the cause of this variation has not been pinpointed, it may be due to slow changes in electronic or phototube parameters (typically several days or more elapse after calibration before the transient is run). If not corrected, this variation would lead to local fuel mass errors and inaccurate determination of initial fuel location. Efficiency corrections and initial fuel location are computed by the program EFFI. When each channel is normalized to have the same efficiency, the hodoscope array provides uniform response to test fuel fission rate.

From the standpoint of reactor accident analysis, however, it is desireable to express fuel motion in terms of mass changes, rather than fission rate changes. In order to provide uniform response to test fuel mass, the reactor flux and power coupling to the test fuel (primarily a truncated-cosine axial shape) must be considered. In addition, a proportionality factor is needed to convert normalized channel count rate changes to mass changes. These requirements can be met by making a second pass through EFFI.

For efficiency adjustment, normally a reference time interval is chosen which is early enough that no significant fuel motion has occurred, is relatively free of spurious noise, and is long enough for excellent count statistics. Then test fuel geometry is known and spatial data fluctuations can be assumed to be due to efficiency variations. EFFI is used to perform minimum-variance fits to two-dimensional parameterized models of test fuel signal and background, leading to efficiency multipliers for each channel. Errors from various sources, of both random and systematic nature, are associated with these efficiency multipliers.

### B2. Mathematical Formalism

EFFI uses a two-dimensional profile model $F(x,y)$ of the expected count rate distribution, where x and y are the horizontal (lateral) and vertical (axial) dimensions at the test plane. The test fuel signal $S(x,y)$ and background components $B(x,y)$ detected by the hodoscope are separately modeled, assuming that

$$F(x,y) = S(x,y) + B(x,y) \quad . \tag{B1}$$

S is composed of a separate profile $s_k$ for each fuel pin and an undetermined overall relative amplitude factor a, as

$$S(x,y) = a \sum_k s_k(x,y) \quad . \tag{B2}$$

Each $s_k$ consists of a Gaussian diametral profile and a predetermined axial profile $f_k$, as

$$s_k = g_k \exp\{-(x - h - d_k)^2/2\sigma^2\}\, f_k(y - v) \quad , \tag{B3}$$

where relative pin amplitudes $g_k$ are determined by pretest calculations and/or experiments and relative lateral pin positions $d_k$ are taken from known initial

geometry. Lateral and axial test bundle center locations h and v and lateral-spread parameter σ may be considered as undetermined parameters to be specified in the fit. Since only three hodoscope columns at most view a single pin, the assumed diametral profile is generally a sufficiently accurate representation of pin signal convoluted with lateral hodoscope response.

The axial pin profile usually consists of pellet-count, γ-ray scan, or fission-wire data convoluted with hodoscope axial response. A typical axial profile is shown in Fig. B-1 along with the experimental data used to obtain it. The effect of the truncated-cosine reactor axial power distribution is evident. To compensate for this effect, a uniform axial pin profile, such as shown in Fig. B-2, is often used in final EFFI fits.

The background, being rather diffuse and smooth, is generally well-represented by a polynomial. The form for B assumed in EFFI is

$$B = \sum_{mn} b_{mn} (x - h)^m (y - v)^n \quad , \tag{B4}$$

where m = 0, 1, 4 and n = 0, 1, 2 in the sum and the combination m = 4, n = 2 is omitted. The exponents chosen characterize mainly a lateral form dominated by test capsule geometry through neutron scattering and an axial form dominated by the truncated-cosine reactor power shape, as displaced from test bundle center.

If an iterative fitting procedure is accepted, F may be linearized in h, σ, and v by choosing initial estimates h', σ', and v', where $h = h' + \alpha$, $\sigma = \sigma' + \beta$, and $v = v' + \gamma$, and by expanding F in a Taylor series about the estimates, keeping only up to first-order terms, obtaining

$$F \approx F(h',\sigma',v') + (\partial F/\partial\alpha)\alpha + (\partial F/\partial\beta)\beta + (\partial F/\partial\gamma)\gamma \quad , \tag{B5}$$

where the derivatives are understood to be taken at $\alpha = \beta = \gamma = 0$. The derivatives with respect to α and β can be performed analytically, while that with respect to γ must be done numerically, noting that $\partial f_k/\partial\gamma = -\partial f_k/\partial y$. Then F can be written as a linear function of twelve fitting parameters $A_\ell$ in the form

$$F \approx \sum_{\ell=1}^{12} D_\ell(x,y)\, A_\ell \quad . \tag{B6}$$

For example, the indices in EFFI are arranged so that $A_1 = a$, $D_1 = \Sigma_k s_k$, $A_4 = a\gamma$, $D_4 = -\Sigma_k s_k(\partial f_k/\partial y)$, $A_5 = b_{0,0}$, $D_5 = 1$, $A_{12} = b_{1,2}$, and $D_{12} = (x - h')(y - v')^2$.

If the efficiencies are assumed to be randomly distributed among hodoscope channels, it makes sense to perform a minimum variance fit to the function

$$V = \sum_{ij} w_{ij} [F(x_i,y_j) - R_{ij}]^2 \quad , \tag{B7}$$

where $R_{ij}$ is the power-normalized count rate for the channel corresponding to hodoscope column i and row j, $w_{ij}$ is a statistical weight, and the sum is over all hodoscope channels. If a good fit is to be obtained, unbiased globally by systematic error, then any systematic error present must vary only locally (among neighboring channels) and not globally (extending over array). From $\partial V/\partial A_\ell = 0$, the following matrix equation is obtained,

$$\tilde{C}\,\vec{A} = \vec{B} \quad , \tag{B8}$$

where the matrix elements are given by

$$C_{p\ell} = \sum_{ij} w_{ij}\, D_p(x_i, y_j)\, D_\ell(x_i, y_j) \quad , \tag{B9}$$

and where

$$B_p = \sum_{ij} w_{ij}\, R_{ij}\, D_p(x_i, y_j) \quad . \tag{B10}$$

Expression B8 is a set of simultaneous linear equations for $A_\ell$. These equations are solved, then $\alpha$, $\beta$, and $\gamma$ are added to h', $\sigma$', and $\nu$', and a new iteration is begun. Iteration is continued until $\alpha$, $\beta$, and $\gamma$ are small compared to h, $\sigma$, and $\nu$. Once the fit parameters are determined, F is computed from Eq. B1 and the efficiency multiplier $e_{ij}$ for column i and row j is calculated for each channel from

$$e_{ij} = F(x_i, y_j)/R_{ij} \quad . \tag{B11}$$

EFFI also computes probable random errors in the fit parameters, to aid in judging the confidence in a given value.

Normally the weights $w_{ij}$ would be the inverse of the variance of $R_{ij}$ as determined from the parent statistical distribution. The variance in $R_{ij}$ caused by count statistics is nearly always small compared to that due to efficiency variation among channels. But the parent distribution of efficiencies is unknown. The functional form $R_{ij}^{-N}$ is assumed in EFFI for $w_{ij}$. The values N = 0, 1, and 2 have been tried. Generally $w_{ij} = 1$ (N = 0) seems to give the most satisfactory fit and is the form usually chosen. This form tends to preserve the ratio of total signal (sum of S over all channels) to total background (sum of B over all channels) to yield an accurate mass calibration factor, while N > 0 depresses this ratio.

In addition to the input described above, EFFI provides a number of options in the fitting procedure. Columns, rows, and/or individual channels may be excluded from the fit, such as may be desired for inoperative or spurious channels. The parameters h, $\nu$, and/or $\sigma$ may be fixed at the initial estimates ($\alpha$, $\gamma$, and/or $\beta$ = 0), thus fixing bundle position and/or lateral signal spread. The upper range of m and n in B may be restricted, simplifying the background profile model. The value of S/B at bundle center (x = h and y = $\nu$) may be fixed at an input value (predetermining a), providing a specified signal-to-background ratio. Or all parameters may fixed at input values to yield an arbitrary profile model.

## B3. Application in Transient Analysis

In normalizing efficiencies for a typical transient, first a fit is usually made to determine test fuel bundle center location (and optionally, pin signal width), using a model of the expected hodoscope response to initial fuel geometry as if each channel had the same efficiency. The best estimates of actual signal strength are used as input for relative pin amplitudes $g_k$ and axial pin profiles $f_k$. No parameters are generally fixed, but best estimates are input for iteration on bundle position. The efficiency multipliers for each channel supplied at this stage would provide uniform response to test fuel fission rate.

Usually uniform response to fuel mass is desired. If so, a second fit is performed to obtain new efficiency multipliers, using uniform pin profiles (constant fission rate over pins convoluted with hodoscope response, as in Fig. B-2, with equal amplitudes $g_k$) and constant background. Bundle location and lateral signal-spread are fixed to those of the first fit above and signal-to-background ratio is fixed to either that obtained in the first fit or that observed in the pretest scan. From knowledge of the total bundle mass and of the fraction of total count rate (as corrected by efficiency multipliers) due to test fuel signal, a mass calibration factor (mass per normalized count rate unit per channel) is derived.

For example, the mass calibration factor $C_P$ for count rates normalized by an average P over hodoscope channels peripheral to the test fuel is easily derived by noting that one may take P = B in the fit above, since B is constant. One obtains

$$C_P = MB/\sum_{ij} S(x_i, y_j) \qquad (B12)$$

as the factor to multiply count rate changes in R/P to yield fuel mass changes, where M is the total mass of the test fuel viewed by the hodoscope. The values of B and S in Eq. B12 are entries in tables output by EFFI. One must be careful in Eq. B12 to sum over the identical set of channels to be used in subsequent analysis. For count rates normalized by any other linear measure of power P', such as the channel array average or a reactor ion chamber, the corresponding mass calibration factor $C_{P'}$ can be obtained from Eq. B12 by noting that $C_{P'} = P'C_P/P$.

## B4. Random Errors

To determine the limits of accuracy of hodoscope data, the magnitudes and propagations of errors associated with the use of EFFI need to be understood. These errors may be random or systematic in nature and may involve the EFFI fit in the reference time interval, count rate changes in succeeding intervals, and residual effects from errors in the SUPRA fit (performed prior to the EFFI fit and described in Appendix A). Errors due directly to count statistics are discussed in the body of the paper and will not be mentioned here. Depending on the magnitude of the nonlinearity corrections in the reference interval, SUPRA errors can propagate errors in efficiency multipliers. SUPRA errors can also affect fuel motion in later time intervals. Errors associated with SUPRA are discussed in Appendix A and will not be further considered here.

Let us consider random errors involved in using EFFI. Those indentified here are associated with the reference time interval. Assuming excellent count statistics, most of this type of error is due to efficiency differences among channels. In fact, EFFI fits are predicated on a random distribution of efficiencies among channels. The uncertainty in test fuel center location for the average transient is perhaps 0.1 column and 0.5 row, leading to average efficiency errors of ~ 6% and ~ 2% (~ 10% for channels near the top or bottom of a fuel pin) per channel, respectively. Uncertainty in pin signal width perhaps averages 0.1 column, leading to ~ 6% efficiency error. Uncertainty in pretest scan S/B is perhaps 4%, leading to ~ 2% efficiency error (assuming S/B ~ 1).

Assuming these errors are uncorrelated, adding by quadrature yields a total random efficiency error for a channel of ~ 9% (~ 13% for channels near pin top ormass displacement errors, so the fuel displacement error due to random efficiency error becomes ~ 18% for a given channel, assuming S/B ~ 1. However, this error is reduced by the square root of the number of channels for

displacements occurring over more than one channel. The mass calibration factor random error becomes ~ 2% due to efficiency error (averaging over roughly a hundred or so channels viewing fuel). Another random error in the mass calibration factor is that in the fuel mass (as weighed). In the reference interval there is no error associated with the TREAT power coupling calibration factor, because it is not used in this normalization process.

B5. Systematic Errors

Unlike the above random errors, systematic errors do not usually fluctuate about an average, but bias the average, and do not add as quadratures, but generally add directly. There are several systematic error sources associated with the reference time interval, all due to deficiencies in the EFFI model. In several transients, pretest scans have revealed slight bowing and/or tilting of the test bundle which could cause ~ 10% average efficiency error in channels at pin top or bottom or at maximum bowing.

The assumption that S/B is constant, to first order, over the hodoscope array is implicit in the efficiency and mass normalizations described in Sec. B3. There is experimental evidence, including hodoscope data, that this is true for at least some experiments, even in cases where flux-shaping collars depress the thermal flux by as much as 50% near test fuel pin ends. Nevertheless, shaping collars are expected to depress the test fuel signal somewhat more than the background, leading to undercompensated efficiencies for test fuel inside the collar and apparent fuel loss when fuel is displaced later to inside the collar (see Appendix C). This loss has been estimated to be no more than 5% for E6, a typical transient in which shaping collars were used.

By the same reasoning, fuel displaced above the shaping collar and neutron filter is expected to register a larger mass gain than actually occurs. The change in thermal-flux magnitude is much greater in this case. In the PINEX-2 transient this factor, combined with decreased self-shielding of dispersed fuel, caused the estimate of fuel ejected into the plenum to be ~ 80% or so too high, according to posttest sectioning and weighing. The extension of collars and filters beyond the expected range of fuel dispersal, where possible, would result in significantly better mass resolution of dispersing fuel.

Another potential systematic error source associated with the reference time interval is the S/B used in the final EFFI fit. The presently used pretest scan S/B value is probably close to the value needed, based on theoretical grounds and comparison of post-test results with hodoscope data. However the initial EFFI fit provides an S/B based on transient data which is usually larger than the pretest scan S/B, sometimes by as much as ~ 50%, apparently due to systematic variation of efficiencies among channels. This variation of efficiencies among channels is not presently understood. If an S/B which is too large (small) were used in the final EFFI fit, the efficiencies outside the reference fueled region would be low (high) relative to the derived mass calibration factor, so that calculated mass displacements outside the reference fueled region would be low (high). This problem is aggravated by a lack of sufficient instrumented peripheral channels to accurately determine background. There are future plans to instrument these channels.

Other sources of systematic error, such as self-shielding, self-multiplication, radiation attenuation, fuel enrichment gradation among pins, control rod motion, and reactor spectrum shifts, come into play only as fuel motion evolves beyond the reference time interval. This is because the efficiency multipliers determined from EFFI provide a uniform mass per normalized count rate unit for each channel for the reference time interval (at least to first order), so that only count rate changes in succeeding time

intervals due to changes in these effects are relevant. Thus, for example, these effects are unimportant in determining sensitivity to small fuel displacements.

## APPENDIX C

## CORRECTIONS FOR FLUX-SHAPING COLLARS

A semi-empirical correction for the effect of flux-shaping collars has been derived (31) and tested against the axial-profile data for AX1 and the L-series transients. The resulting equation is:

$$\Omega' = (\pi\tau\Sigma_a^c/\Sigma_a^m)\,[x_2/(\rho^2 + x_2^2) - x_1/(\rho^2 + x_1^2) + 1/\rho\,[\tan^{-1}(x_2/\rho) - \tan^{-1}(x_1/\rho)]], \quad (C1)$$

with the following definitions:

$\Omega'$ = the effective solid angle subtended by the collar at a point on the fuel axis

$\tau$ = thickness of the collar

$\Sigma_a^c$ = total macroscopic absorption cross section of the collar

$\Sigma_a^m$ = total macroscopic absorption cross section for absorbing material of uniform density assumed by the model to be inside the collar.

$\rho$ = radius of the collar

$x_{1,2}$ = axial position of the ends of the collar.

The geometry is shown in Fig. C-1.

The correction has been used (additively) for multiple-collar configurations with no compensation for fine details such as spectrum hardening through multiple collars. This lack of compensation for spectrum shift is not expected to significantly affect the above results because the cross sections enter as a ratio.

R. Simms (32) has noted that the presence of shaping collars does not result in abrupt flux changes internally, and has approximated the filter discontinuity by assuming the effect is proportional to the solid angle subtended by the collar at the "dose point." An additional factor sinθ was derived (33) and used in obtaining Eq. C1.

Certain applications have been made of the formalism. In experiment AX1, the only power-profile data available came from a fuel-pellet count. As a result, the corrections were applied (for the purposes of testing the correction) only over the central region where fuel self-shielding effects are constant. The results are shown in Fig. C-2, which also displays the relative collar and fuel configurations. The change in self shielding is readily seen by the poorness of the fit near the ends of the fuel.

In another case, the L-series experiments, the methodology developed must apply over a greater length and larger errors must be expected. An axial monitor wire traverse (using 30-mil-dia uranium-zirconium wire, 3.5 w/o U @ 93.3% $U^{235}$) is available for the L-series mockup with an L8 trial transient. Two-inch segments of the wire were counted.

By using the axial-flux profile given by Kirn, et al. (34) in the collar-correction program, a result qualitatively in good agreement with experiment was obtained. Although a close fit may be had by adjusting the program parameters, there is little justification for this approach. It is likely that the flux shape given by Kirn does not in fact faithfully represent the flux near the test loop.

Hodoscope data for Tests AX1, L8 and L8(SCAN) were used to determine a chopped-cosine axial-flux profile having a half-wavelength of $\lambda/2 \sim 141$ cm. This is to be compared with a $\lambda/2 \sim 180$ cm that corresponds to the TREAT buckling of $B^2 = 3.1 \times 10^{-4}$ cm$^{-2}$.

These results motivated calculations (35) for the TREAT flux vs. axial position, for two groups, >0.82 MeV and <0.68 eV. The results confirm the above findings and generally show the fast flux dropping off substantially faster than the low-energy group as the flux approaches the axial-reflector boundary. This behavior is also a well-known result of the two-group diffusion method for multiregion reactors. However, the fission rate near the test loop apparently follows the fast-flux profile. The reasons for this are not understood. Because the signal is proportional to the fission rate and the background is proportional to the fast flux (to first order), the EFFI normalization may be accurate to first order without a collar correction.

The value of $\lambda/2 = 141$ cm was used in the collar-correction program along with an increase in the overall constant K from 1.85, found to optimize the fit for AX1, to 2.775; the resulting fit is shown in Fig. C-3. The poorness of the fit in the region of row 5 is due to the assumption of a simple cosine flux profile.

The comparisons made above to test the collar correction are sensitive to the assumed shape of the axial-flux profile. (It should be emphasized that the collar correction is based on geometrical considerations and does not require knowledge of the actual flux profile.) Although there is no real substitute for having a monitor-wire traverse in the L-series mockup without fuel or collars, some mechanism of approximating the perturbations of the test loop on the axial flux is desirable. One approach might be to make a better fit to the hodoscope efficiency data than the simple cosine.

The collar-correction program has recently been integrated with the existing hodoscope data-processing programs. Preliminary results for the L7 transient show that the magnitude of the correction is generally less than 20%, but could be much larger in some regions. This correction program is still in a development stage and has not been tested on an independent data source, such as posttest examination.

ACKNOWLEDGMENTS

The authors are indebted to D. Burrows, Doug Ray, and others at TREAT for operation and maintenance of the hodoscope and to R.R. Stewart and J.P. Regis for constant support in the handling and processing of data.

REFERENCES

[1] A. De Volpi, R.J. Pecina, R.T. Daly, D.J. Travis, R.R. Stewart, and E.A. Rhodes, "Fast-Neutron Hodoscope at TREAT: Development and Operation," Nucl. Techn. 27: 449 (1975).

[2] A. De Volpi, R.R. Stewart, J.P. Regis, G.S. Stanford, and E.A. Rhodes, "Fast-Neutron Hodoscope at TREAT: Data Processing, Analysis, and Results," Nucl. Techn. 30: 398 (1976).

[3] A. De Volpi, "Fuel and Cladding Motion Surveillance," Proceedings of the Intl. Mtg. on Fast Reactor Safety and Related Physics, USERDA CONF-761001 II: 846 (1977).

[4] A. De Volpi, P. Bertoncini, C. Fink, A. Klickman, L.W. Person, E. Rhodes, G.S. Stanford, and R. May, "Current and Advanced Methods for Determining Quantitative Fuel Dispersion Using Hodoscope Data," p. 2279, Proceedings of the International Meeting on Fast Reactor Safety Technology, American Nuclear Society (1979).

[5] E. Rhodes, A. De Volpi, C. Fink, G. Stanford, and R. Pecina, "TREAT Fast-Neutron Hodoscope: Improvements in Time and Mass Resolution of Fuel Motion," IEEE Trans. Nucl. Sci. NS-26 (1): 809 (1979).

[6] A. De Volpi, A.R. Jamrog, R.J. Pecina, D.J. Travis, C.L. Fink, R.R. Stewart, N.A. Kramer, and P.H. Hofhine, "Design, Installation, and Operation of New Hodoscope Collimator at TREAT," Trans. ANS 24: 273 (1976).

[7] C.L. Fink, D.L. Smith, and R. Daly, "Efficiency Measurements on a Hornyak Button Detector and a Fission Counter Using Mono-Energetic Neutrons," ANL/RAS 77-09 (Apr. 1977), (unpublished).

[8] C.L. Fink, A. De Volpi, and G. Stanford, "Advances in Clad Blockage Detection," Transactions of the Second Technical Exchange Meeting on Fuel- and Clad-motion Diagnostics for LMFBR Safety Test Facilities, ANL/RAS 76-34 (unpublished Argonne National Laboratory report) (1979).

[9] R. Simms, "An Interpretation of Fuel Motion in Recent TREAT Experiments with LMFBR Fuel," ANL/RAS 79-18 (July 1979).

[10] C.L. Fink, A. De Volpi, and C.A. Ford, "Status Report on Clad-Blockage and Sodium Void Detection," Specialists' Meeting on Fuel and Cladding Motion Diagnostics, Los Alamos, NM (Dec. 1977), (unpublished).

[11] A. De Volpi, "High-resolution Fast-neutron and Gamma Digital Radiography," IEEE Trans. Nucl. Sci. NS-23 (1), 350 (1976).

[12] A. De Volpi, "High Resolution Radiography by Means of a Hodoscope," U.S. Patent 4092542 (30 May 1978).

[13] E. Rhodes, A. De Volpi, C. Fink, G. Stanford, and R. Stewart, "Hodoscope In-Situ Radiography", Transactions of the Second Technical Exchange Meeting on Fuel- and Clad-Motion Diagnostics for LMFBR Safety Test Facilities, ANL/RAS 76-34 (unpublished Argonne National Laboratory report) (1979).

[14] A. De Volpi, W.C. Kaiser and J.J. Eichholz, "Multi-Detector Integrated Fission Counter Array," IEEE Trans. Nucl. Sci. NS-23 (1), 307 (1976).

[15] O. Gailar and A.E. Klickman, "The Effects of Fuel Distribution on Fission Density in TREAT Experiments," Proceedings of the International Meeting on Fast Reactor Safety Technology, American Nuclear Society (1979).

[16] e.g., R.W. Albrecht, private communication (Sept. 30, 1979).

[17] A. De Volpi, "Estimates of Variance and Merit Ratios from Measured Quantities of Fluctuating Origin and Inherent Correlation," Intl. J. Appl. Rad. & Iso. 22: 103 (1971).

[18] G.J. Berzins and A.H. Lumpkin, "PINEX-2: Pinhole-TV Imaging of Fuel Ejection from an Internally Vented Capsule," p. 2235, Proceedings of the International Meeting on Fast Reactor Safety Technology, American Nuclear Society (1979).

[19] A.H. Lumpkin, G.J. Berzins, R.A. Cosimi, T.E. O'Hare, and J.R. Davidson, "Developments in the LASL Fuel Pin Imaging System: PINEX-3A," p. 2243, Proceedings of the International Meeting on Fast Reactor Safety Technology, American Nuclear Society (1979).

[20] A. De Volpi, G.S. Stanford, C.L. Fink, E.A. Rhodes, and M.R. Fenrick, "Text Processing for the Professional Staff," Industrial Research/Development, p. 22 (Jan. 1980).

[21] Argonne National Laboratory unpublished reports 75-57, 76-16, 76-79, 76-130, 77-25, 77-44, 77-54, 77-93, 78-24, 78-73, 79-67 (1975-1979).

[22] C.E. Dickerman, A.B. Rothman, A.E. Klickman, B.W. Spencer, and A. De Volpi, "Summary of TREAT Experiments on Oxide Core-Disruptive Accidents," Argonne National Laboratory Report ANL-79-13 (1979).

[23] H.U. Wider, A.M. Tentner and P.A. Pizzica, "The PLUTO2 Overpower Excursion Code and a Comparison with EPIC," p. 120, Proceedings of the International Meeting on Fast Reactor Safety Technology, American Nuclear Society (1979).

[24] A.M. Tentner and H.U. Wider, "LEVITATE - A Mechanistic Model for the Analyses of Fuel and Cladding Dynamics Under LOF Conditions for SAS4A," p. 1988, Proceedings of the International Meeting on Fast Reactor Safety Technology, American Nuclear Society (1979).

[25] K. Bohnel and H. Bluhm, "First Results of the CABRI Neutron Hodoscope," p. 2261, Proceedings of the International Meeting on Fast Reactor Safety Technology, American Nuclear Society (1979).

[26] E.A. Rhodes, "Evaluation of Ex-core Imaging Apertures for STF," Transactions of the Second Technical Exchange Meeting on Fuel- and Clad-motion Diagnostics for LMFBR Safety Test Facilities, ANL/RAS 76-34 (unpublished Argonne National Laboratory report) (1977).

[27] K.T. Stalker, L.M. Choate, and L.D. Posey, "The Potential of High Speed X-Ray Cinematography as a Fuel Motion Diagnostic for Safety Test Facilities," p. 2270, Proceedings of the International Meeting on Fast Reactor Safety Technology, American Nuclear Society (1979).

[28] J.G. Kelly, K.T. Stalker, D.A. McArther, K.W. Chu and J.E. Powell, "Theory and Application of the Coded Aperture Fuel Motion Detection System" p. 2302, Proceedings of the International Meeting on Fast Reactor Safety Technology, American Nuclear Society (1979).

[29] R.W. Engstrom and E. Fischer, "Effects of Voltage-Divider Characteristics on Multiplier Phototube Response," Rev. Sci. Instr. 28: 525 (1957).

[30] L.O. Johnson, "A High Rate NaI Detector System," IEEE Trans. Nucl. Sci. NS-26, 465 (1979).

[31] A.K. Gupta and N. Nath, "Gain Stability in High-Current Photomultipliers at High Variable Counting Rates," Nucl. Instr. and Methods 53, 352 (1967).

[32] Unpublished information (Memo to L.J. Harrison from R. Simms dated 30 May 1974, entitled "Filtering at Pump Clamp of Mark-IIC and its Effects on Loop Safety.")

[33] Argonne National Laboratory unpublished report ANL-RDP-88 (Reactor Development Program Progress Report Oct. 1979)

[34] F. Kirn, J. Boland, H. Lawroski, and R. Cook, "Reactor Physics Measurements in TREAT," ANL-6173 (1960).

[35] Unpublished information (Memo to G.E. Marsh from G. Klotzkin dated 8 August 1979, entitled "Transmittal of TREAT Axial Flux Profile.")

## LIST OF FIGURES

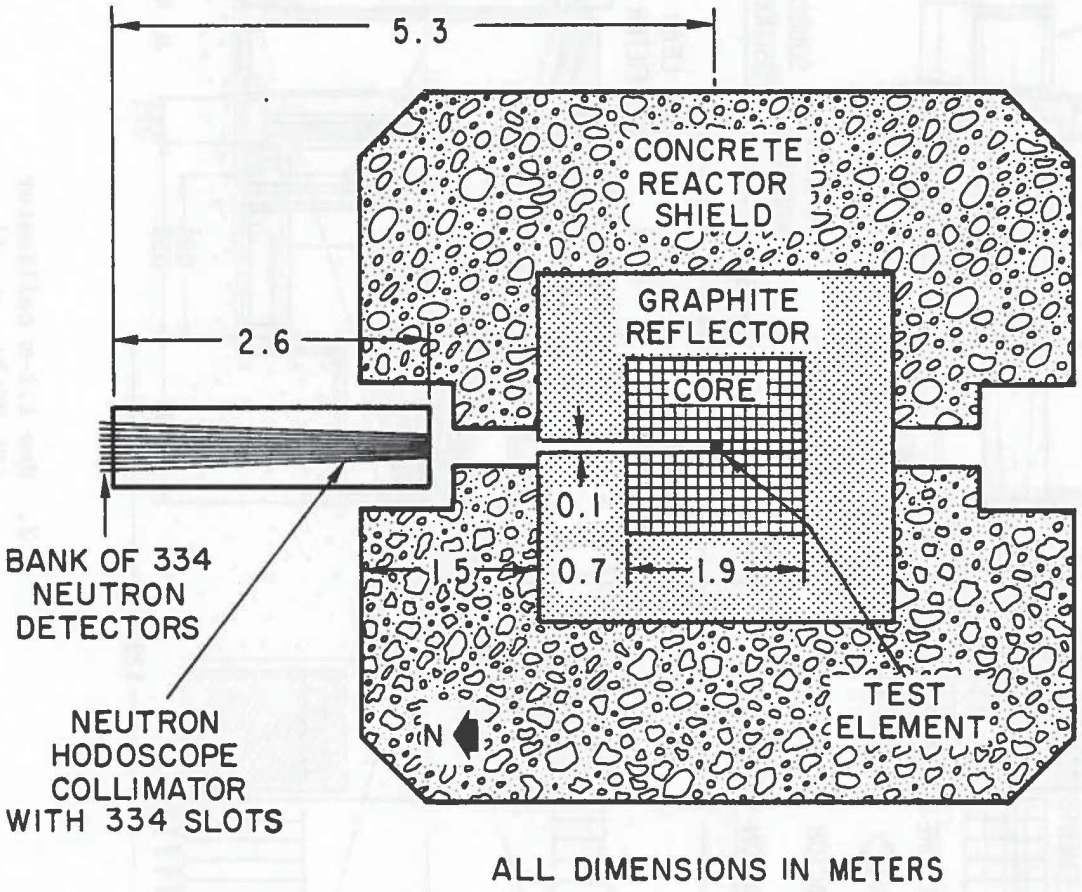


1. Plan view of 0.5-m hodoscope collimator at TREAT
[DE VOLPI, et al]

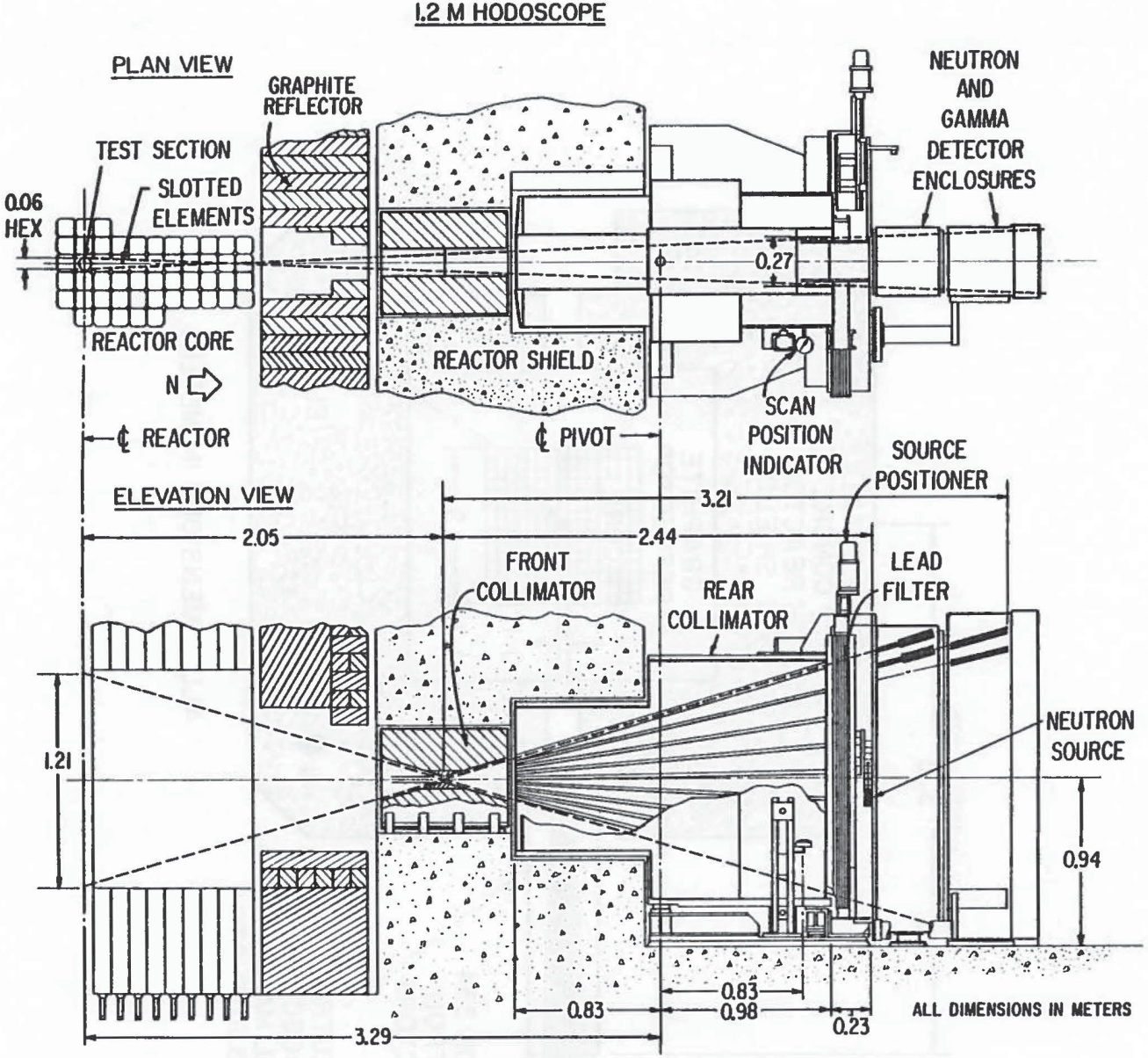


2. New 1.2-m collimator
[DE VOLPI, et al]

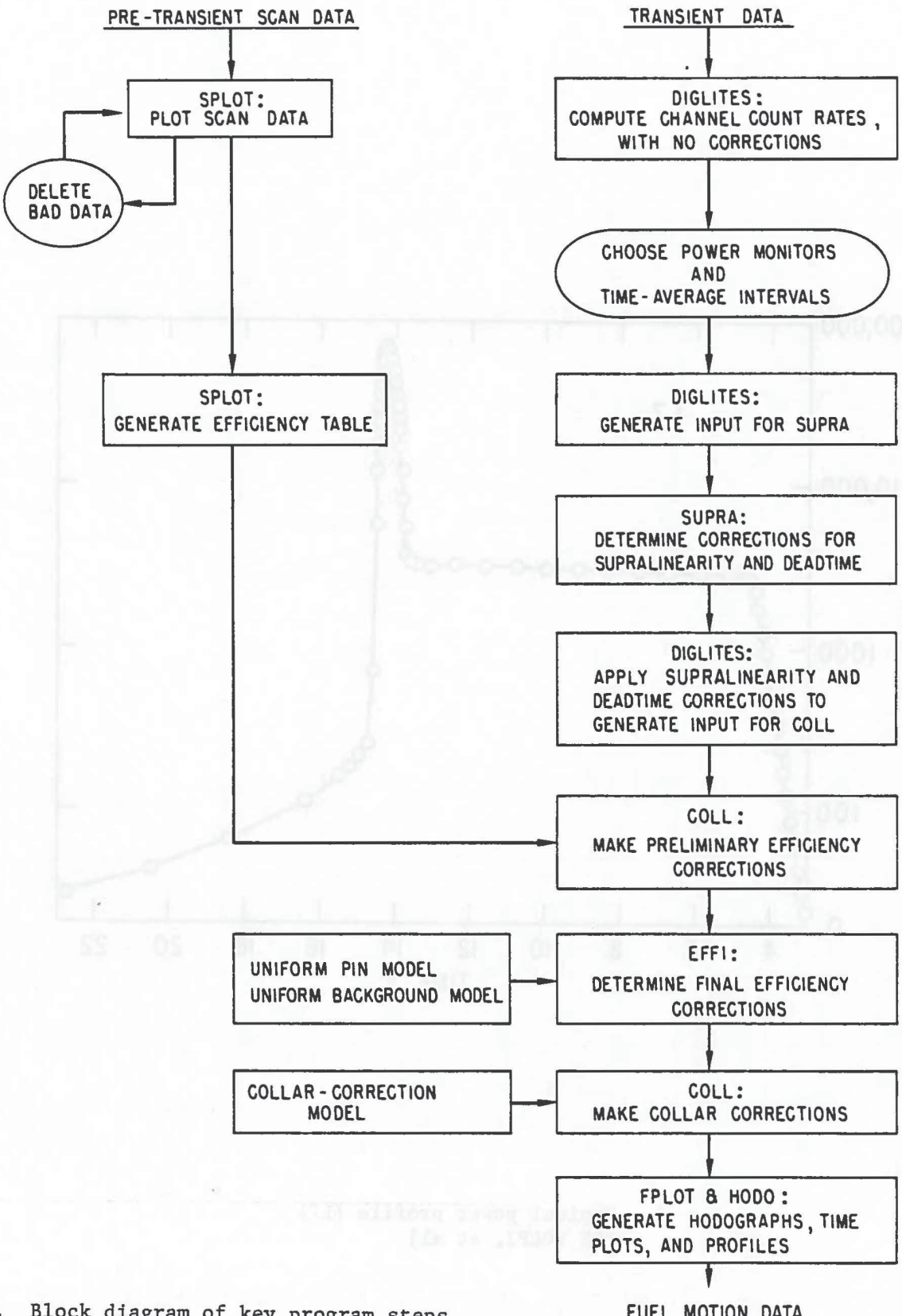


3. Block diagram of key program steps [DE VOLPI, et al]

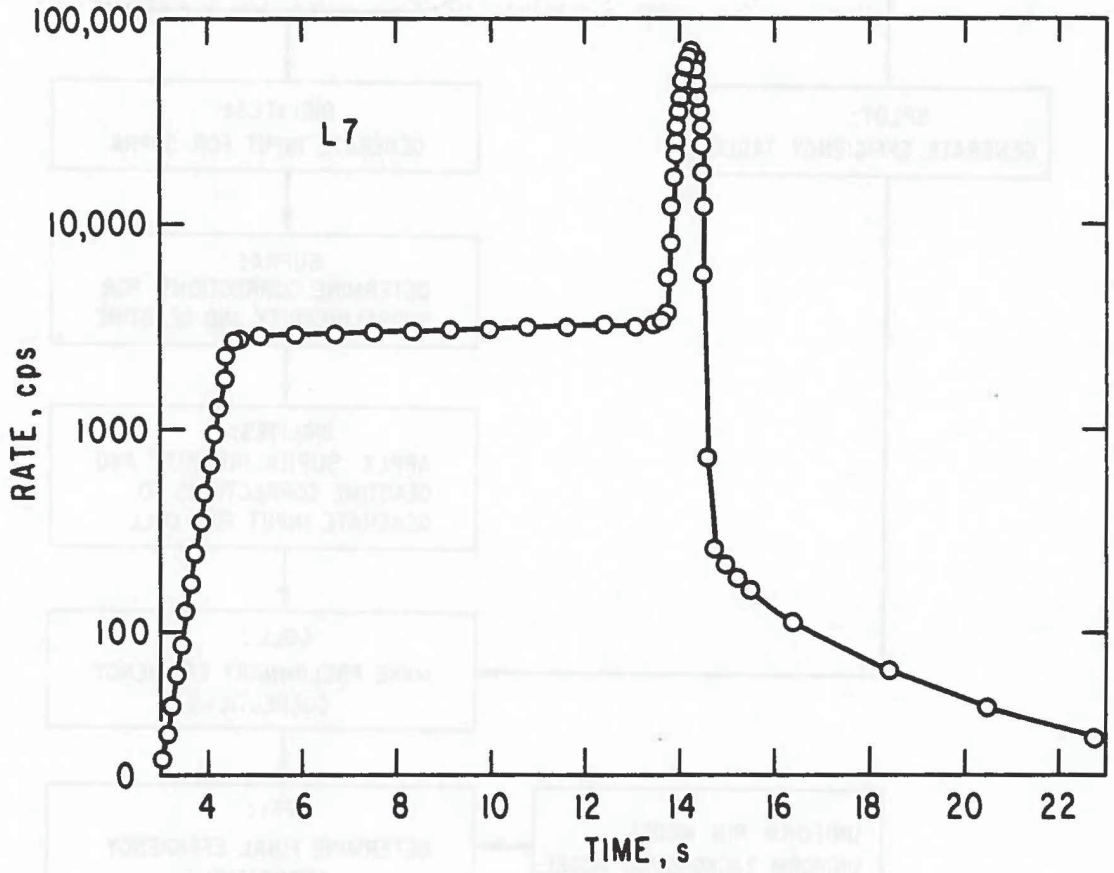


4. Typical power profile (L7)
[DE VOLPI, et al]

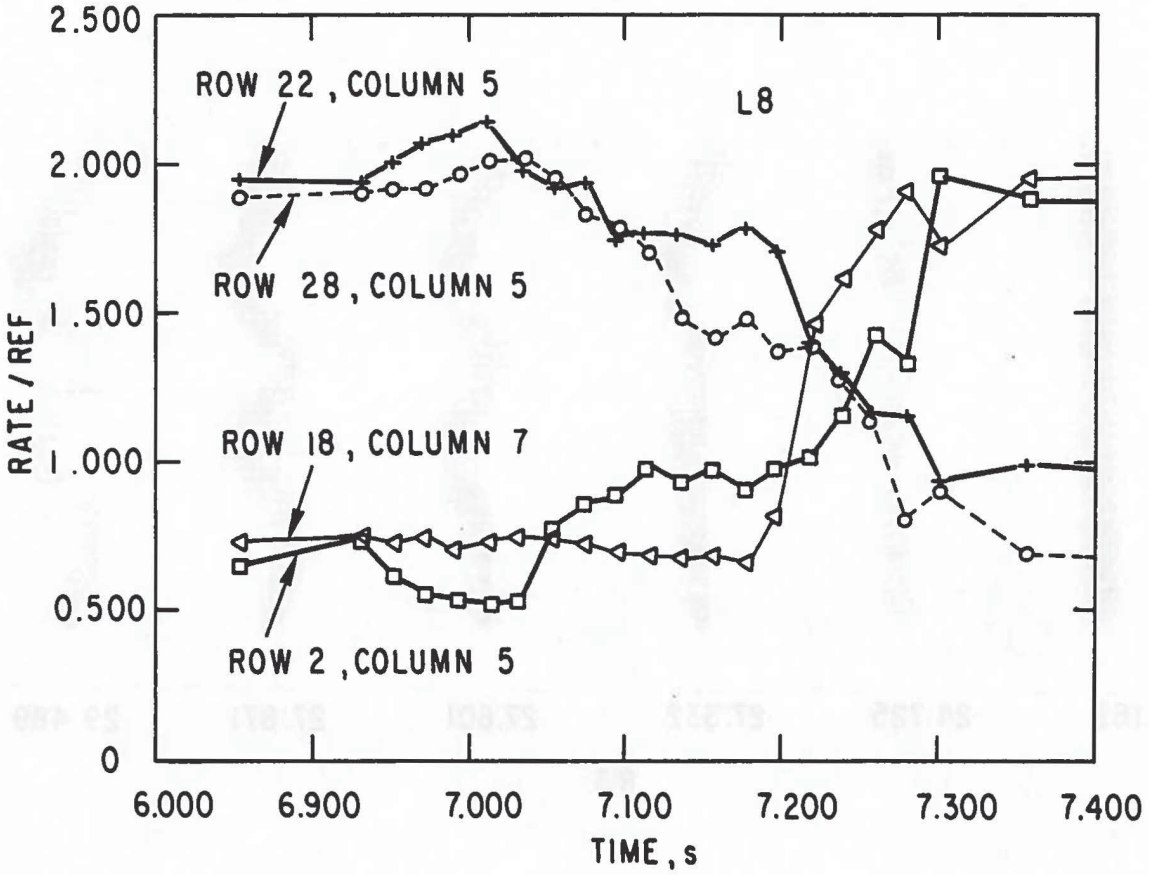


5. Power-normalized count-rate history (L8) [DE VOLPI, et al]

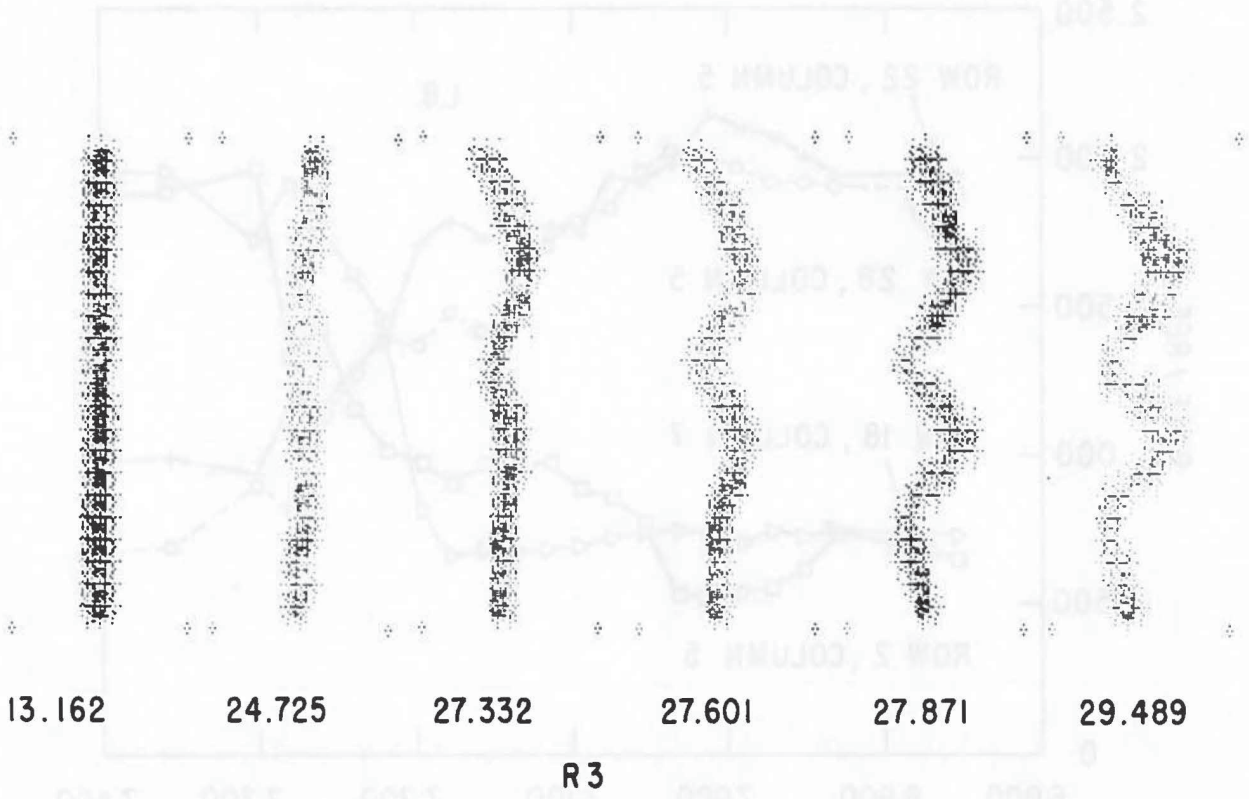


6. Intensity-modulated hodographs (R3)
[DE VOLPI, et al]

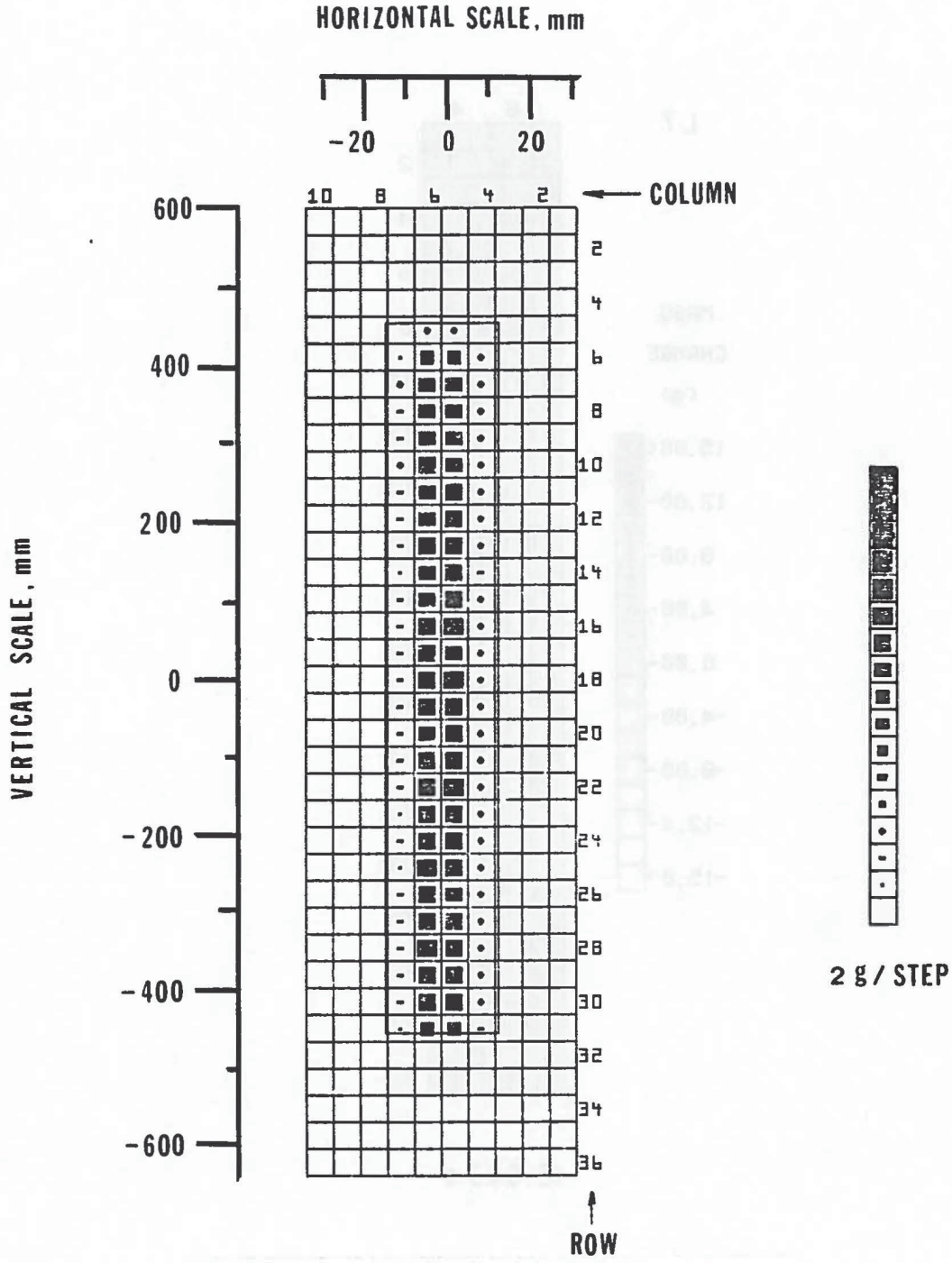


7. Symbolic hodographs (R8)
[DE VOLPI, et al]

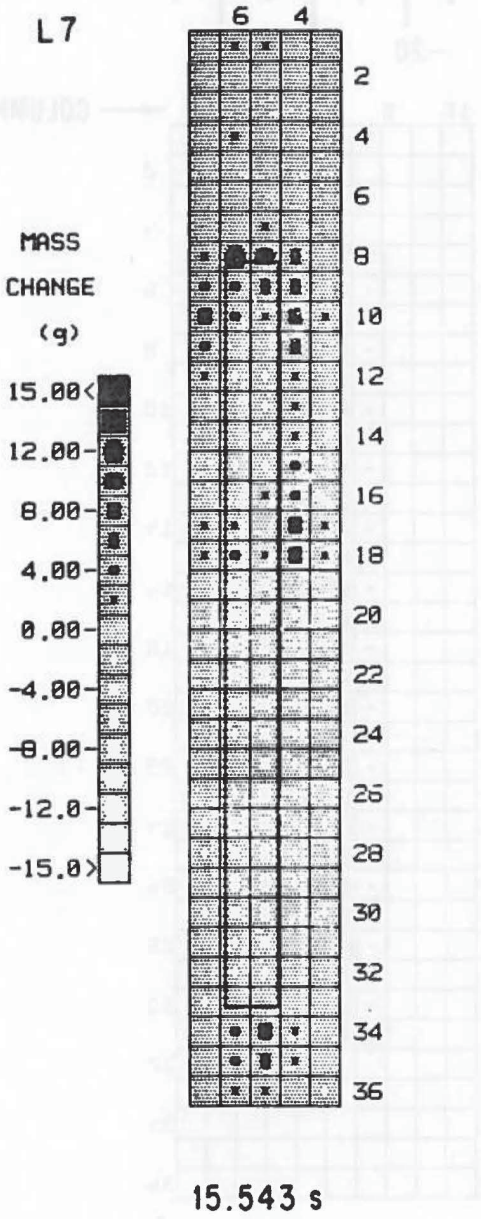


8. Differential hodographs (L7)
[DE VOLPI, et al]

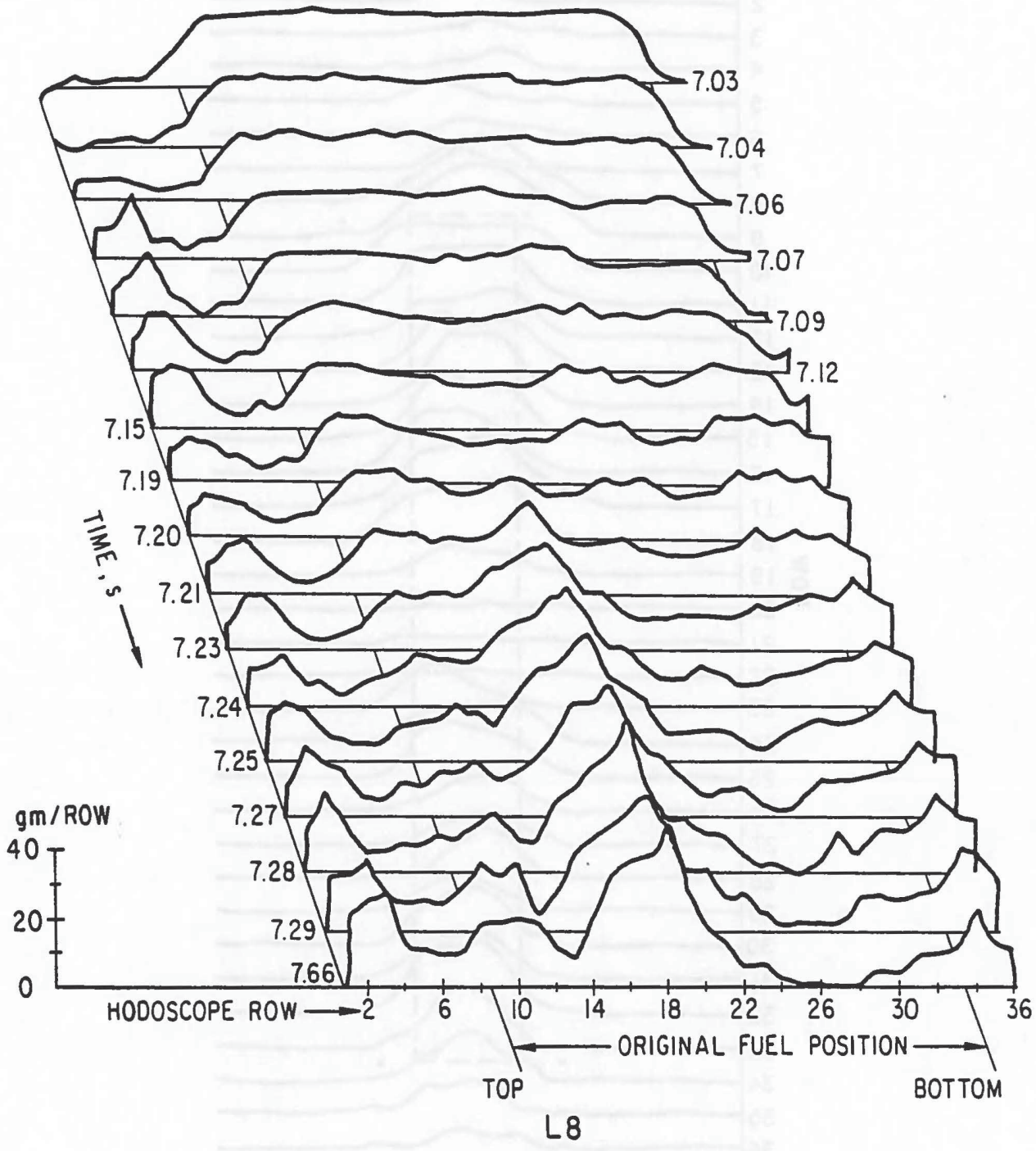


9. Three-parameter axial profiles (L8)
[DE VOLPI, et al]

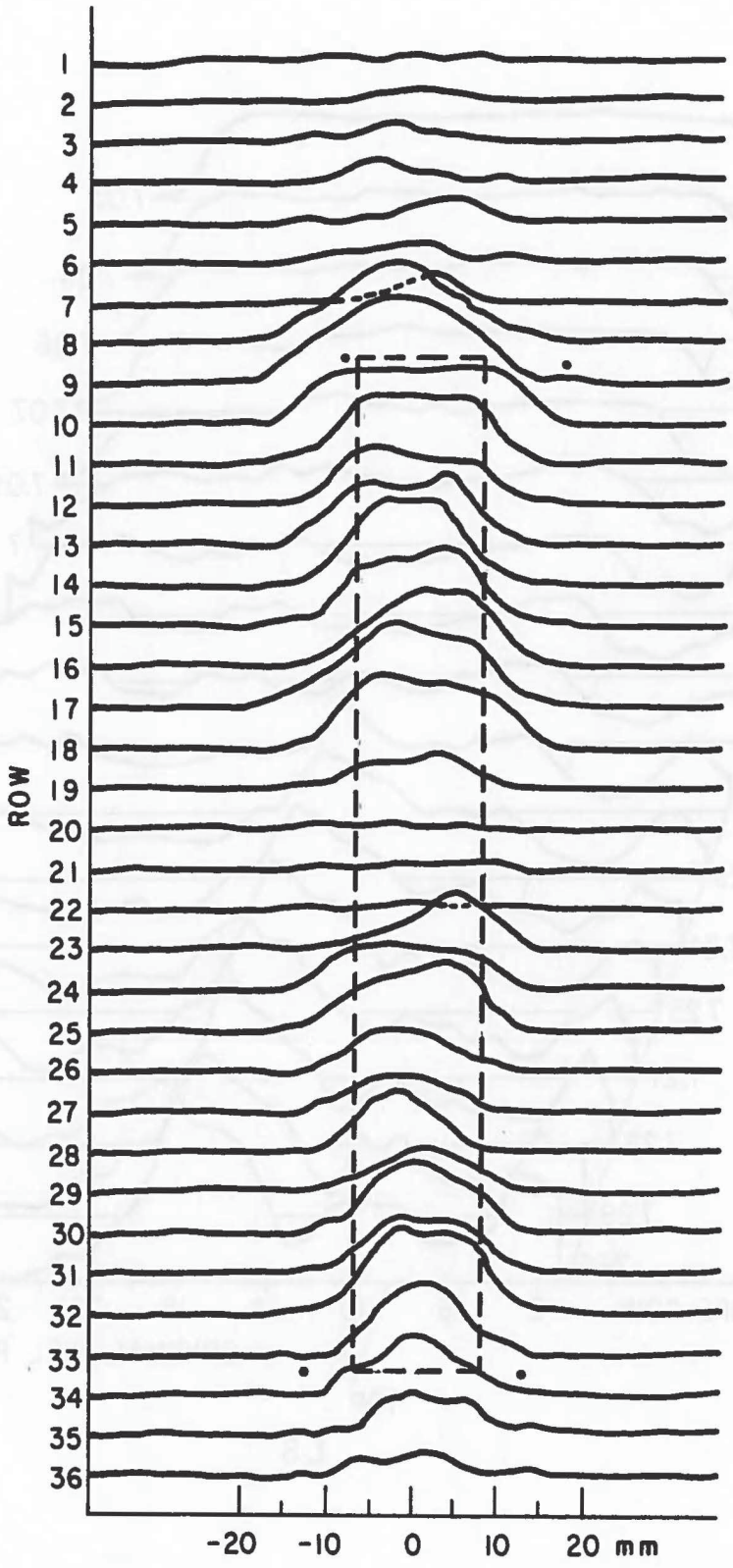


10. Post-transient in-situ fast neutron radiographic scan profile (L7) [DE VOLPI, et al]

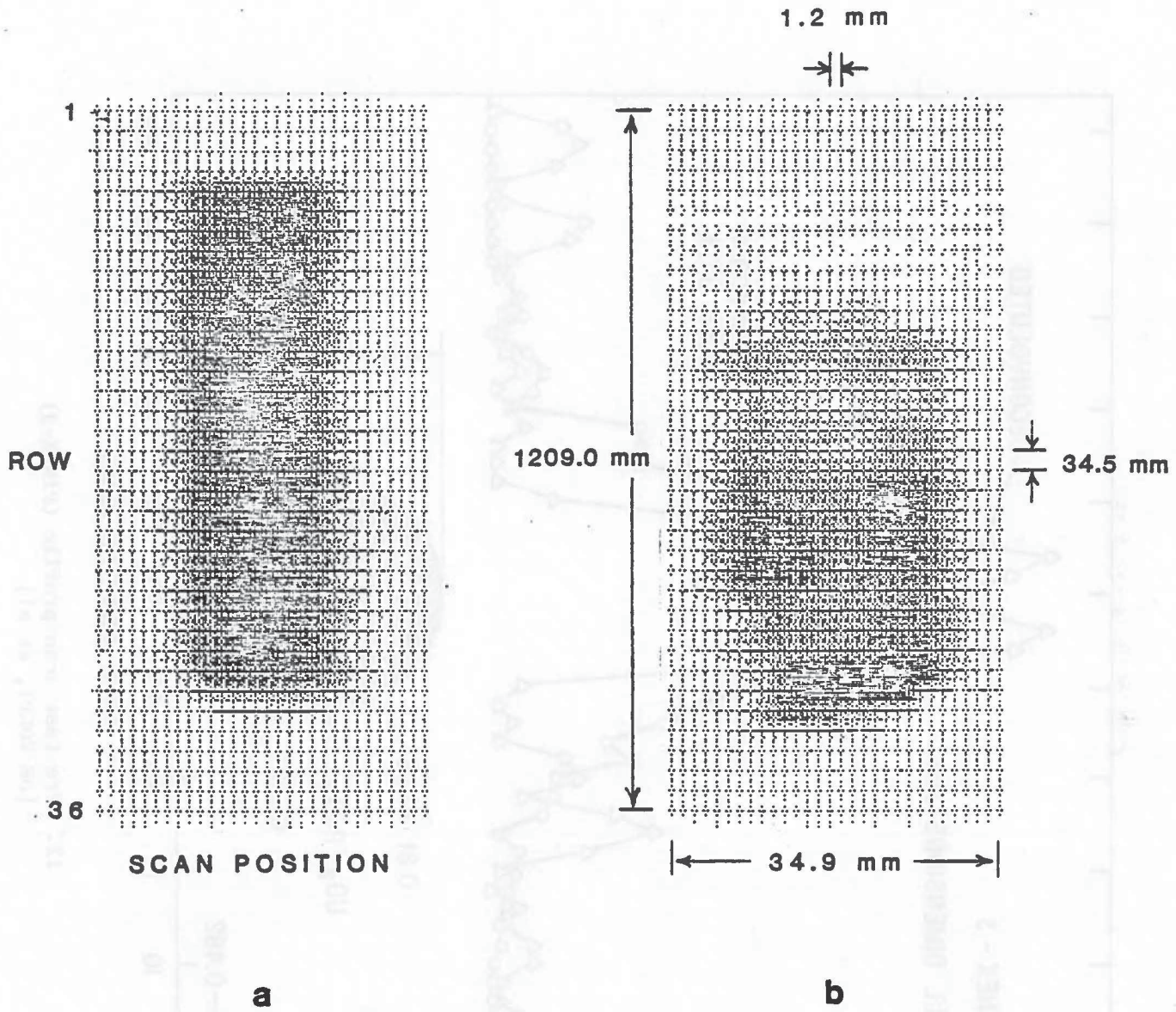


11. Hodographs depicting pretest (a) and posttest (b) fuel disposition (R8) [DE VOLPI, et al]

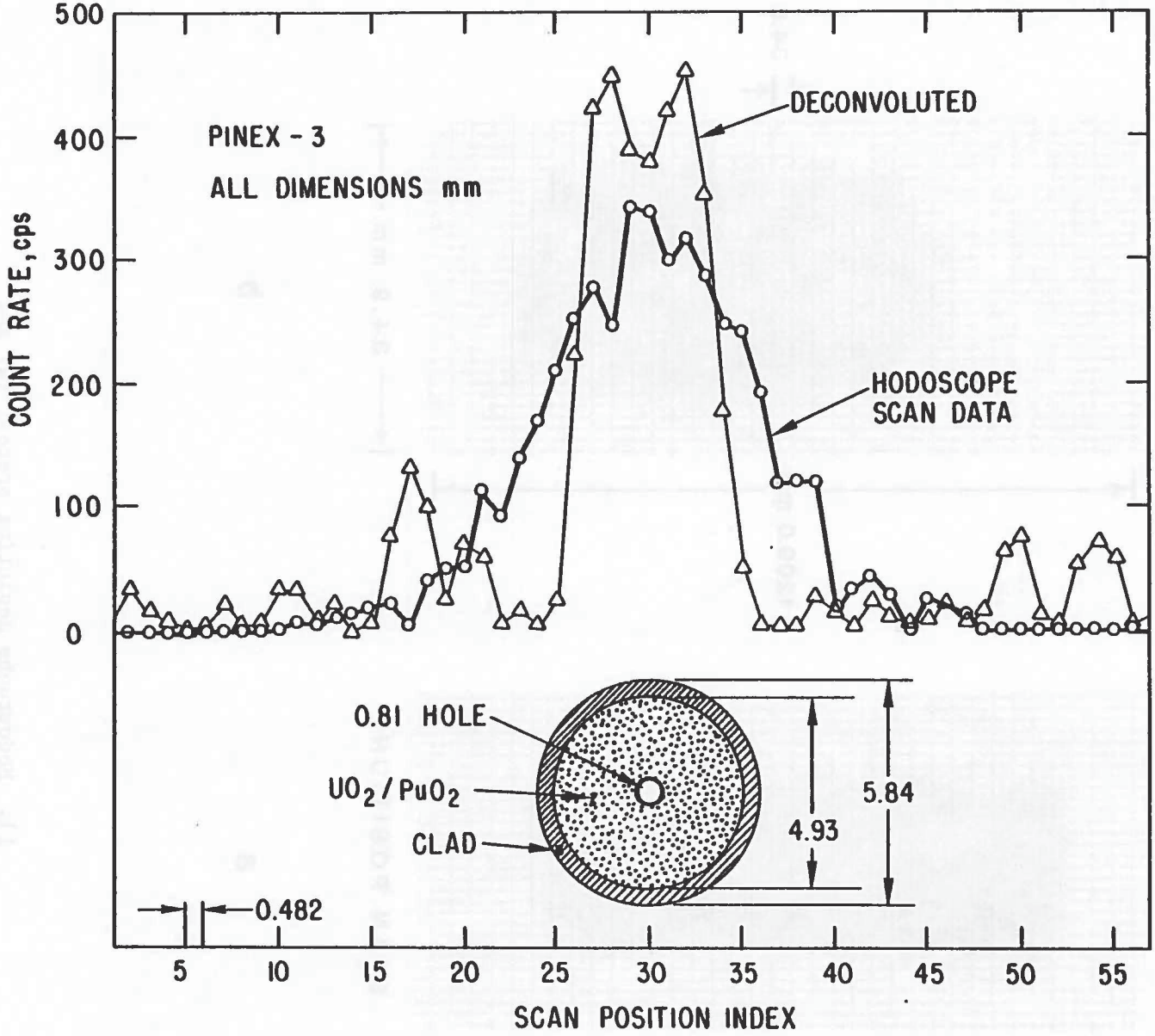


12. Pre test scan profile (PINEX-3)
[DE VOLPI, et al]

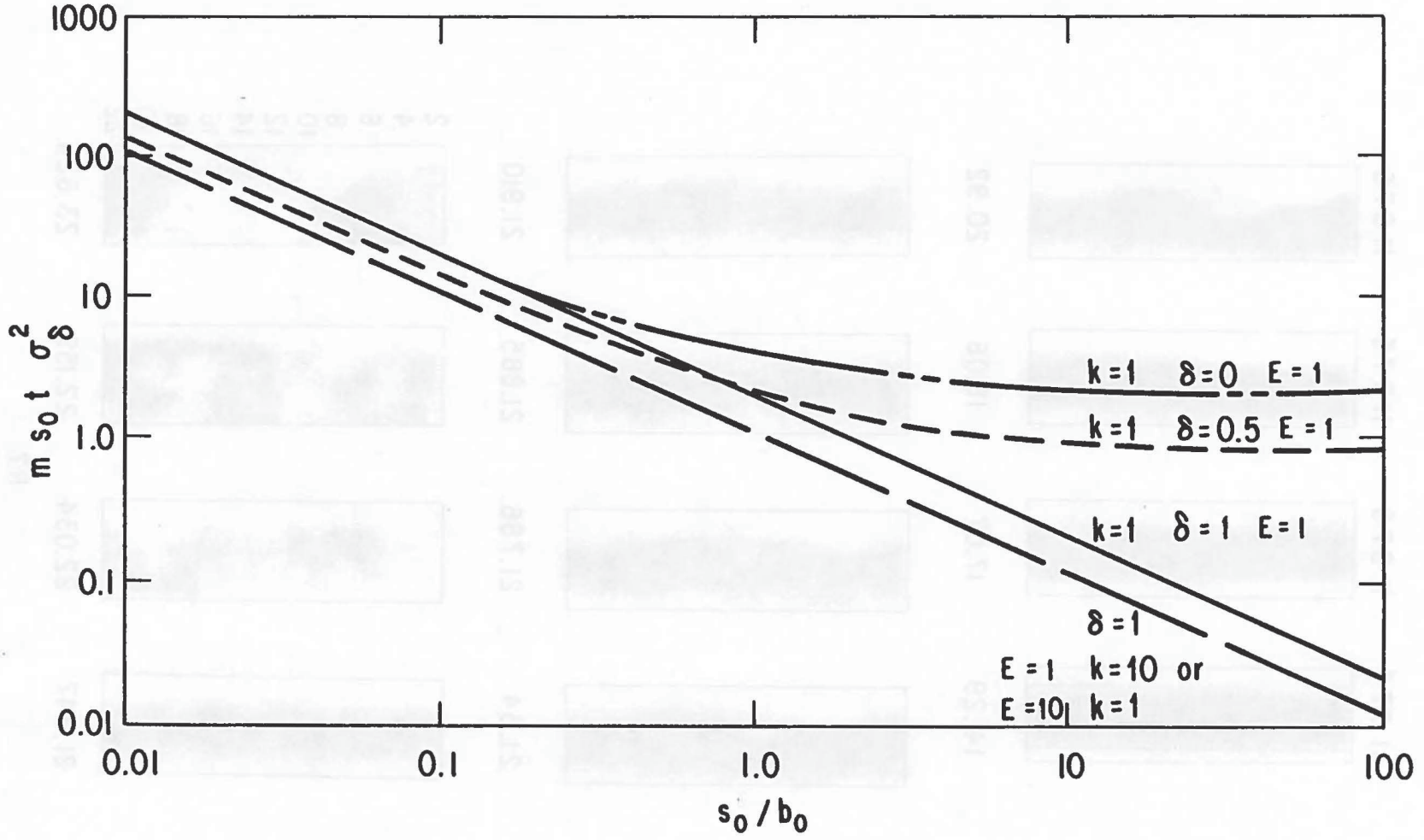


13. Parametric dependence of detection sensitivity upon signal/background ratio
[DE VOLPI, et al]

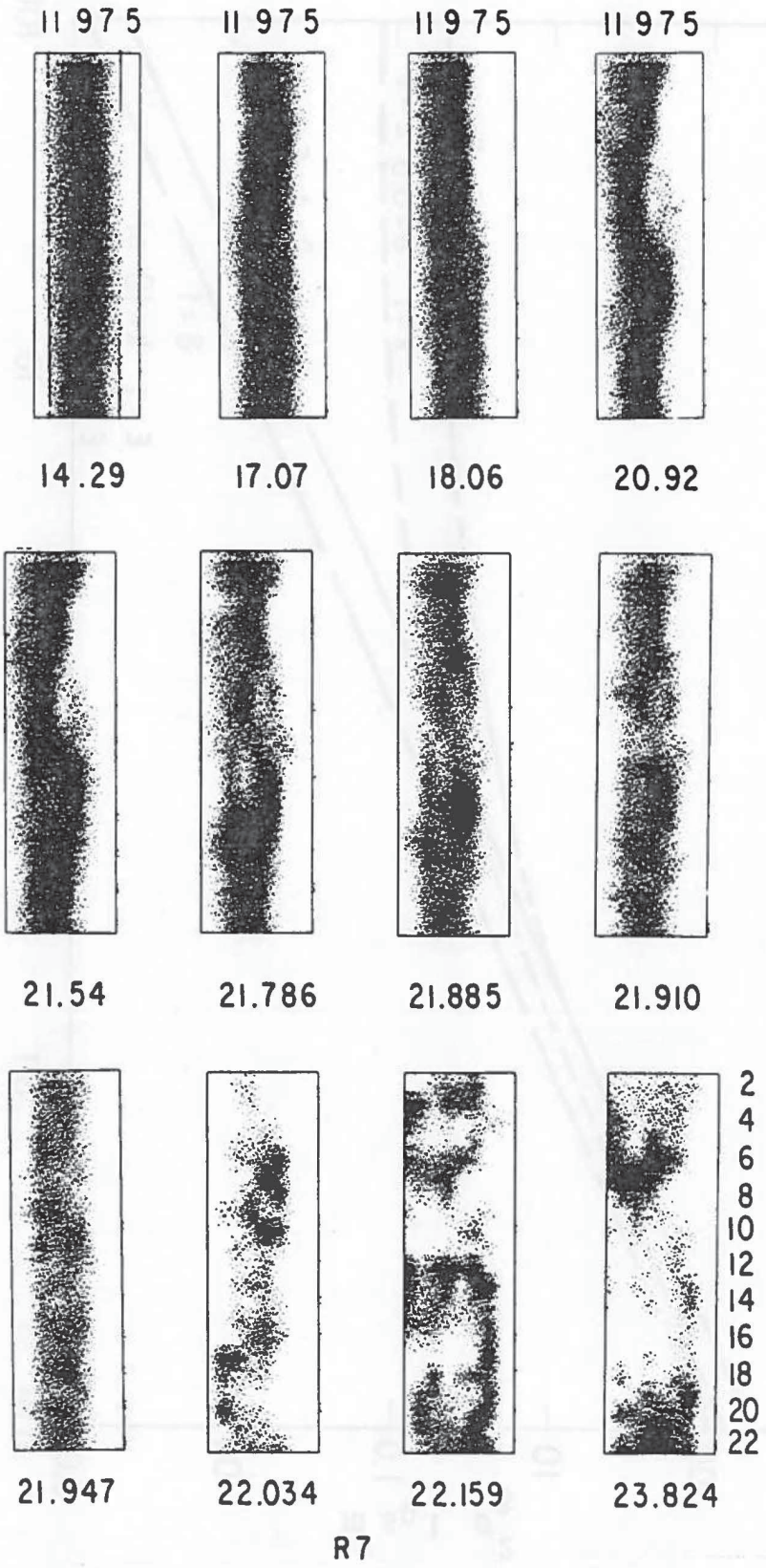


14. Destruction of a 7-pin cluster (R7)
[DE VOLPI, et al]

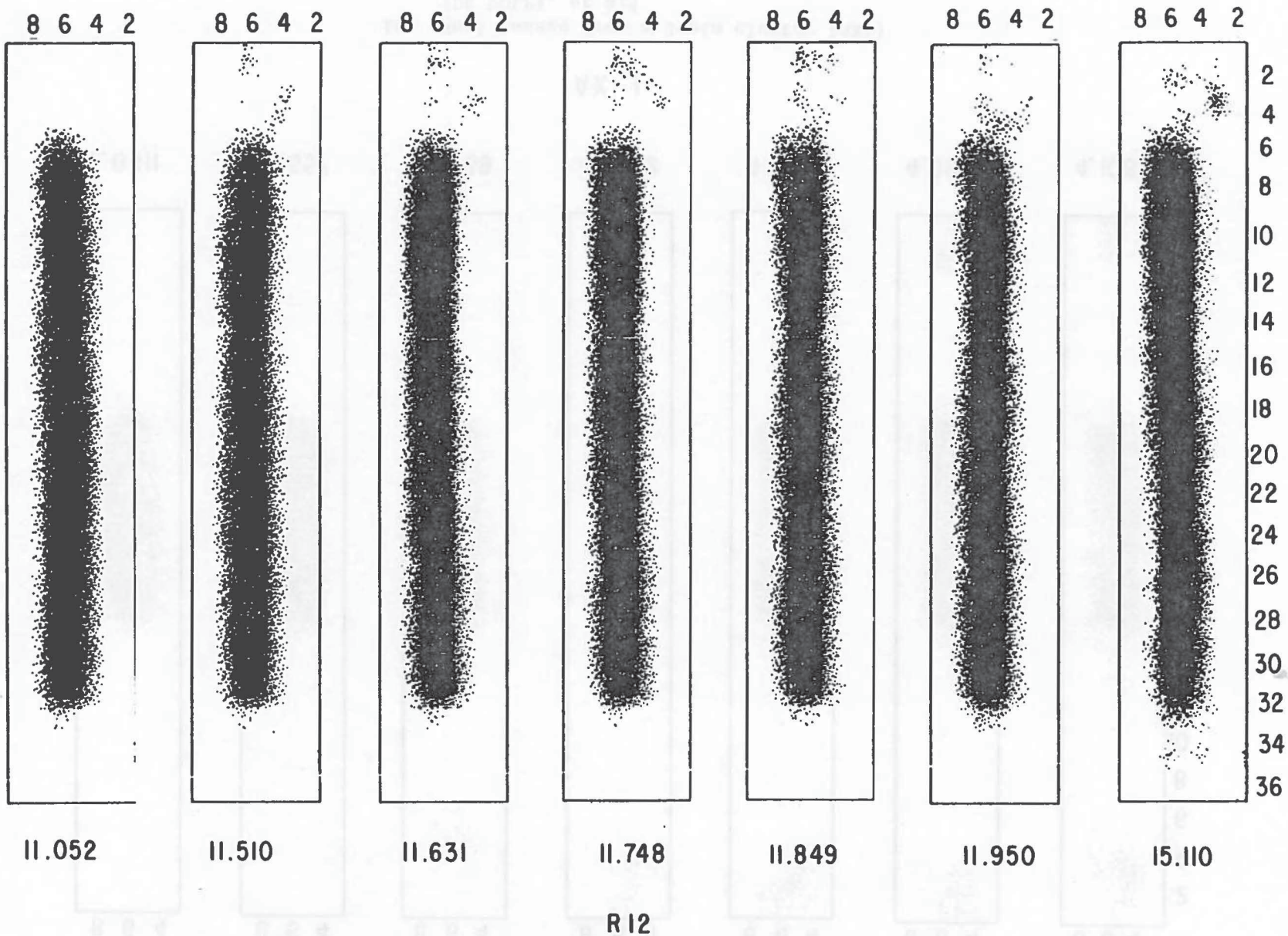


15. Partial loss of fuel from a 7-pin cluster (R12)
[DE VOLPI, et al]

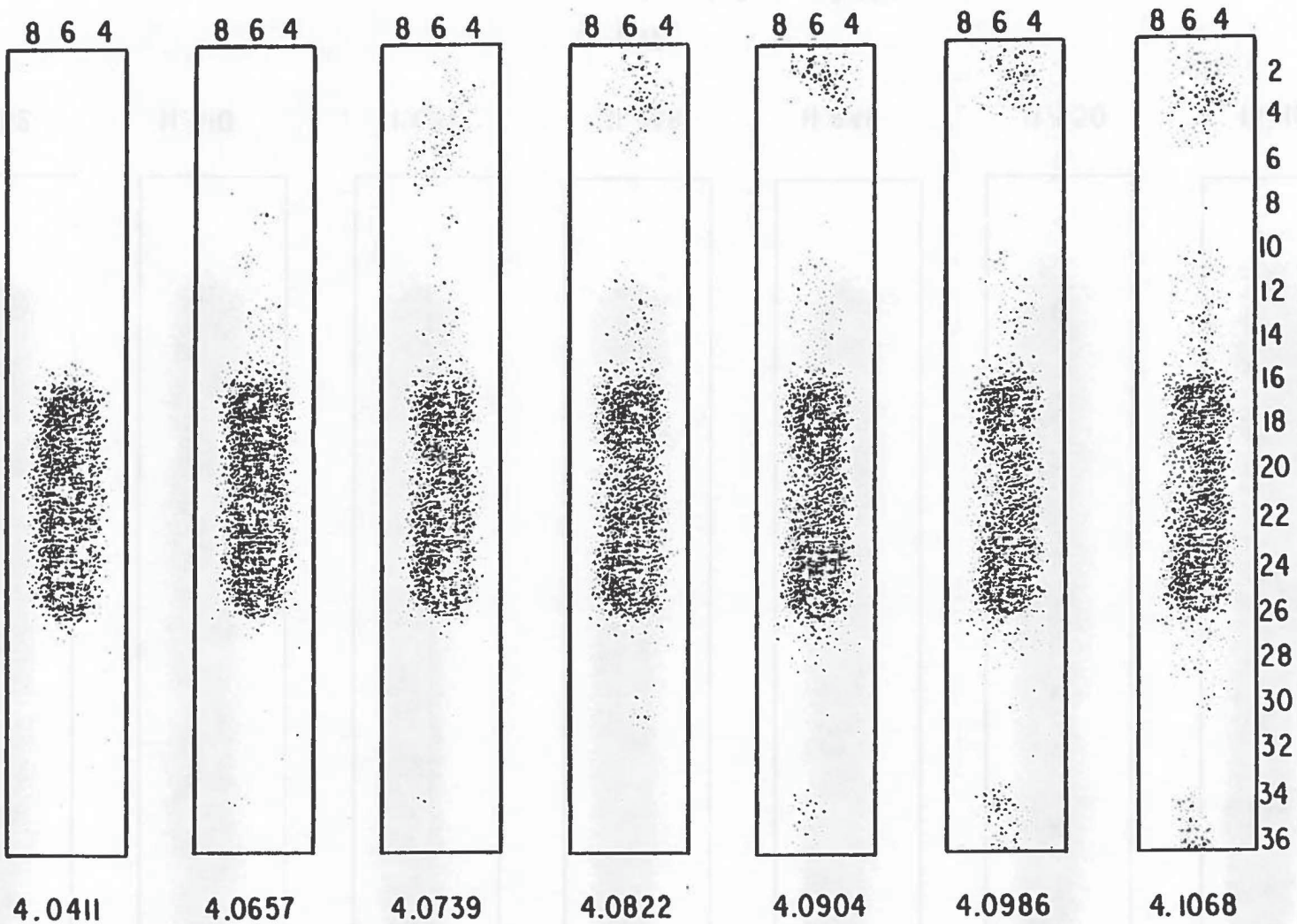


16. Fuel losses from a 3-pin cluster (AX1)
[DE VOLPI, et al]

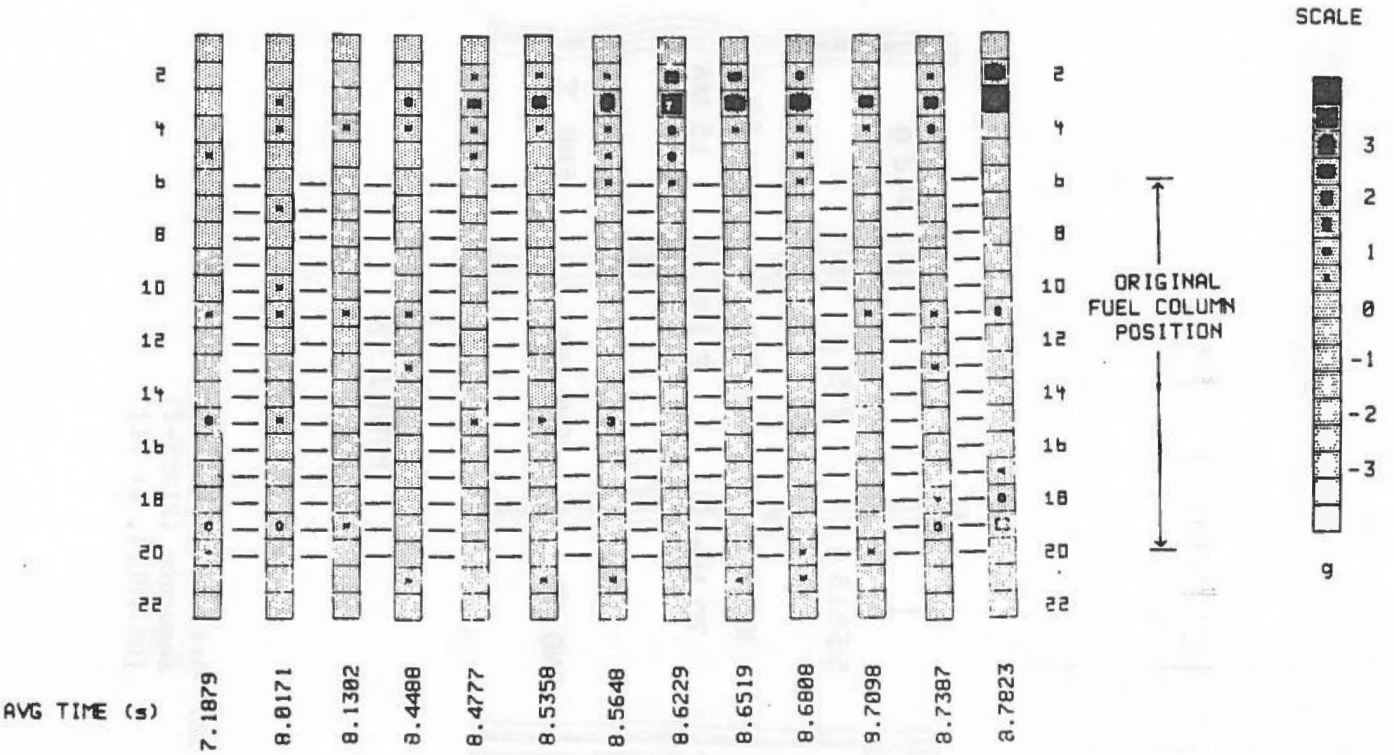


SC1A

17. Axial component of fuel motion (SC1A)
[DE VOLPI, et al]

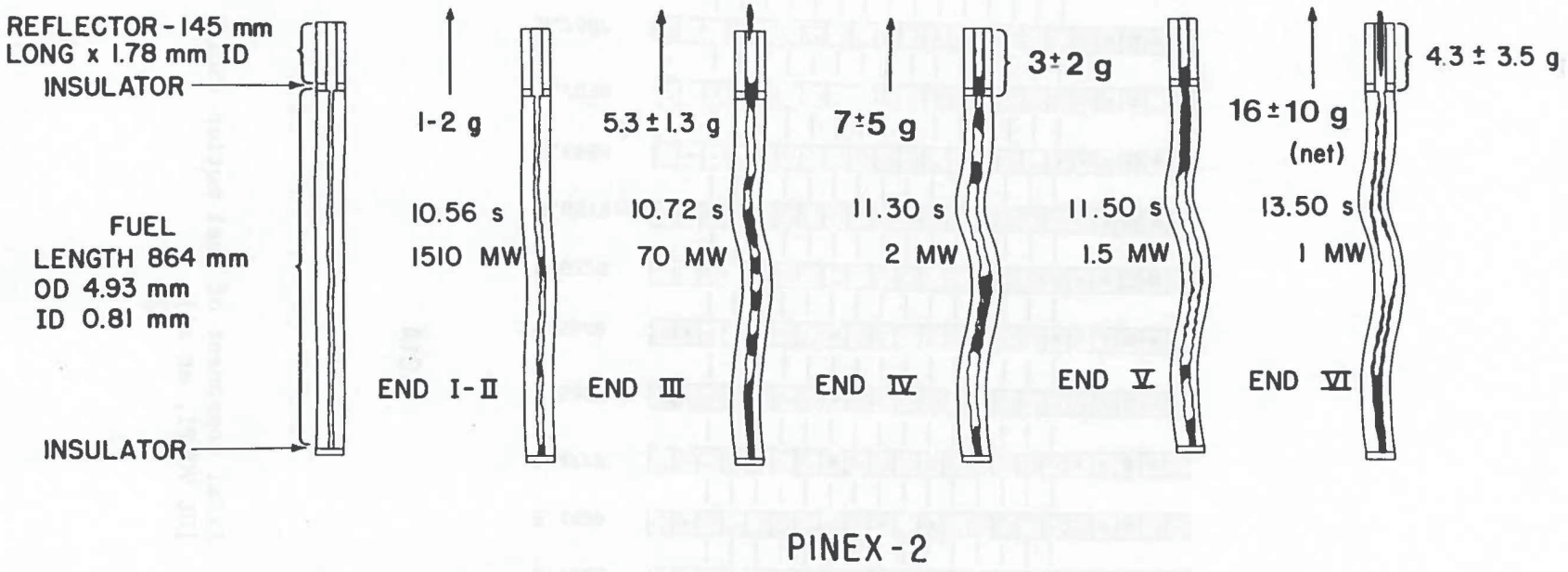


18. Artists reconstruction of motion sequence (PINEX-2) [DE VOLPI, et al]

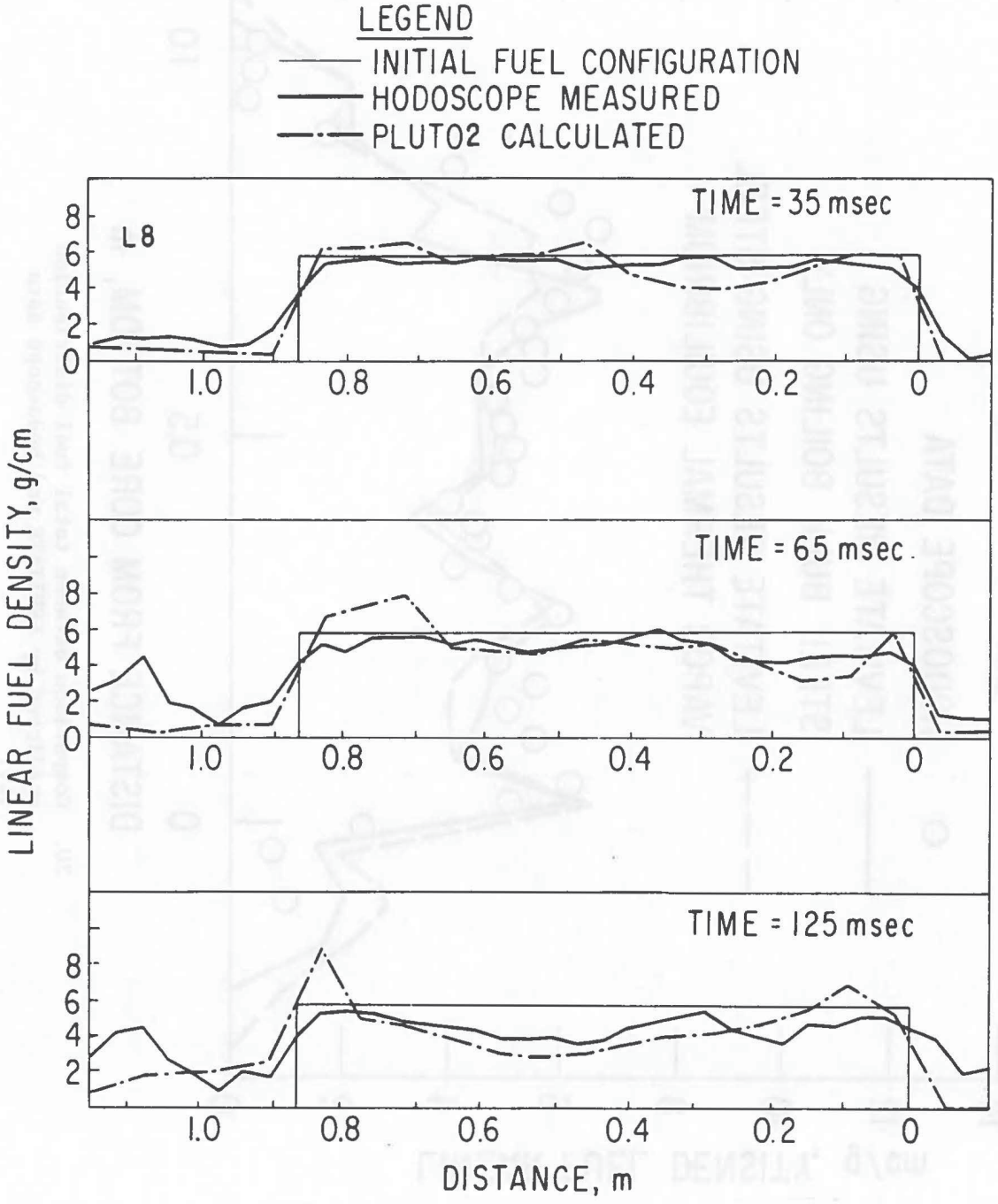


19. Comparison of hodoscope data and PLUTO2 calculations of fuel density at several different times (L8)
[DE VOLPI, et al]

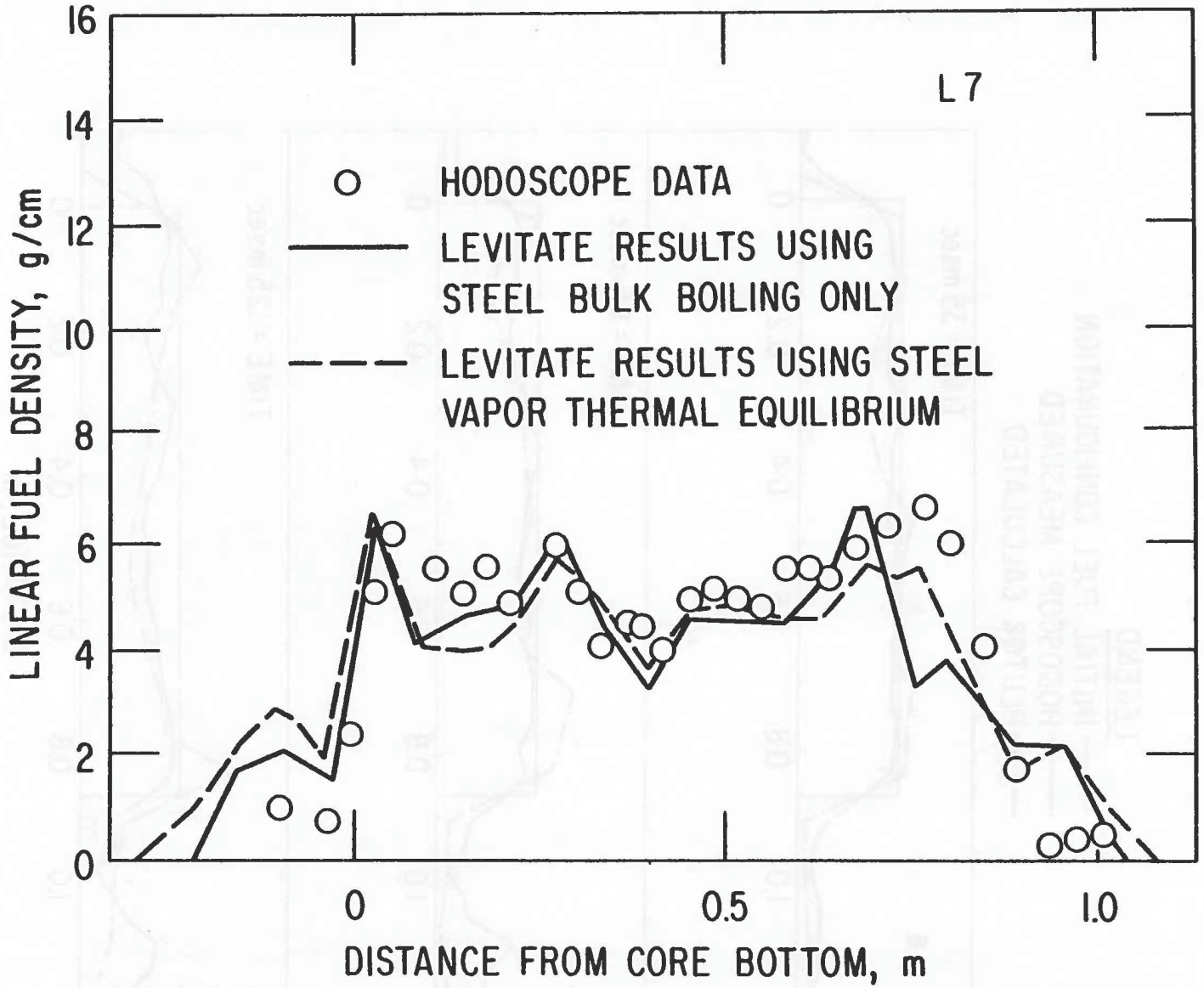


20. Comparison between total fuel distribution predicted by LEVITATE and hodoscope data (L7)
[DE VOLPI, et al]

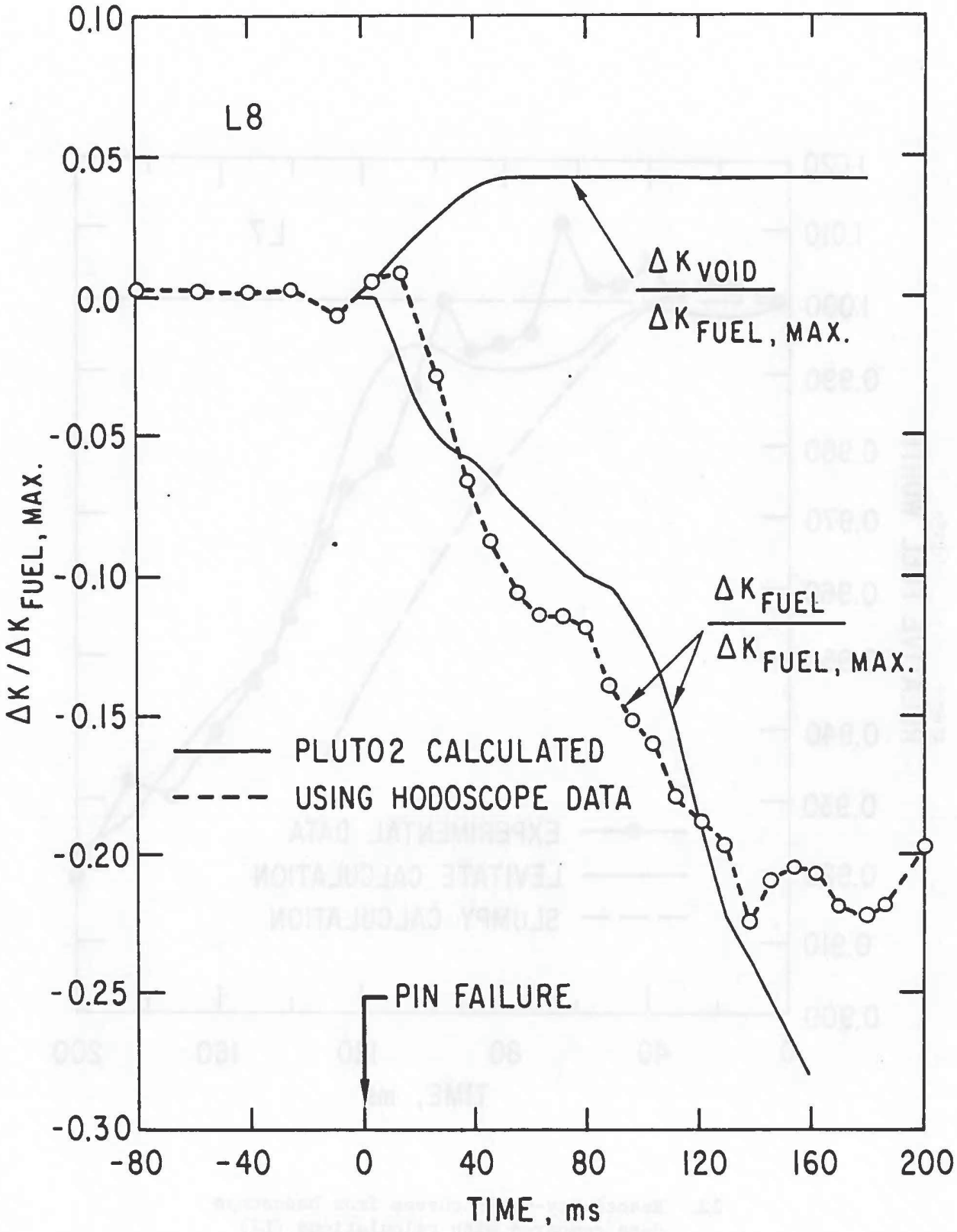


21. Comparison of hodoscope data and PLUTO2 calculations of reactivity worth as a function of time (L8)
[DE VOLPI, et al]

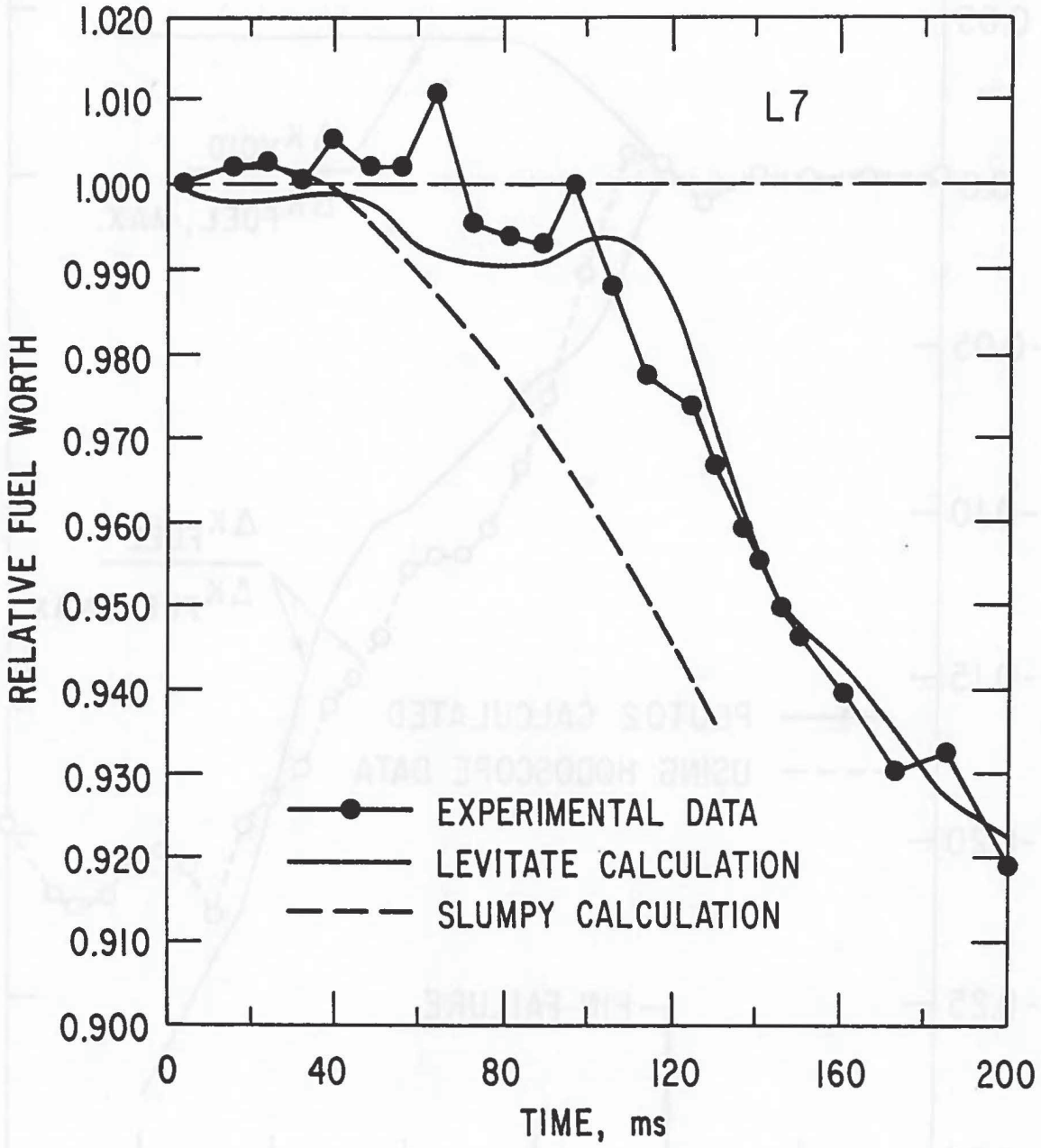


22. Reactivity-worth curves from hodoscope data compared with calculations (L7) [DE VOLPI, et al]

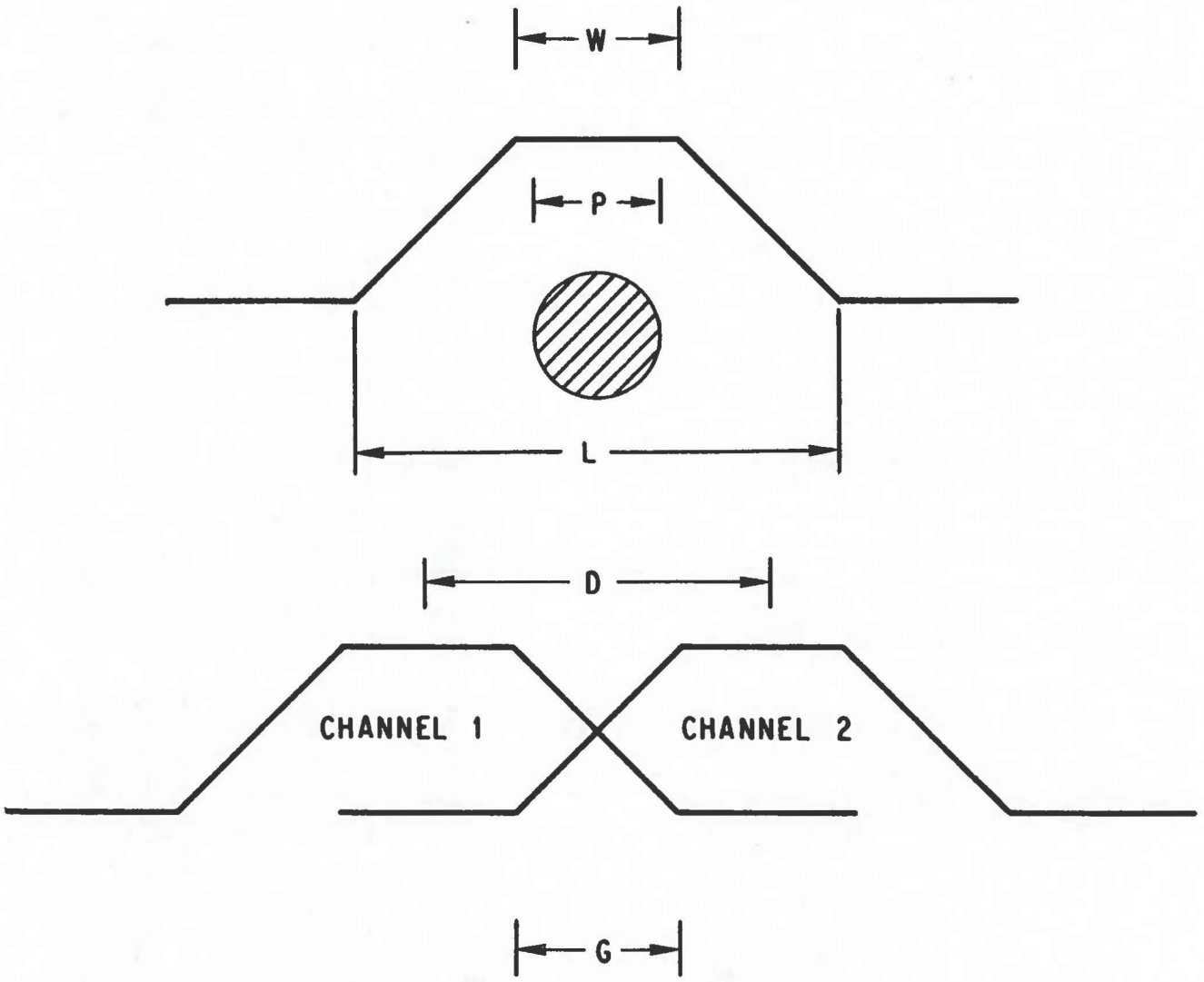


23. Simplified model of hodoscope collimator spatial response function
[DE VOLPI, et al]

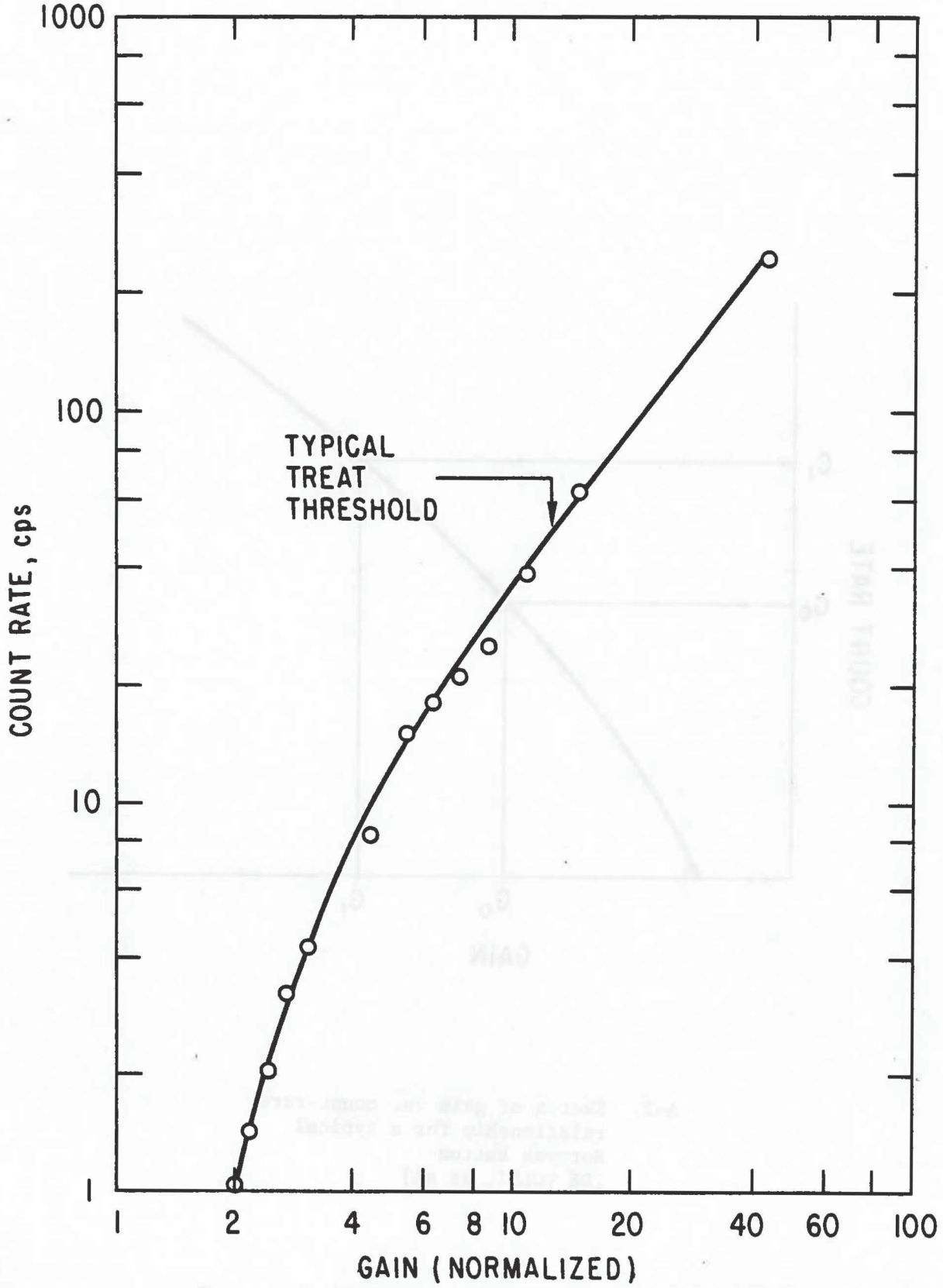


A-1. Count rate vs. gain for typical Hornyak-button detector [DE VOLPI, et al]

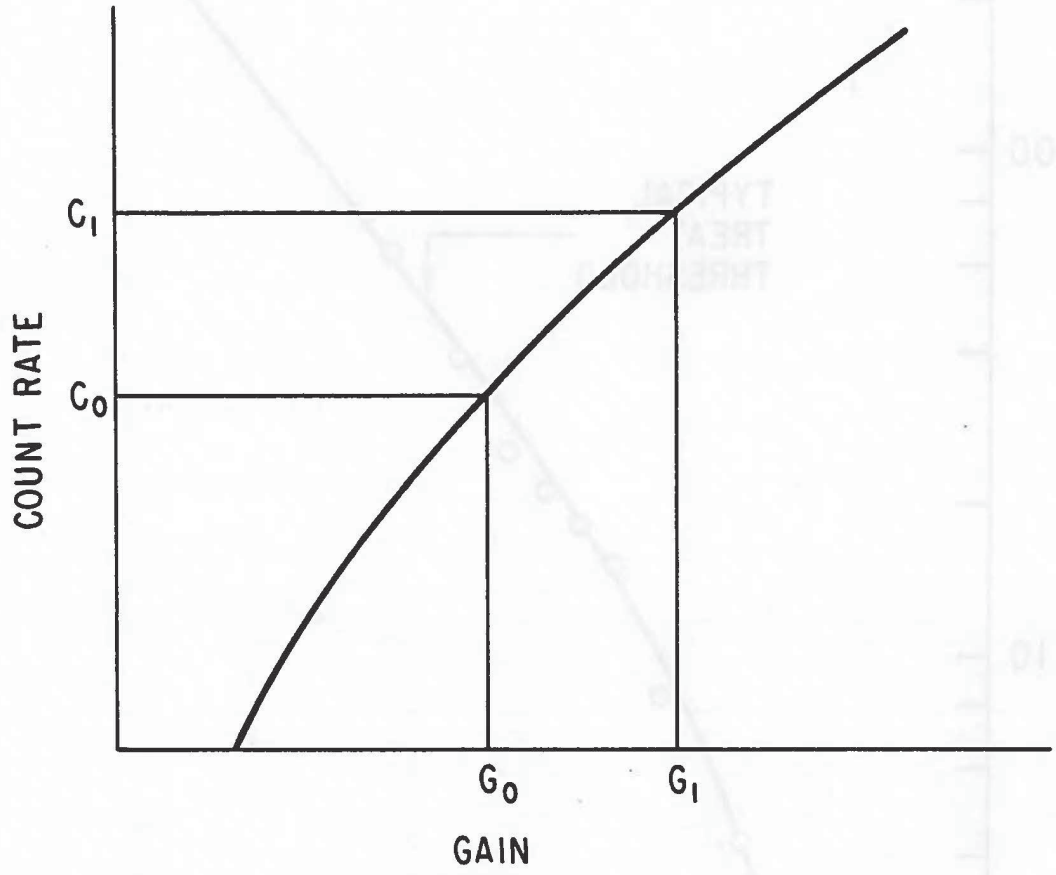


A-2. Sketch of gain vs. count-rate relationship for a typical Hornyak button
[DE VOLPI, et al]

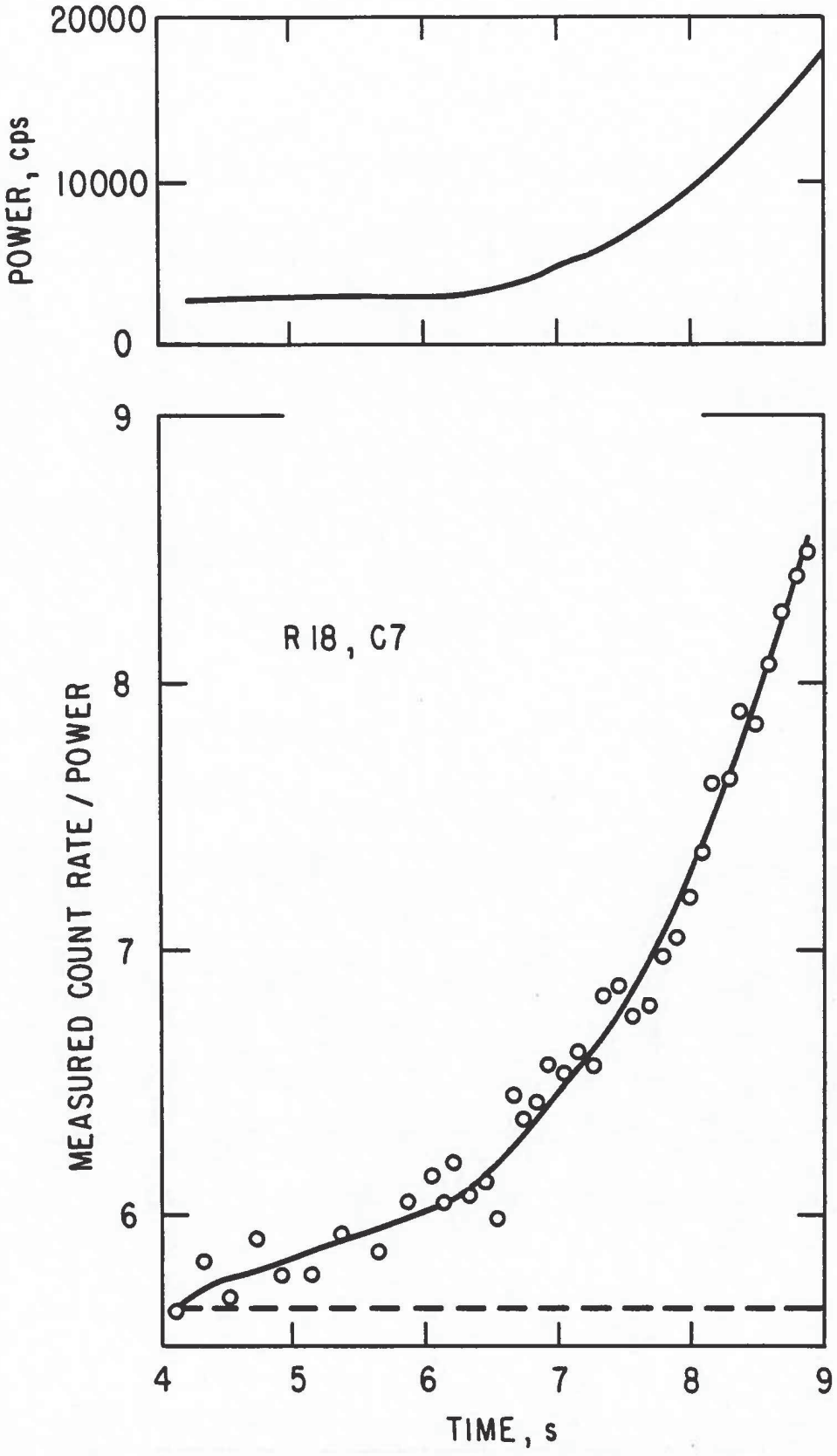


A-3. Comparison of supralinearity model with experimental measurements [DE VOLPI, et al]

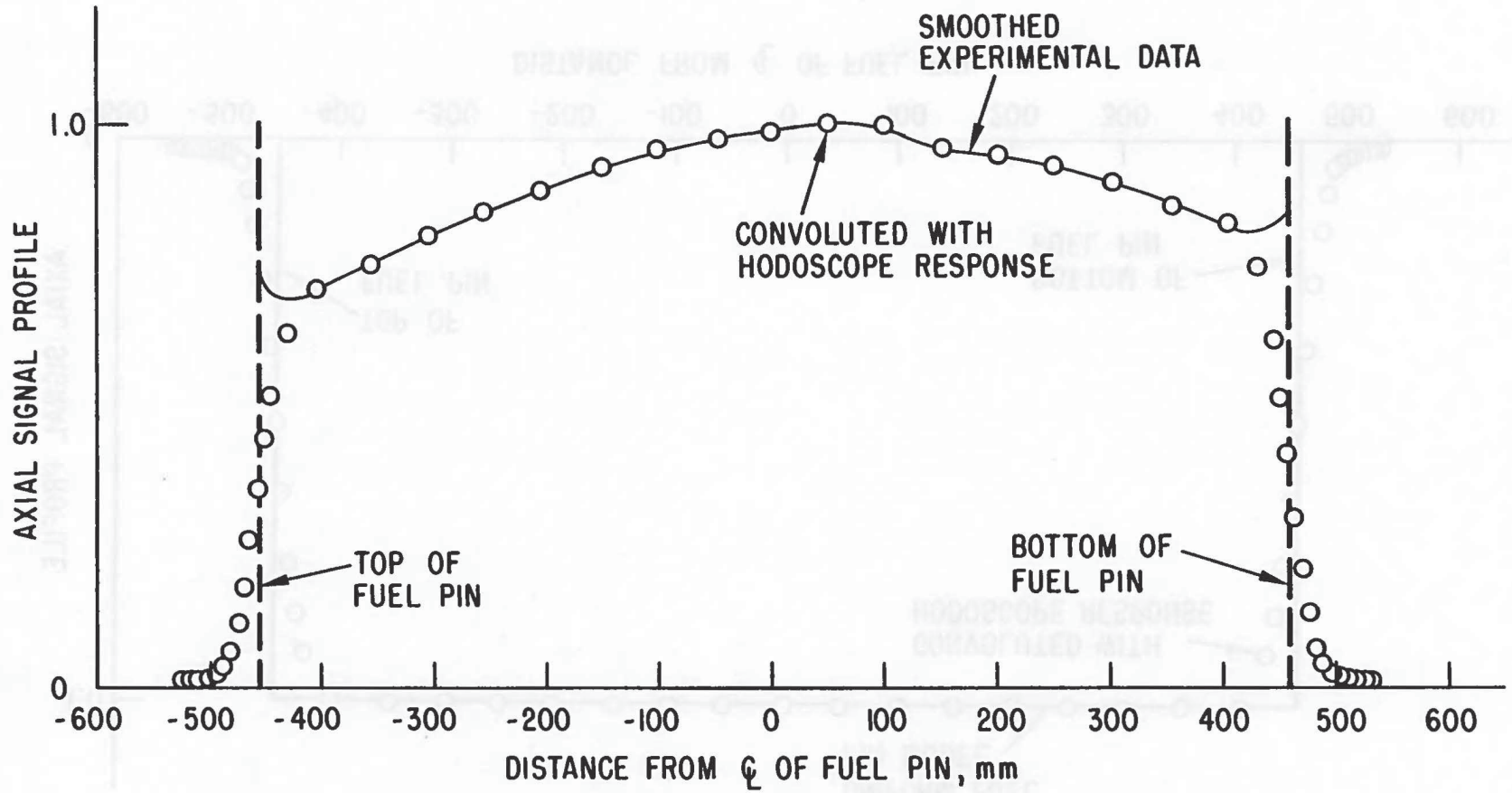


B-1. Typical axial profile
[DE VOLPI, et al]

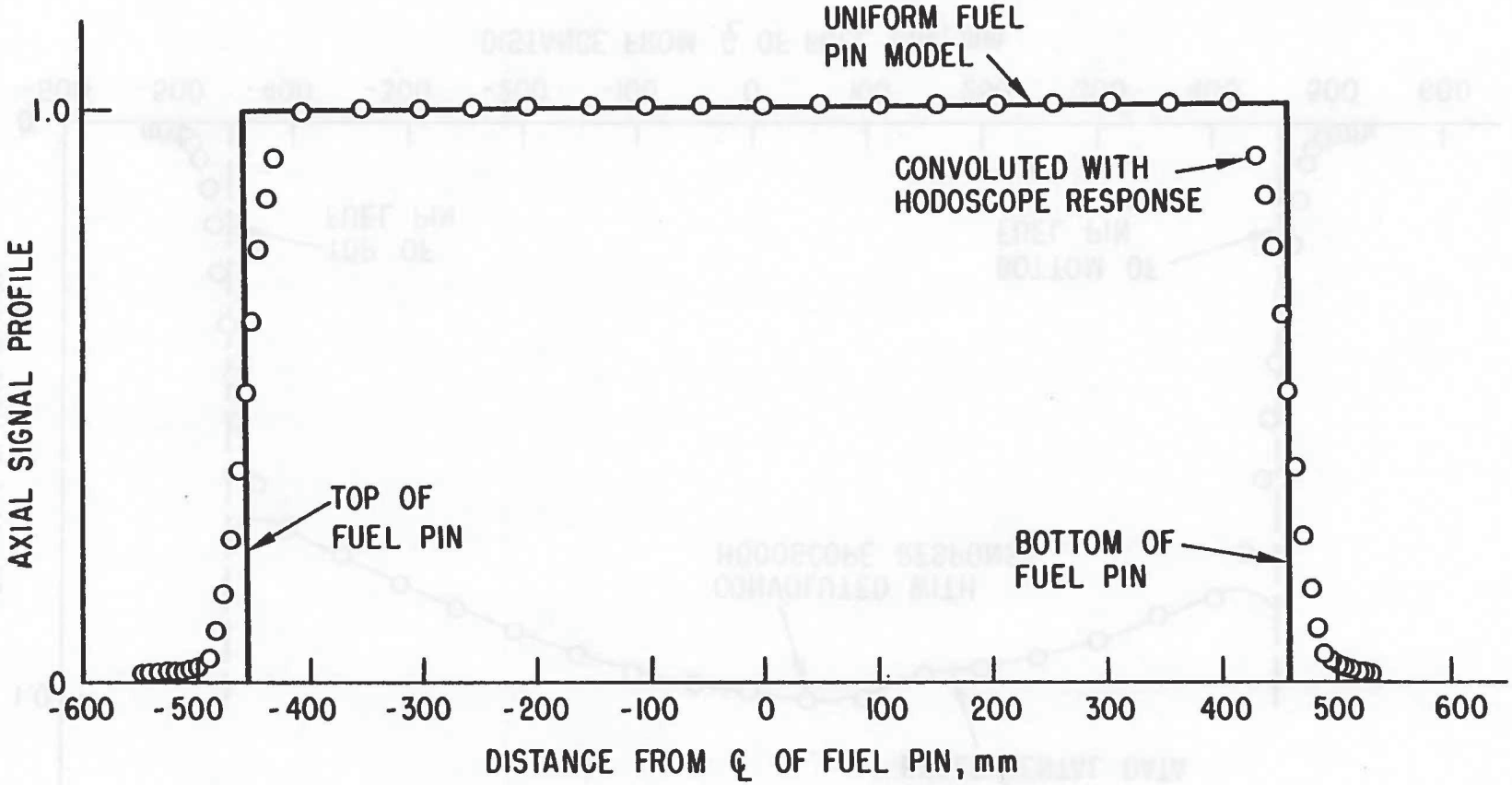


B-2. Uniform axial-pin profile model
[DE VOLPI, et al]

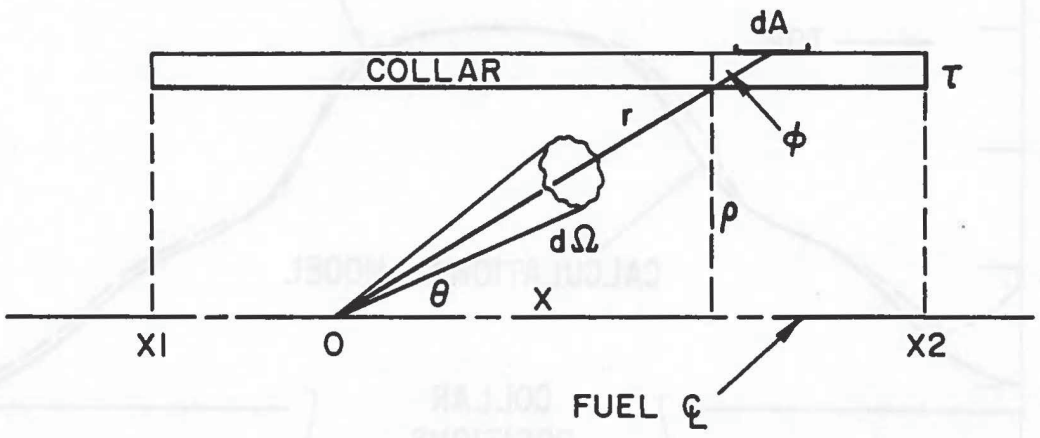


C-1. Geometry for collar corrections
[DE VOLPI, et al]

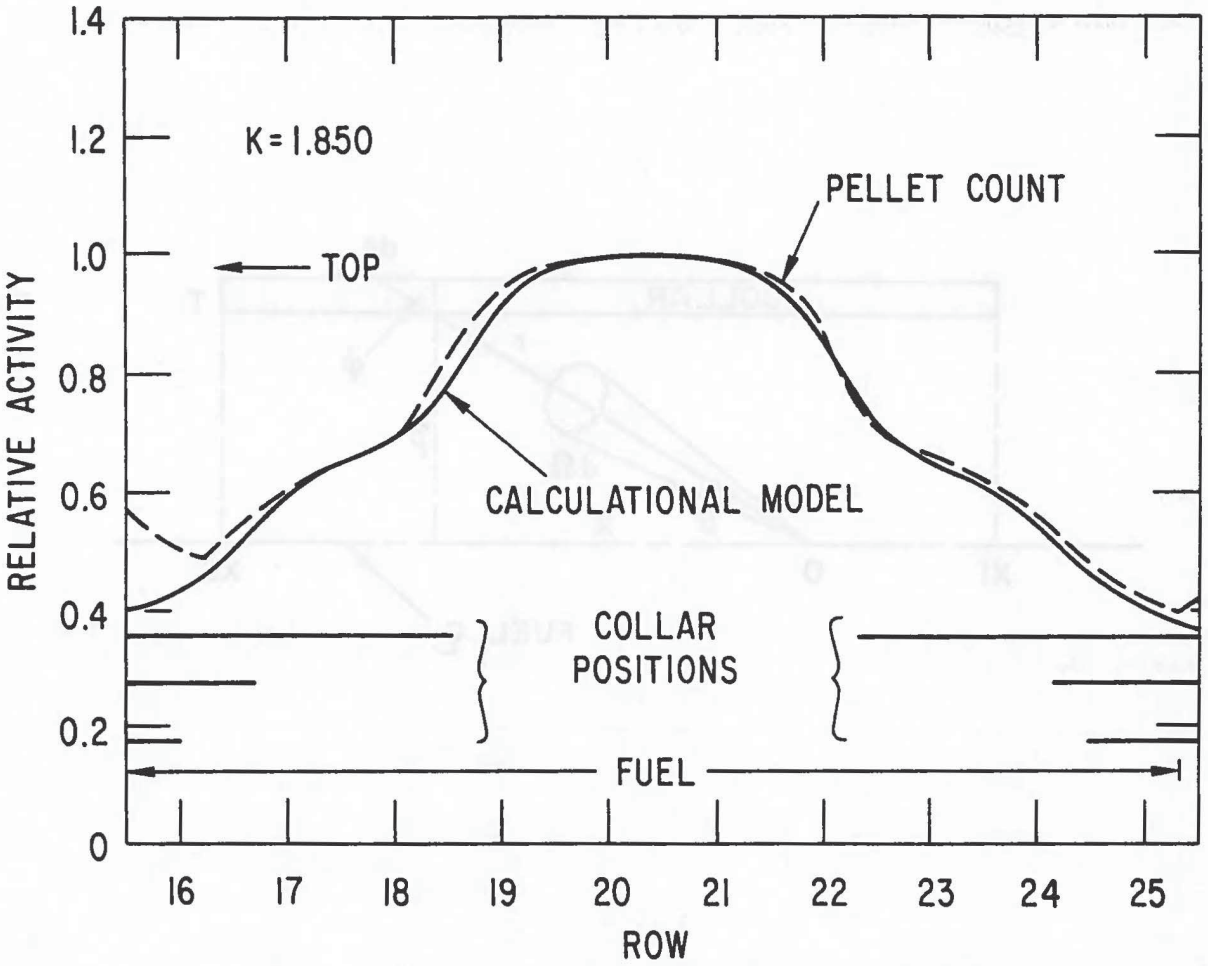


C-2. An example of results for collar corrections [DE VOLPI, et al]

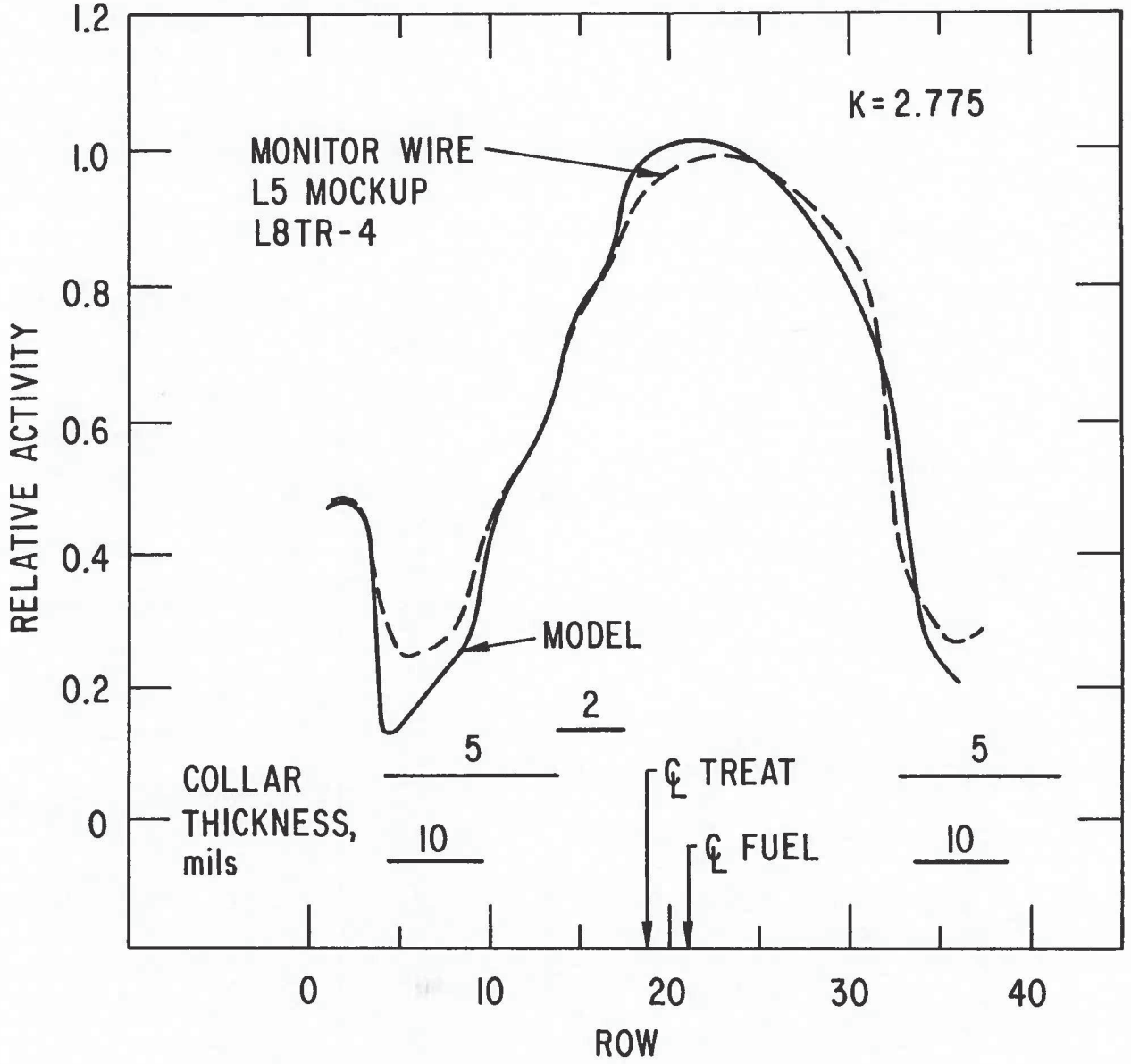


C-3. Collar-correction fit for AX1
[DE VOLPI, et al]